Controlling Chaos Using Synchronization

by

Ali Azimi Olyaei

A Thesis submitted to the Faculty of Graduate Studies of

The University of Manitoba

in partial fulfilment of the requirements of the degree of

Doctor of Philosophy

Department of Mechanical Engineering

University of Manitoba

Winnipeg, Manitoba

(*xxiii*/129/11/163)

I would like to dedicate this thesis to my beloved parents

Iran and **Asad**, and to my dear sister **Shima**.

Abstract

The main contribution of this thesis can be formulated in terms of a synchronization problem describing interactions between a system of harmonic oscillators (HO) and a given dynamical system, called HO synchronization. This thesis investigates the applications of HO synchronization in the area of controlling chaos. It proposes an innovative feedback stabilization technique, called HO feedback control, that utilizes an output of the synchronized system to stabilize periodic orbits of dynamical systems. A particularly attractive application of this stabilization technique is found in controlling chaotic systems, where the aim is to stabilize unstable periodic orbits embedded in the chaotic attractors. This thesis utilizes the same concept of synchronization to develop a novel method of detecting unstable periodic motions in chaotic time series, called HO time series analysis. To do so, the proposed method does not require any information about the underlying dynamics beyond a recorded time history. Therefore, it is appealing in experimental situations. The information obtained from the HO time series analysis can be used in various methods of controlling chaos, including the HO feedback control. In a different, but related application, this thesis proposes a novel transformation of a time delay system to a system of ordinary differential equations featuring the same concept of synchronization, called HO transformation. This transformation yields an efficient finite dimensional approximation to the original time delay system. It is practically important as it allows implementation of classical theories and conventional tools, developed for finite dimensional systems, to analyze time delay systems. This thesis utilizes the HO transformation to reveal the relation between the delayed feedback control and the HO feedback control.

Acknowledgments

I would like to express my sincere gratitude to my advisor Professor Christine Wu for her continuous support of my PhD study and research, for her patience, and motivations. She is a great mentor, who introduced new dimensions to my life. I feel so fortunate having the opportunity to work with her, and learn from her during the last four years. I am also grateful to my co-advisor Professor Wiltold Kinsner for his guidance and support throughout writing of this thesis.

I would like to express my deepest respect and gratitude to my parents, Iran and Asad, and to my sister, Shima, who have always supported me throughout my life.

I thank my dear friends Ehsan Alishahi and Dr. Alireza Armioon for their spiritual supports and inspirations during writing of this thesis.

Contents

List of Tables

List of Figures

List of Acronyms

CPG	Central pattern generator
DFC	Delayed feedback control
EDFC	Extended delayed feedback control
HO	Harmonic oscillator
NFFC	Notch filter feedback control
OPF	Occasional proportional feedback
ODE	Ordinary differential equation
OGY	Ott Grebogi Yorke
PFC	Proportional feedback control
PSD	Power spectral density
RMS	Root mean square
SNA	Strange nonchaotic attractor
UPO	Unstable periodic orbit

List of Symbols

Scalars

Scalars are denoted by italic letters

d	Number of vriables in Nelder-Mead simplex algorithm
D	State space dimension
E	Error signal
E_k	Truncation error
f_c	Control perturbations
f_N	Nyquist frequency
i	Imaginary unit
j	Running index
k	Truncation limit
l	Running index
K_D	Control gain of DFC/EDFC
K_H	Control gain of HO feedback control
κ_n	The n^{th} coupling strength of HO feedback control
K_N	Control gain of NFFC
K_P	Control gain of PFC

L	Number of samples in the time series y
m	Running index
n	Running index
N	Number of samples in one period of the target orbit
N_ω	Resolution of the frequency discretization
r_c	Radios of convergence of Taylor series
p	Running index
R	Memory coefficient of EDFC
R_ω	Root mean square deviation of the system from HO manifold
$\bar{R}_\omega$	Weighted time average of R_ω
s	Laplace variable
$\mathfrak{s}$	Complex variable
t	Time
t'	Arbitrary time
t_0	Initial time
T	Period of UPO
w_l	The l^{th} averaging weight
y	Recorded time history
u_{in}	Input of dynamical system
u_{out}	Output of dynamical system
V_{in}	Input voltage of the electrical circuit
V_{out}	Output voltage of the electrical circuit
x_j	The j^{th} component of the state vector
α	The exponent of the averaging weight

γ	Control parameter of the system described by Eq. (2.9)
β	Control parameter of the system described by Eq. (2.9)
δ	Initial deviation of nearby trajectories/orbits
Δt	Sampling period
ϵ	Final deviation of nearby trajectories/orbits
ε	Threshold for identifying periodic orbits
λ	Floquet exponent
λ_Ψ	Eigenvalue of Ψ
λ_{Ψ_m}	The m^{th} eigenvalue of Ψ
μ_m	A complex variable defined by $\mu_m = \frac{\tau}{2}(\lambda + im\omega_{_T})$
ξ	Notch filter damping
τ	Delay time
ω	Frequency constant
ω_{max}	The upper limit of the desire frequency rage for UPOs detection
ω_{min}	The lower limit of the desire frequency rage for UPOs detection
$\omega_{_T}$	The fundamental frequency of UPO

Vectors and Matrices

Vector and matrices are denoted by bold letters

$\mathbf{a}_{nm}$	The m^{th} Fourier coefficient of $\mathbf{A}_{n\,T}$
$\mathbf{A}$	Vector of harmonic oscillator
$\mathbf{A}_n$	The n^{th} harmonic oscillator
$\mathbf{A}_{n_T}$	Periodic solution of the n^{th} harmonic oscillator
$\mathbf{B}$	A complex matrix defined by $e^{\mathbf{B}\,T} = \Phi(0)^{-1}\Phi(T)$

$\mathbf{c}_n$	A complex vector defining the n^{th} Fourier coefficient of $\mathbf{x}/\delta\mathbf{x}$
$\mathbf{f}$	Vector field
$\mathbf{F}_l$	A constant vector defining the l^{th} eigenvalues of Ψ
$\mathbf{I}$	$D \times D$ identity matrix
$\mathbf{I}'$	Identity matrix defined by the cardinality of set $\mathbb{U}$
$\mathbf{J}$	Jacobian of nonlinear system
$\mathbf{K}$	Generalized coupling matrix
$\mathbf{K}_D$	Control gain matrix of DFC/EDFC
$\mathbf{K}_H$	Control gain matrix of HO feedback control
$\mathbf{K}_n$	The n^{th} coupling matrix of HO feedback control
$\mathbf{K}_P$	Control gain matrix of PFC
$\mathbf{P}$	A complex matrix defined by $\mathbf{P}e^{\mathbf{B}t} = \Phi(t)$
$\mathbf{P}_\Psi$	Eigenvector of Ψ
$\mathbf{P}_{\Psi_m}$	The m^{th} eigenvector of Ψ
$\mathbf{R}$	Memory matrix of EDFC
$\mathbf{u}$	Solution of a dynamical system
$\mathbf{u}_n$	Floquet eigenfunction associated with $\mathbf{A}_n$
$\mathbf{u}_\mathbf{x}$	Floquet eigenfunction associated with $\mathbf{x}$
$\mathbf{v}$	Solution of a dynamical system
$\mathbf{x}$	State vector
$\mathbf{x}_0$	Initial state vector
$\mathbf{x}_m$	The m^{th} Fourier coefficient of $\mathbf{x}_T$
$\mathbf{x}_T$	Periodic solution
$\mathbf{z}$	Delay variable

Λ	Eigenvalue matrix of Ψ
Φ	Fundamental matrix solution
Ψ	Coefficient matrix of $\mathbf{A}$

Sets

$\mathbb{C}_\bullet$	Neighborhood of the set $(\bullet)$
$\mathbb{D}$	Domain of convergence of Padé approximation
$\mathbb{R}$	Real number set
$\mathbb{T}$	Time set
$\mathbb{U}$	Defining set of frequency content of HO synchronization
$\mathbb{V}$	Complement of $\mathbb{V}^c$ with respect to $\mathbb{Z}$
$\mathbb{V}^c$	Defining set of frequency content of $\mathcal{H}_0$
$\mathbb{V}_\lambda$	$\mathbb{V}_\lambda = \mathbb{V}$ for $\lambda = 0$, otherwise $\mathbb{V}_\lambda = \emptyset$
$\mathbb{X}$	State space
$\mathbb{X}_a$	Attractor of a dissipative system
$\mathbb{Z}$	Integer set

Operators and Other Symbols

$g_D(s)$	Transfer function of DFC/EDFC
$g_H(s)$	Transfer function of HO feedback control
$g_N(s)$	Transfer function of NFFC
$\mathcal{H}_0$	Defining function of the truncated term of HO manifold
$\mathcal{H}_\omega$	Defining function of HO manifold
$\mathcal{H}^k_{\omega_T}$	Defining function of the truncated HO manifold

$\mathcal{I}$	Identity map
$\mathcal{M}_{\mathcal{H}}$	HO manifold
$(\bullet)^{\top}$	Transpose of the matrix $(\bullet)$
φ^t	Evolution operator
$\Upsilon_{(\bullet)}$	Orbit through $(\bullet)$
$\det(\bullet)$	Determinant of matrix $(\bullet)$
$(\dot{\bullet})$	Derivative of $(\bullet)$ with respect to time
$(\bullet)^c$	Complement of set $(\bullet)$
$\lvert\bullet\rvert$	Absolute value of $(\bullet)$
$\equiv$	Equivalence operator (is equivalent to)
$\lVert \bullet \rVert$	Norm of the vector $(\bullet)$
$\exists$	Existential quantification (there exists)
$\rightarrow$	Function arrow (from . . . to)
$\Rightarrow$	Implication operator (implies that)
$\in$	Set membership operator (in the set)
$\subset$	Subset operator (subset of)
$\forall$	Universal quantification (for all)

List of Definitions

Chapter 1

Introduction

The world and every single component of it are continuously changing according to certain rules. These rules govern the evolution of the system from an initial state to a final state. The governing rules are often deterministic, i.e., they guarantee a unique evolution for a given set of initial conditions. Here, an important question to address is how sensitive this evolution is to initial conditions. Answering this question is of a particular interest, since the initial conditions can only be measured or assigned within a limited range of accuracy. In deterministic systems, the present state always determines the future state. However, for a class of dynamical systems (defined in Sec. 2.2) known as chaotic systems (defined in Sec. 2.5), an approximation of the present state does not lead to an approximation of the future state. In such systems, infinitesimal small errors in assigning initial states lead to large deviations in the final states. This is an undesirable property that deteriorates the predictability of the system's response. The significance of this property is well clarified by the following question raised by Edward Lorenz,

one of the discoverers of chaos [1]: "Does the flap of a butterfly's wings in Brazil set off a tornado in Texas?" [2] He argued that in chaotic systems, small causes can have large effects. The flapping wings represents a small change in initial conditions that can lead to a tremendous, large scale effect. This phenomenon is known as the butterfly effect [3; pp. 181-184], and serves as a metaphor for what in the technical language is called "sensitive dependence on initial condition". It adversely effects the outcome of chaotic systems, and therefore, needs to be avoided in many practical situations.

1.1 Problem Statement

Chaos (defined in Sec. 2.5) in dynamical systems manifests itself by an irregular, aperiodic behaviour that restricts the operating range of many physical systems, and renders their long-term prediction impossible [1]. This section describes the general properties of chaos, and points out the need for developing an effective method to suppress the destructive effects, and exploit the inherently rich properties of it.

1.1.1 Motivation

The ability of predicting the outcome of real-world dynamical systems is critically important. It allows us to take a suitable action to avoid undesirable effects, and exploit the potential benefits of them. This is a fundamental concept based on which we often live our everyday lives. This concept also plays an important role in engineering. Engineers design, control, and optimize systems based on their prediction about the system's response. They sometimes fail to predict the

outcome correctly due to their limited knowledge, or understanding of the system. However, this is not always the reason of failing. They may also fail due to their limited accuracy in measuring, or assigning the system's state. No matter how accurately the system's state (defined in Sec. 2.2) is measured or assigned, the error is quickly magnified when the system is chaotic. As a consequence, the ability to predict the system's response is totally lost after a short period of time. An example of such a behavior can be found in turbulent flows in fluid mechanics, where individual realizations of identical experiments are always different, no matter how accurately the experiments are conducted. Notice that sensitive dependence on initial conditions alone does not produce chaos. A bounded long-term behaviour is also required. Consider a simple dynamical system that doubles the current value at each iteration. This system exhibits sensitive dependence on initial conditions, as arbitrarily close initial states becomes widely separated after a few iterations. However, this dynamics yields an unbounded response, and therefor has no chaos [4; pp. 3]. In other words, deterministic chaotic systems yield non-intersecting trajectories (defined in Sec. 2.3.2) that are globally bounded while locally divergent. These seemingly contradictory properties of chaos induce a complex mixing of trajectories leading to an irregular, aperiodic response that sensitively depends on initial conditions. This is an undesirable behaviour, and needs to be avoided in many applications.

1.1.2 Problem Definition

Chaos is a common phenomenon in nature, and has been observed in a wide range of dynamical systems of various physical nature. It has been known

as a source of seriously destructive effects, and therefore, needs to be averted in many practical situations. One approach to prevent chaos might be making large alterations in the physical structure of the system. However, this approach not only changes the system's original dynamics, but also it may not be feasible or financially justifiable in many situations. Therefore, one needs to seek solutions that prevent manifestation of chaos in dynamical systems by applying only small perturbations, or making slight alterations. This is where the term "controlling chaos" (defined in Sec. 2.1) emerges [5].

It is worth mentioning that not all the properties of chaos are undesirable. Interestingly, chaos has great potential in producing an infinitely large number of periodic motions from the same dynamical system under small control actions [5]. In fact, the skeleton of chaotic systems is made up of infinitely many unstable periodic orbits (UPOs) [5]. The question then arises as to what happens if one can stabilize the periodic orbits embedded in chaotic systems? The answer to this question seems to be a promising way of solving the problem called chaos. Stabilizing the system's periodic orbits eliminates the sensitivity of the system to initial conditions. All the trajectories that start sufficiently close to the orbit (inside the basin of attraction (defined in Sec. 2.4)), remain arbitrarily close to it for ever. Therefore, the dynamical system will be no longer unpredictable. Furthermore, it transforms the irregular, aperiodic behaviour of the system to a regular, periodic one, while the intensity of the control perturbations remains vanishingly small. From this perspective, the presence of chaos can also be beneficial. Not only are there infinitely many unstable orbits among which one can stabilize the motion that fits the best to the design and operation criteria, but also there is the

possibility of switching between different modes of periodic motion by stabilizing different unstable orbits in systems for multipurpose uses. Section (2.6) provides two applications of chaos control techniques in practical situations.

The first attempt of controlling chaos is known as OGY method proposed by Ott, Gerbogi, and Yorke [5]. This method applies wisely chosen small perturbations to an accessible system's parameter once per cycle of the periodic motion to keep the system close to the target orbit. The well-known OGY method has been applied successfully to control chaos in many physical systems [6], however, it suffers from the following limitations:

(i) The control rule is valid only in a small neighborhood of the target orbit. This can lead to a long chaotic transient, before the system enters the vicinity of the target orbit;

(ii) Due to the discrete nature of the control method, inevitable noise in the experimental data can lead to occasional outbursts of the system to the regions far from the target orbit;

(iii) It is not able to stabilize high-period periodic orbits with relatively large Lyapunov exponents (defined in Sec. 2.5); and

(iv) It requires comparatively large amount of information about the system's dynamics, which is not easy to obtain, specially from noisy time series.

To overcome the limitations of OGY method, Pyragas proposed a time-continuous method of controlling chaos known as the delayed feedback control (DFC) [7]. It is one of the most powerful and widely used methods of controlling

chaos. This method continuously injects control perturbations whose intensity is proportional to the deviation of the current state of the system form its state at one period of the target orbit in the past. So, the intensity of the control perturbations vanishes, once the target orbit is stabilized. This control method does not require *a priori* analytical knowledge about the dynamical system, and it is relatively easy to implement in practical situations. However, it suffers from the following limitations:

(i) The dynamics of the controlled system takes place in an infinite dimensional function space. As a consequence, it has a complicated theory;

(ii) Evaluating the stability properties of the controlled orbit requires special simplifications and numerical efforts; and

(iii) Periodic orbits of nonautonomous systems (defined in Sec. 2.2.2) with odd number of real Floquet multipliers greater that unity (torsion free or directly unstable orbits) are never stabilized by this method. This limitation is known as the odd number limitation [8, 9], and has been considered as the most important analytical limitation of the delayed feedback control.

Another practical approach of suppressing chaos in dynamical system is known as the notch filter feedback control (NFFC) proposed by Ahlborn and Parlitz [10]. The underlying idea of using notch filter feedback is to suppress a selected frequency from the power spectrum of the system. This method is particularly suitable for fast dynamical systems, as it can easily be implemented in analogue hardware. In contrast to OGY and Pyragas method, this method is an invasive method. Consequently, it suffers from the following critical limitation:

NFFC changes the system's original dynamics by applying relatively large control perturbations.

Knowing the advantages and disadvantages of the main contributions in the area of controlling chaos, this thesis seeks a practically effective method of controlling chaos that integrates the main advantages of the previously proposed method, while reduces their critical limitations.

1.1.3 Proposed Solution

This thesis addresses the problem of controlling chaos from a new perspective using synchronization (defined in Sec. 2.7) techniques. It introduces a synchronization problem describing the interactions between a system of harmonic oscillators and the chaotic system. It employs an invariant property of the synchronized system to develop a feedback method of controlling chaos. The feedback is designed such that the synchronous motion of the harmonic oscillators and the controlled system on the target periodic orbit become stable.

1.2 Thesis Formulation

1.2.1 Thesis Statement

This thesis aims to develop a new stabilization technique capable of controlling chaos in a wide range of dynamical systems with various physical nature, and to demonstrates its capabilities through analytical investigations, numerical simulations, and experimental implementations.

1.2.2 Thesis Objectives

The primary objectives of this thesis is to develop an effective method of transforming unpredictable chaotic system to a predictable periodic one, which consists of two parts:

(i) Developing an effective method of controlling chaos that has the following desirable properties:

- It is a noninvasive method that stabilizes the system's periodic orbit by applying small control perturbations.
- It is able to control chaos without having *a priori* analytical knowledge about the system's dynamics.
- It is a time-continuous method whose control rules is valid everywhere in the state space.
- It does not suffer from the so-called odd number limitation.
- It has a simple structure that allows straightforward evaluation of the stability properties of the controlled orbit.

(ii) Demonstrating the capabilities of the proposed method to control chaos in real world physical systems:

- Implementing the proposed method successfully to control chaos in a real-world physical system.

1.2.3 Research Questions

Several methods of controlling chaos have been proposed in the past few decades [11]. They have limitations and advantages. The question then arises:

1. Is there any relation between the method proposed in this thesis and previously proposed methods of controlling chaos?
2. What are the relative advantages and disadvantages of the proposed method compared with the previously proposed methods?

In order to answer this question, one needs to quantify the performance of the control method. Therefore, this research tries to answer the following question:

3. What are the key factors that quantify the performance of the proposed method?

As a general rule, chaos control methods are supposed to preserve the system's original dynamics. Therefore,

4. Can the proposed method be classified as a noninvasive method?

From the practical point of view, chaos control methods should be able to effectively control chaos in a real-world physical systems. Consequently,

5. Does the proposed method effectively control chaos in practical situations?
6. What are the limitations in the experimental implementation of the new method?

7. How can one reduce the limitations and improve the performance of the proposed method in experimental implementations?

1.2.4 Scope of the Thesis

The methods proposed to improve the behaviour of chaotic systems can be classified into two major groups: (*i*) noninvasive methods of controlling chaos that stabilizes the existing periodic orbits by applying vanishingly small perturbations, and (*ii*) invasive methods that suppress chaos that creates a new periodic orbits by applying relatively large perturbations. This thesis focuses on noninvasive methods mainly, as they match with the classical definition of controlling chaos [5]. Some methods of suppressing chaos are also discussed to study the relations, or making comparisons between different methods.

The main contribution of this thesis can be formulated in terms of a synchronization problem describing interactions between a system of harmonic oscillators and a given dynamical system. It is called HO synchronization, due to the central role of harmonic oscillators in its structure. This thesis investigates the applications of the HO synchronization in the following areas:

(i) **Controlling chaotic systems:** a particularly important application of the HO synchronization manifests itself in an innovative feedback method of controlling chaos, called HO feedback control. This thesis investigates the performance of the HO feedback control in the context of linear stability analysis of the target orbit, and demonstrates its success in controlling chaos in real-world physical systems through an experimental implementation.

(ii) **Time series analysis of chaotic systems:** this thesis utilizes the concept of HO synchronization to develop a systematic approach of extracting unstable periodic motions from a single time history of chaotic systems, called HO time series analysis. It argues that the proposed approach is superior to the classical methods of detecting unstable periodic orbit, as it does not require state space reconstruction, or any analytical knowledge about the dynamical system. It demonstrates that information obtained from the HO time series analysis can be used in various methods of controlling chaos including the HO feedback control.

(iii) **Analysis of time delay systems:** an interesting application of the HO synchronization is found in analysis of time delay systems. This thesis reveals that a class of HO synchronization serves as an effective and accurate transformation of a time delay system to a well-organized system of ordinary differential equations (ODE), called HO transformation. This thesis investigates the performance of the proposed transformation in evaluating stability properties of time delay systems through numerical demonstrations and analytical investigations. It utilizes the HO transformation to study the relation between DFC and HO feedback control of chaos.

1.2.5 Organization of the Thesis

This thesis is divided into five chapters. In addition to the introduction, it consists of the following chapters:

Chapter 2 provides a theoretical background on some of the core topics

in nonlinear dynamics and chaos. It provides a technical description of chaos, and introduces practical ways to improve the system's performance when chaos emerges.

Chapter 3 introduces the concept of HO synchronization, and addresses its applications in controlling chaos (HO feedback control), extracting unstable periodic orbits from chaotic time series (HO time series analysis), and analyzing time delay systems (HO transformation).

Chapter 4 investigates the success of the proposed methods described in Chapter 3 through numerical demonstrations and experiments. It addresses experimental realization of the HO feedback control in practical situations by controlling chaotic behaviour of a transistor-based electrical circuit [12]. The capabilities of the HO time series analysis in detecting periodic orbits is addressed by extracting UPOs from time series obtained from both numerical simulations and experiments. The success of the HO transformation in evaluating the stability properties of time delay systems is investigated numerically. The relation between EDFC and the HO feedback control is also discussed through the HO transformation by comparing the stability properties and the configuration of the stabilized orbits in the state space. Finally, stabilizing torsion free orbits of nonautonomous system using HO feedback control is addressed.

Chapter 5 answers the research question raised in section 1.2.3. It addresses the main contributions of this thesis, and points out the limitations of the current work. It also provides suggestions and recommendations for the improvement or further extensions of the present work.

Chapter 2

Background

2.1 Introduction

Controlling chaos is defined as the process of stabilizing an unstable periodic orbit embedded in the attractor of a chaotic system that according to certain operating criteria corresponds to a desired system's performance [5]. There are several components to this definition such as dynamical system, stability, attractor, and chaos, which will be addressed throughout this chapter.

This chapter starts with a formal definition of a dynamical system, and different classifications of it. Stability as an important property of the solution of a dynamical system is addressed next. The concepts of stability relevant to the context of this thesis, namely Lyapunov and Poincaré stability are explained. The attractor of a dissipative system as a subspace of the state space in which the steady state evolution takes place is then discussed. This chapter explains essential properties of attractors with emphasis on the properties of the system's evolution

in a chaotic attractor. The phenomenon called chaos is defined, and its advantages and disadvantages are pointed out. Finally, two strategies of suppressing the destructive effects and exploiting the inherently rich properties of chaos, namely controlling and synchronizing chaos are explained.

2.2 Definition of a Dynamical System

The notion of dynamical system can be describe by a set of its possible states (state space), and the evolution law that defines the change of the state in the course of time. Therefore, a dynamical system consists of three components: (*i*) time, (*ii*) state space, and (*iii*) the evolution law [13; pp. 1]. A formal definition of a dynamical system requires a further discussion about its main ingredients as discussed as follows:

Time: in dynamical systems, time is often considered as the independent variable. It is measured in terms of the events that change the state of the system. This quantity is identified by an element $t \in \mathbb{T}$, where $\mathbb{T}$ is the set of either real, or integer numbers. Accordingly, two types of dynamical systems can be distinguished: (*i*) systems with continuous time, which corresponds to $\mathbb{T} = \mathbb{R}$, and (*ii*) systems with discrete time, which corresponds to $\mathbb{T} = \mathbb{Z}$. The systems of the first type are described by differential equations, and called continuous-time dynamical systems, while those of the second type are described by algebraic equations (map), and called discrete-time dynamical systems. There also exists a third type of dynamical system known as hybrid systems that exhibit both continuous and discrete dynamical be-

haviour. This thesis deals with continuous-time dynamical systems mainly, although a particular type of discrete-time systems known as Poincaré map is also addressed.

State space: the *state space* of a dynamical system is a set $\mathbb{X}$ that includes all the possible states of the system. The *system's state* can be specified by an element $\mathbf{x} \in \mathbb{X}$. In fact, $\mathbb{X}$ is a space in which the system's state $\mathbf{x}$ evolves in the course of time t. The state corresponding to the initial time t_0 is called the initial state, and is denoted by $\mathbf{x}_0$. It is worth mentioning that the dimension of the state space $\mathbb{X}$ can be either finite, or infinite. This thesis deals with the finite-dimensional state space, although time delay systems, which are examples of infinite-dimensional systems, are also discussed. A finite-dimensional state space can be defined by $\mathbb{X} = \mathbb{R}^D$, where D is a positive integer representing the dimension of the state space. This implies that a finite dimensional state space can be represented by a set of D coordinates each of which corresponds to a state variable of the system. In such a space, the state of the system $\mathbf{x}$ can be described by a vector of dimension D.

Evolution law: the main component of a dynamical system is the evolution law that determines the state $\mathbf{x}$ of the system at any given time t. The most general way to specify the evolution is to assume that for a given $t \in \mathbb{T}$ a map φ^t is defined in the state space $\mathbb{X}$,

$$\varphi^t : \mathbb{X} \to \mathbb{X} \tag{2.1}$$

which transforms an initial state $\mathbf{x}_0$ into some state $\mathbf{x} \in \mathbb{X}$ at time t according

to

$$\mathbf{x} = \varphi^t \mathbf{x}_0 \tag{2.2}$$

The map φ^t is often called the *evolution operator* of dynamical system that satisfies the following property.

$$\varphi^{t_0} = \mathcal{I} \tag{2.3}$$

where $\mathcal{I}$ is the identity map on $\mathbb{X}$, such that $\mathcal{I}\mathbf{x} = \mathbf{x}$ for all $\mathbf{x} \in \mathbb{X}$. This property implies that the system does not change its state spontaneously. Changes in the system's state correspond to the events based on which the time is measured. In continuous-time systems, the family $\{\varphi^t\}_{t\in\mathbb{T}}$ of evolution operators is called the *flow* of the system [13; pp. 5].

Defining the components of a dynamical system enables giving a formal definition of it, as follows: a *dynamical system* is a triple $\{\mathbb{T}, \mathbb{X}, \varphi^t\}$, where $\mathbb{T}$ is the time set, $\mathbb{X}$ is the state space, and $\varphi^t : \mathbb{X} \to \mathbb{X}$ is the evolution operator [13; pp. 5].

2.2.1 Deterministic vs Stochastic Models

This thesis deals with ordinary differential equations that model the time evolution of real physical systems. Nature can be characterized reasonably by a deterministic behaviour even if, in opposition, several reasons to support the idea of random behaviour of nature can be provided [14]. Regardless of deterministic or stochastic nature of physical systems, an accurate mathematical model should involve some random parameters, or be formulated in terms of random equations. Two reasons to support this claim can be provided [15]: (i) a real physical system is not fully isolated. It interacts with its environment continuously. However, the

mathematical model cannot take into account all the interactions of the system and the environment. Consequently, random disturbances caused by these interactions need to be added to the mathematical model of the artificially isolated physical systems. (*ii*) The mathematical model cannot take into account all the variables involved in the evolution of the system. Consequently, some variables are inevitably missing from the mathematical description of the system. This deficiency suggests that the state variables of the mathematical model do not need to satisfy a deterministic evolution, but a stochastic one that includes some probabilistic terms to take into account the effects of the missing variables. On the other hand, deterministic models are significantly simpler that stochastic models. Although they are not as inclusive as stochastic models, they have proven their validity in modeling of a large number of physical systems. In many applications, deterministic models effectively describes the system's dynamics without being involved in a complicated stochastic modeling of the system. In fact, it is the dominant approach in many engineering applications. To this end, this thesis addresses the dynamical behavior of deterministic models. Notice that the evolution of deterministic models is fully determined by the initial conditions for the fixed values of the system's parameters.

2.2.2 Conservative vs Dissipative Systems

Dissipation is an important concept based on which dynamical systems can be classified. *Dissipation* in the flow of a system means that a set of final states occupies the region smaller in size than that occupied by the corresponding initial states. Based on this concept, a dynamical system can be either dissipative, or

conservative. A *conservative system* preserves the size of the volume in which the initial conditions are defined, while a *dissipative system* contracts the size of the volume in the state space. In other words, the evolution of a conservative system takes place in the full state space of the system, while a dissipative system evolves in a contracting subspace of the state space. This means that the trajectories of a dissipative system started from different initial conditions are finally attracted to a subspace of the state space with zero volume. This phenomenon is called attraction, and the final set to which the trajectories are attracted is called the attracting set. A special and important type of attracting sets is called an attractor, which is covered in detail in Sec. 2.4.

In this section a formal definition of a dynamical system is provided, and different classifications of it are presented. Among different classes of dynamical systems, this thesis mostly deals with finite-dimensional deterministic time-continuous dissipative systems, which indeed represent a wide range of real-word dynamical systems. More rigorously, such systems can be described by

$$\dot{\mathbf{x}} = \mathbf{f}(t, \mathbf{x}) \tag{2.4}$$

where $\mathbf{x} \in \mathbb{R}^D$ is the state vector, $t \in \mathbb{R}$ is the time, and $\mathbf{f}$ is often referred to as the vector field describing the system's dynamics. Throughout this thesis, $\dot{\bullet}$ denotes the derivative with respect to time. A dynamical system is said to be *autonomous*, if the associated vector field does not depend on time explicitly, otherwise, it is *nonautonomous*.

2.3 Concepts of Stability

A dominant subject in analysis of dynamical systems is the stability of the resulting motion. Over the years, concepts of stability have been advanced either by modifying old ideas, or by creating new concepts. This section addresses the stability of the solutions of finite-dimensional time-continuous systems under small perturbations of initial conditions. Among different concepts of stability, the stability in the sense of Lyapunov [16] and the stability in the sense of Poincaré [17] are discussed.

2.3.1 Lyapunov Stability

The solution $\mathbf{u}(t)$ of either an autonomous, or a nonautonomous system is said to be *Lyapunov stable* if, given a small number $\epsilon > 0$, there exists $\delta = \delta(\epsilon) > 0$ such that any other solution $\mathbf{v}(t)$ for which $\| \mathbf{u} - \mathbf{v} \| < \delta$ at initial time $t = t_0$ satisfies $\| \mathbf{u} - \mathbf{v} \| < \epsilon$ for all time $t > t_0$. In nonautonomous systems, δ is also a function of initial time t_0 [18; pp. 21]. Here, $\| \bullet \|$ denotes a norm defined in the state space, which does not need to be the usual Euclidean norm [19; pp. 97]. More rigorously, the solution $\mathbf{u}(t)$ is stable if [19; pp. 48]

$$\forall \epsilon > 0, \exists \delta > 0, \| \mathbf{u}(t_0) - \mathbf{v}(t_0) \| < \delta \qquad \Rightarrow \qquad \forall t > t_0, \| \mathbf{u}(t) - \mathbf{v}(t) \| < \epsilon \quad (2.5)$$

In other words, if $\mathbf{u}(t)$ is Lyapunov stable, any other solutions that start sufficiently close to it (in the δ neighborhood of $\mathbf{u}(t)$), will remain arbitrarily close to it (in the ϵ neighborhood of $\mathbf{u}(t)$) for all time $t > t_0$. The solution $\mathbf{u}(t)$ is said to be asymptotically stable, if it is Lyapunov stable, and $\lim_{t \to \infty} \| \mathbf{u}(t) - \mathbf{v}(t) \| = 0$.

The concept of stability in the sense of Lyapunov provides a strong basis to investigate the stability of equilibrium solutions of dynamical systems. However, the direct implementation of this concept can be very challenging. Establishing the $\epsilon - \delta$ requirement can be very difficult for nonlinear systems. In fact, for arbitrarily designated values of ϵ, a values for δ needs to be found such that the trajectories starting from the δ neighborhood of the equilibrium point never leaves the ϵ neighborhood of it. Therefore, this strong concept of stability needs to be supported by practically effective ways of investigating the stability of equilibrium solutions. Two practical ways of determining the stability of equilibrium solutions of dynamical systems are Lyapunov's linearization and Lyapunov's direct methods. If the linearization of a nonlinear system around an equilibrium solution exists, Lyapunov's linearization method infers the stability of the equilibrium solution of the nonlinear system from the stability of the equilibrium solution of the linearized system. Lyapunov's direct method has a different approach. It is based on a fundamental physical observation: a system eventually settles down to an equilibrium state, if the total energy of the system continuously decreases. Therefore, this method investigates the rate of change of a scalar energy-like function known as the Lyapunov function along the trajectory of the system to determine the stability of the equilibrium solution. A detailed description of the both methods is provided in [20; pp. 111-156].

2.3.2 Poincaré Stability

The notion of stability proposed by Lyapunov determines the stability by examining how close two trajectories started from different initial conditions are

at the same instant of time. This approach is typically used to study the stability of equilibrium solutions of dynamical systems. Employing this concept of stability to dynamic solutions of nonlinear systems is very restrictive. The key point in the description of this restriction is understanding the difference between the trajectories and the orbits of dynamical systems. A *trajectory* or an *integral curve* of a dynamical system is referred to as the graph of solution $\mathbf{x}(t, t_0, \mathbf{x}_0)$ over time, while an *orbit* $\Upsilon(\mathbf{x}_0)$ corresponds to a set of points in the state space that lie on the trajectory passing through $\mathbf{x}_0$ at an arbitrary time t'. In other words $\Upsilon(\mathbf{x}_0) = \Upsilon\big(\mathbf{x}(t', t_0, \mathbf{x}_0)\big)$ [21; pp. 2].

According to the concept of Lyapunov stability, periodic solutions of nonlinear systems are always unstable. The reason can be described based on the fact that the frequency of periodic oscillations of nonlinear systems depends on the amplitude, which in turn is determined by the initial conditions. Hence, periodic solutions started from slightly different initial conditions oscillate with two different frequencies. Consequently, they do not stay close to each other after a sufficiently large period of time. Even though, the two orbits stay close, the periodic solution is not stable in the sense of Lyapunov, as the integral curves do not stay close. To remedy this situation, Poincaré proposed the notion of *orbital* or *Poincaré stability* to study the stability of dynamic solutions of nonlinear systems. Suppose that the orbits of solutions $\mathbf{u}(t)$ and $\mathbf{v}(t)$ are denoted by $\Upsilon_{\mathbf{u}}$ and $\Upsilon_{\mathbf{v}}$, respectively. $\Upsilon_{\mathbf{u}}$ is said to be orbitally stable if, given a positive number $\epsilon > 0$, there exists $\delta = \delta(\epsilon)$ such that if $\| \mathbf{u}(t = t_0) - \mathbf{v}(t = t') \| < \delta$ for some $t' > t_0$, then there exist $t_1 > t_0$ and $t_2 > t_0$ for which $\| \mathbf{u}(t = t_1) - \mathbf{v}(t = t_2) \| < \epsilon$. Furthermore, $\Upsilon_{\mathbf{u}}$ is said to be asymptotically stable, if $\Upsilon_{\mathbf{v}}$ tends to $\Upsilon_{\mathbf{u}}$ as $t \to \infty$ [18; pp. 26]. In

other words, the notion of Poincaré stability examines how close the orbits are in the state space.

Similar to Lyapunov stability, the definition of Poincaré stability does not provide an explicit approach to determine the stability of periodic orbits. The stability of such orbits can be investigated through the linearization of nonlinear system around the periodic orbit. If such a linearization exists, the stability of the periodic orbit of the nonlinear system can be inferred from the stability of the equilibrium solution of the linearized system through Floquet theory [22]. This theory is one of the essential tools in evaluating the performance of many chaos control techniques. It deals with linear systems with periodic coefficient as defined by

$$\dot{\mathbf{x}} = \mathbf{J}(t)\mathbf{x} \tag{2.6}$$

where $\mathbf{J}(t)$ is a $D \times D$ matrix such that $\mathbf{J}(t) = \mathbf{J}(t+T)$. This equation can be though of as the linearized equation around a periodic orbit, which defines the deviation of the nonlinear system from the target orbit. In this situation, $\mathbf{J}(t)$ is the Jacobian matrix associated with the nonlinear system evaluated on the periodic orbit. Equation (2.6) has a fundamental matrix solution denoted by $\Phi(t)$, whose columns are linearly independent solutions of the linearized system. Floquet theory states that $\Phi(t+T)$ is also a fundamental matrix solution satisfying

$$\Phi(t+T) = \Phi(t)\Phi^{-1}(0)\Phi(T) \tag{2.7}$$

where $\Phi^{-1}(0)\Phi(T)$ is known as the *monodromy matrix*. For any complex matrix $\mathbf{B}$ satisfying $e^{\mathbf{B}T} = \Phi^{-1}(0)\Phi(T)$, there exists a complex matrix function $\mathbf{P}(t)$ such

that

$$\Phi(t) = \mathbf{P}(t)e^{\mathbf{B}t} \tag{2.8}$$

where $\mathbf{P}(t)$ is a periodic matrix with the minimum period T. The representation $\Phi(t) = \mathbf{P}(t)e^{\mathbf{B}t}$ is called a Floquet normal form for the fundamental matrix solution. The eigenvalues of $e^{\mathbf{B}T}$ is called *Floquet multipliers* of the system. A *Floquet exponent* is a complex number λ such that $e^{\lambda T}$ is a Foquet multiplier. The periodic orbit is stable, if the real part of the Floquet exponents are all negative. If an exponent with a positive real part is found, the orbit is unstable.

2.4 Attractors in Dissipative Systems

In a general setting, an *attracting set* is a subspace of the state space to which the system's trajectories initiated from different initial conditions may finally be attracted. An attracting set is called an *attractor*, if it satisfies some supplementary conditions, as described as follows [18; pp. 29-30]:

1. **Invariance:** an attractor $\mathbb{X}_a$ is an invariant set of the flow of the system $\{\varphi^t\}_{t\in T}$. In other words, if a trajectory starts from an initial condition inside an attractor, it never leaves the attractor. Formally, $\varphi^t\mathbb{X}_a \in \mathbb{X}_a$.

2. **Attractivity:** there exists a neighborhood $\mathbb{C}_{\mathbb{X}_a}$ of the attractor $\mathbb{X}_a$ such that the trajectories starting from initial conditions inside $\mathbb{C}_{\mathbb{X}_a}$ approaches $\mathbb{X}_a$ as $t \to \infty$. Formally, $\varphi^t\,\mathbb{C}_{\mathbb{X}_a} \subset \mathbb{C}_{\mathbb{X}_a}$ for $t > t_0$, and $\varphi^t\,\mathbb{C}_{\mathbb{X}_a} \to \mathbb{X}_a$ as $t \to \infty$. The largest subspace of such initial conditions is called *basin of attraction* or the *stability region.*

3. **Recurrence:** trajectories initiated from a state in an open set of $\mathbb{X}_a$ repeat-

edly come arbitrarily close to this initial state after sufficiently large values of time.

4. **Indecomposability:** an attractor cannot be split up into two nontrivial pieces.

Notice that all attracting sets possess Properties 1 and 2, but only certain type of attracting sets known as attractors possess Properties 3 and 4 as well. Unstable solutions can be a part of an attracting set. However, Property 3 excludes unstable and transient solutions from being attractors. Furthermore, attracting sets can be composed of more than one attractors, which violates Property 4.

In general, there are four types of attractors in dissipative systems. They are geometrical objects in the state space that exhibit the exclusive properties of attractors. The simplest one is a point attractor forming an isolated point in the state space. From the mathematical point of view, the corresponding state of the system on this attractor can be characterized by a fixed value. The asymptotically stable equilibrium solution of dynamical systems is an example of a point attractor. In contrast to the point attractor, the other types of attractors are dynamic solutions, as the corresponding state variable evolves in the course of time.

The second type of attractors is a periodic attractor. This type of attractor forms an isolated closed curve in the state space. The motion of the system along this curve can be characterized by a fixed frequency. An asymptotically stable limit cycle is an example of a periodic attractor.

The third type of attractors are quasiperiodic attractors. Such an attractor

is characterized by a set of incommensurate frequencies. The simplest form of this type of attractors is a two-period quasiperiodic attractor. It forms a surface of two-torus in the state space. The motion of the system on this surface can be defined by two incommensurate frequencies along the poloidal and toroidal directions of the torus. Since the ratio of the frequencies are irrational, the trajectory of the system never closes itself. Although the wave form of a quasiperiodic signal may look complex, calculating its spectrum reveals its simplicity.

The forth type of attracts in dissipative systems are known as chaotic attractors. In contrast to the point, periodic and quasiperiodic attractors, chaotic attractors do not form regular geometrical objects in the state space. From the mathematical point of view, the evolution of the system on chaotic attractors cannot be expressed by any known mathematical functions. This type of attractors exhibits interesting geometrical, as well as dynamical properties, which are explained in Sec. 5.2.

Figure 2.1 illustrates different types of attractor of a four dimensional system described by Eq. (2.9) for different values of the parameters γ and β [23].

$$\begin{bmatrix} \dot{x}_1 \\ \dot{x}_2 \\ \dot{x}_3 \\ \dot{x}_4 \end{bmatrix} = \begin{bmatrix} 35(x_2 - x_1) + 35x_2x_3 \\ 25x_1 - 5x_1x_3 + x_2 + x_4 \\ x_1x_2 - \gamma x_3 \\ -\beta x_2 \end{bmatrix} \tag{2.9}$$

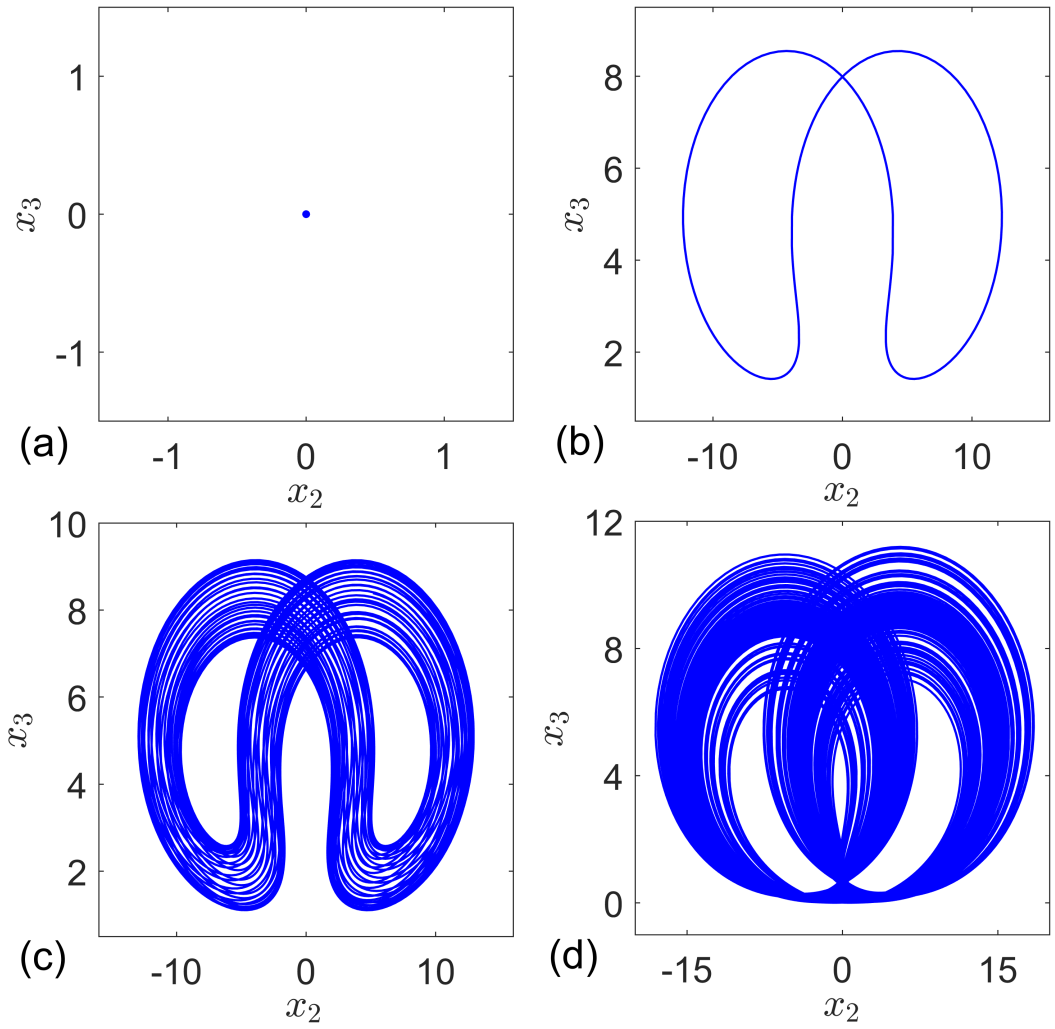

Figure 2.1: Two dimensional projection of attractors of the system described by Eq. (2.9). (a) Point attractor for $\gamma = 20$ and $\beta = 1000$. (b) Periodic attractor for $\gamma = 25$ and $\beta = 100$. (c) Quasiperiodic attractor for $\gamma = 22$ and $\beta = 100$. (d) Chaotic attractor for $\gamma = 35$ and $\beta = 100$.

2.5 Chaos and Chaotic Attractors

As a matter of fact, there is no universally accepted mathematical definition for chaos (a definition of chaos based on the transitivity is presented in Appendix D). This phenomenon cannot be expressed by any known mathematical function. However, it can be identified by its unique properties. This section describes exclusive properties of chaos, and explains the erratic nature of the system's evolution

on a chaotic attractor.

Typically, a chaotic motion is [24; pp. 21]

1. Irregular in time: it is an aperiodic response.

2. Unpredictable in the long-term: it is sensitive to initial conditions.

3. Complex, but ordered in the state space: it has a fractal structure.

The union of these properties are exclusive to chaotic dynamics, and may be used to define chaos. Based on these properties, *chaos* can be defined as a bounded aperiodic long-term behavior of a deterministic system that creates a complex, but well-organized structure in the state space, while exhibits sensitive dependence on initial conditions [25; pp. 323].

It is worth mentioning that the skeleton of chaotic attractors is made up of infinitely many unstable periodic orbits. As a result, in an arbitrarily small neighborhood of each point inside a chaotic attractor, an unstable periodic orbit can be found. A chaotic trajectory starting inside this neighborhood approaches the nearby unstable orbit along its stable manifold, shadows the orbit for *a priori* unknown period of time, and then jumps along its unstable manifold to a different orbit. This process is repeated irregularly such that the trajectory visits arbitrarily small neighborhood of every point on each periodic orbits during its temporal evolution on the attractor. This suggests a random-like evolution of a typical chaotic trajectory among the unstable orbits embedded in the chaotic attractor. Consequently, a chaotic evolution never repeats itself.

As a matter of fact, the number of periodic orbits inside a chaotic attractor increases with their length. In other words, the longer the orbit, the more orbits of the same length can be found in the attractor. For sufficiently long orbits, this number increases exponentially with the length [24; pp. 154]. This exponential rate of increase is characterized by a quantity called *topological entropy*. This is an important property of a chaotic attractor that describes the first aspect of chaos: chaotic attractors have a positive topological entropy reflecting the existence of infinite number of unstable periodic orbits in the chaotic attractor, and the absence of stable ones.

The size of chaotic attractors is finite, and the periodic orbits are dens on it. The existence of this densely packed set of unstable orbits leads to a phenomenon known as the sensitivity to initial conditions. As mentioned earlier, in any arbitrarily small neighborhood of each point on the attractor, an unstable periodic orbit exists. Thus, the distance between trajectories initiated close to this point increases exponentially according to the repelling eigenvalue of the nearby orbit. The rate at which the trajectories diverge locally in the state space can be used to define the local Lyapunov exponent associated with a specific point on the attractor. This exponent is a positive number reflecting the unstable nature of the periodic orbit. Such a positive number can be assigned to any point on the attractor, and therefore, it depends on the initial condition. However, the average of local Lyapunov exponents over the entire attractor is independent of initial condition. The *Lyapuonve exponent* associated with an attractor is a global quantity that measures the average rate at which a perturbation to a trajectory grows in time as it evolves on the attractor. Notice that this quantity can be defined in

different directions corresponding to different coordinate axes spanning the state space of the system. The average Lyapunov exponent characterizes the second aspect of chaos: *chaotic attractors* have at least one positive Lyapunov exponent reflecting the sensitivity of the system to initial conditions.

Trajectories on a typical chaotic attractor remain confined to a bounded region of the state space, yet they separate exponentially fast from their neighbors. These seemingly contradictory properties of chaos are the results of repeated folding and stretching of the space of initial states. Dissipation in the flow continuously contracts this space towards the attractor, while the sensitivity of the system to initial conditions continuously stretches it along the attractor. It is important to note that the stretching process does not take place in a fixed direction in the state space. Otherwise, it violates the boundedness of the system. Therefore, the flow of the system folds the surface of stretching, and bends it around to somewhere inside the attractor. This description of the system's dynamics on the attractor illustrates that chaotic systems have the minimum of three dimensions corresponding to contracting, stretching, and folding. Repeated process of stretching and folding creates an irregular geometrical object in the state space that has a fractal structure. In a general setting, *fractals* are geometrical shapes with fine structures at arbitrarily small scales [25; pp. 398]. They usually show some degree of self-similarity at each scale. In contracts to a regular geometrical object that has an integer dimension, the dimension of a fractal is a non-integer real number. The deviation of this dimension from an integer number reflects its complexity, and the existence of such a dimension indicates an ordered state space structure associated with the chaotic motion, which explains the third aspect of

chaos. A unified approach toward the fractal dimension of a given set of points is presented in [26].

An attractor with a fractal geometry is called a *strange attractor* [27]. Therefore, all chaotic attractors are strange. However, a strange attractor is not necessarily chaotic [28]. Such an attractor is called a strange nonchaotic attractor (SNA), and is generic in systems where there is a quasiperiodic forcing term [29]. Notice that the dynamics of a chaotic system determines the configuration of its attractor in the state space. However, the geometry of the attractor does not reveal all the information about the underlying dynamics. Yet, there is a strong connection between chaos theory and fractal geometry at very deep levels.

2.6 Controlling Chaos

The idea of controlling chaos is based on the fact that the skeleton of a chaotic attractor is made up of infinitely many unstable periodic orbits. This motivates developing a method of controlling chaos that transforms a chaotic behavior to a periodic one by stabilizing an unstable periodic orbit embedded in the chaotic attractor [5]. Since, the unstable orbit is a solution of the free system, the control can be achieved by applying vanishingly small perturbations. The existence of an infinite number of densely packed unstable periodic orbits offers a large number of candidates to stabilize. This property of chaotic systems allows different outputs from the same system by applying only small control perturbations

An interesting application of chaos control has been found in robotics [30].

Controlling sensor-motor systems in complex robots is a challenging problem, since the control signals need to be coordinated to a broad behavioral spectrum quickly. Conventional robotics solutions are mostly restricted to few behavioral patterns with limited autonomy. The idea of chaos control seems to be an effective way of controlling robots with complex and broad behavioral pattern. This idea has been utilized in an interesting application, in which an artificial hexapod was prototyped to create typical walking patterns emerging in insects [30]. In this system, 18 sensors drive 18 motors by means of a simple neural control to generate 11 complex behavioral patterns. A simple module of two neurons was used in the central pattern generator (CPG) unite. Without control, this simple neural circuit exhibits a chaotic behavior with a large number of unstable periodic patterns embedded in its attractor. Using a simple approach of delay feedback control, 11 distinct periodic patterns of the neural circuit were stabilized and successfully coordinated into 11 basic walking patterns of the robot.

In a different application, chaos control methods have been used to stabilize the behavior of mechanical linkages with clearance joints [31]. It is important to note that clearance is inevitable in mechanical joints due to manufacturing tolerances and wear between different parts of the system. Clearance is not only necessary to allow the relative motion between connected bodies, but also to permit the assemblage of the components. However, it leads to a dramatic degradation of the system's performance. The repeated process of impacts and rebounds between the connected bodies in a clearance joint generates impulsive forces and undesirable vibrations. The presence of clearance in mechanical joints has been known as the source of chaotic behavior in many mechanical linkages [32]. The classical

methods of reducing undesirable clearance effects have practical restrictions [33]. They make large alterations to the structure of the linkage, which can lead to the failure of the mechanism to accomplish the assigned task. The concept of controlling chaos provides an alternative approach to solve this problem. Using chaos control methods, an unstable periodic orbit embedded in the chaotic attractor of the system can be stabilized such that the contact between the connected bodies in the clearance joint is preserved for the whole cycle of the motion [31]. This approach minimizes the undesirable effects of the clearance and enables the system to accomplish the assigned task by applying only small perturbations.

These two examples along with a large number of theoretical and experimental studies [11] illustrate that the concept of controlling chaos has a wide range of applications in various fields of engineering and science. Several methods of controlling chaos have been proposed in the last few decades. A brief review on the major contributions is presented in this section.

2.6.1 OGY Method

The first attempt of controlling chaos is the seminal work of Ott, Grebogi, and Yorke known as OGY method [5]. This approach aims to stabilize an unstable periodic orbit embedded in the chaotic attractor by applying small time-dependent alterations to an accessible system's parameter. It is known as an effective method of control chaos in time-discrete dynamical systems. When applying this method to a time-continuous system, the associated Poincaré map needs to be considered.

Implementation of this approach requires relatively large amount of infor-

mation about the system's dynamics. The first step is to identify the location of the fixed point associated with the target orbit on a Poincaré section of the attractor. To extract the target fixed point on a Poincaré section different methods have been proposed in the literature [18; pp. 572-573]. The next step is to obtain a linear approximation of the system's dynamics around the desired fixed point, based on which the stability properties of the target fixed point, as well as a linear approximation of its stable and unstable manifolds can be evaluated. It is worth noting that the location of the target fixed point and the accompanying stable an unstable manifolds varies with respect to the system's parameters. Due to the recurrence behavior of the chaotic system, a typical trajectory repeatedly visits small neighborhoods of the target fixed point during its evolution on the attractor. It approaches the fixed point along its stable manifold and moves away along the unstable manifold. The underlying idea is to vary accessible system's parameters when the uncontrolled system approaches the fixed point. Once the system's state comes close to the fixed point, a wisely chosen perturbation is applied to accessible parameters in such a way that the subsequent state lands on the stable manifold of the original fixed point. The same process is repeated for each intersection of the trajectory and the Poincaré section. Consequently, the evolution approaches the fixed point as $t \to \infty$.

The OGY method is a special case of a general technique called pole placement in control theory. In this technique, the perturbations to the system's parameters are considered in the form of the state proportional feedback. The aim is to choose control gains so that all of the eigenvalues associated with the fixed point of the controlled system are inside the unite circle in the complex plane.

The choice of parameter perturbations in OGY method corresponds to a special case of control gains that transfers the unstable eigenvalues of the free system to the origin of the complex plane without changing the location of the stable ones [18; pp. 582].

One of the attractions of OGY method in practical situations is the independence of this approach from the mathematical model of the system. Using a single output of the system, the chaotic attractor can be reconstructed in a pseudo state space using embedding techniques such as the well-known method of delays [34]. The required information necessary to generate the control signal, then can be obtained using the reconstructed attractor. The first experimental application of OGY method was realized by Ditto, et al [35]. They stabilized a period-one orbit embedded in the chaotic oscillations of a magnetoelastic ribbon. Since then, OGY method has been successfully applied to a large number of physical systems [36] ranged from electrical circuits and chemical reactions to nonlinear optics and biological systems. In spite of the long list of successful implementation of OGY method in practical situation, this method suffers from critical limitations. It requires comparatively large amount of information about the system's dynamics to establish the control. Furthermore, the control rule is only valid in the linear region of the fixed point. This is a restrictive factor, since the time taken for the trajectory to come to the vicinity of the fixed point can be long leading to undesirably long chaotic transients. To shorten this time, one can exploit the sensitivity of the system to initial conditions and employ the so-called targeting scheme [37] to steer the trajectory to the vicinity of the fixed point, but this requires further information and more computational resources. In addition, the implementation

of OGY method to time-continuous systems is restricted to the level of noise in the experiment. Due to the discrete nature of the method, the inevitable noise can lead to occasional outbursts of the system to the regions far from the target orbit. Consequently, the control process needs to be halted, and resumed only when the system's state returns to the vicinity of the target fixed point, again.

It is worth mentioning that before OGY method a non-feedback perturbative technique to transfer a chaotic behavior to a regular periodic one was proposed by Lima and Pettini [38]. In this approach, an accessible system's parameter is perturbed by an oscillatory signal with a fixed frequency and variable amplitude. The implementation of this approach can be complicated by the fact that extensive preliminary learning task of the system's response is required. Since the amplitude of the perturbations is relatively large, the resulting motions do not belong to the set of periodic orbits embedded in the attractor of the free system. Such a method is called suppression of chaos by the same author, and cannot be classified as a method of controlling chaos.

2.6.2 OPF Method

To overcome the limitations of OGY methods different extensions and modifications of it have been proposed [39]. One of the major modifications of OGY method is known as the occasional propositional feedback (OPF) proposed by Hunt [40]. OPF is an effective method to find, stabilize and switch between different modes of periodic motion embedded in the attractor of chaotic systems. In contrast to the OGY method, OPF method does not require detailed knowledge about the system's dynamics nor the initial location of the target fixed point and

the accompanying stable and unstable manifolds to establish the control. The underlying idea of OPF is to sample the state of the system, when the trajectory hits a Poincaré section on which the sampled state exhibits a local minimum (or maximum). If the sampled state falls within a prescribed range or window, the system's parameter is perturbed proportionally to the deviation of the sampled variable from the center of the window. The value at the center may be the desired value (a one-dimensional projection of the target fixed point) of the sampled state.

In contrast to OGY method, the implementation of OPF is not restricted to low-period periodic orbits with small leading Lyapunov exponent. In addition, this method of control does not require digital processing of the system's output to generate the control signal. In fact, OPF can be implemented in analogue hardware, which makes it very appealing to control chaos in fast dynamical systems. The major drawback associated with OPF is the fact that the amplitude of the parameter perturbations is not always restricted to small values. Consequently, this method can alter the structure of the chaotic attractor, and lead to periodic orbits that do not belong to the attractor of the free system. In these situations, OPF turns to be an invasive method that suppresses chaos, but not control it.

2.6.3 PFC Method

The well-known OGY method and the extensions or modifications of it deal with a Poincaré section in the state space of time-continuous systems, and therefore, are discrete in nature. As a consequence, their practical implementation is very sensitive to the level of noise in the experimental data. The fluctuating noise may lead to occasional bursts of the system to regions far from the target

orbit. In such situations, the control process needs to be halted. It is resumed only when the system returns to the vicinity of the target orbit after a period of chaotic transient. For the same reason, OGY method is not able to stabilize periodic orbits whose leading Lyapunov exponent is large compared to the reciprocal of the time between the control perturbations (period of the target orbit). For high-period periodic orbits with large leading Lyapunov exponent, the next intersection of the system's trajectory and the Poincaré section takes place in a region far from the target orbit, where the control rule is not valid any more.

To overcome these limitations, Pyragas proposed a time-continuous method of controlling chaos known as the proportional feedback control of chaos (PFC) [7]. Similar to OGY, this method of control requires detailed information about the target orbit in the state space. In practical situations, such information can be obtained by reconstructing the system's attractor from a single output of the system using delay embedding techniques [34]. Then, one can search for a set of periodic orbits in the reconstructed attractor, among which an orbit can be selected based on the certain operating criteria. Once the orbit is extracted, PFC applies control perturbations based on the difference between the current state of the system and its state corresponding to the evolution of the system along the extracted orbit in the form of negative feedback. Equation (2.10) describes a dynamical system controlled by PFC, in which the control perturbations are applied as an external force.

$$\dot{\mathbf{x}} = \mathbf{f}(t, \mathbf{x}) + \mathbf{K}_P\big(\mathbf{x}_T(t) - \mathbf{x}(t)\big) \tag{2.10}$$

Here, $\mathbf{x}_T(t)$ represents the time evolution of the system along the desired periodic

orbit, and $\mathbf{K}_P$ is a $D \times D$ matrix that denotes the control gain. This control scheme suggests a noninvasive method, since the control perturbations practically vanishes once the target orbit attains its stability.

In contrast of OGY method that applies control perturbations once the system's state is sufficiently close to the target fixed point on a Poincaré section in the state space, PFC method can switch on the control perturbations at any moment, regardless of the location of the system's state. However, similar to OGY method, the performance of PFC highly depends on the quality of the extracted periodic motion, and the level of noise in the experiment. In cases where the periodic motion is not accurately extracted, this control method turns to an invasive method. In such situations, PFC transfers a chaotic behavior to a periodic one by applying relatively large control perturbations. Consequently, it changes the system's original dynamics. However, in contrast to OGY method, a noisy time series does not lead to unexpected bursts of the system to regions far from the desired orbit, but to smearing-out the target motion [7].

2.6.4 DFC Method

PFC method of controlling chaos requires an explicit expression of the time evolution of the system's state along the target periodic orbit to establish the control. To release this constraint, Pyragas proposed another time-continuous method known as delayed feedback control (DFC) [7]. It is one of the most powerful and widely used methods of controlling chaos in real world dynamical systems. This method continuously injects control perturbations whose intensity is proportional to the difference between the current state of the system and its state at one period

of the target orbit in the past. Thus, the intensity of the control perturbations practically vanishes once the desired orbit is stabilized. Equation (2.11) describes a dynamical system controlled by DFC, in which the control perturbations are applied as an external force.

$$\dot{\mathbf{x}} = \mathbf{f}(t, \mathbf{x}) + \mathbf{K}_D\big(\mathbf{x}(t - T) - \mathbf{x}(t)\big) \tag{2.11}$$

where T is the period of the target orbit, and $\mathbf{K}_D$ is a $D \times D$ control gain matrix. Equation (2.11) shows that DFC automatically meets the criteria required by the periodicity of the target motion, regardless of the dynamics of the chaotic system.

Different extensions and modifications of the original DFC have been proposed [11]. The extended delayed feedback control (EDFC) [41] presumably is the most important modification of DFC. This method incorporates infinitely many previous states of the system at integer multiples of the period of target orbit into the control loop. Equation (2.12) describes a dynamical system controlled by EDFC.

$$\dot{\mathbf{x}} = \mathbf{f}(t, \mathbf{x}) + \mathbf{K}_D\Big((1 - R)\sum_{m=1}^{\infty} R^{m-1}\mathbf{x}(t - mT) - \mathbf{x}(t)\Big) \tag{2.12}$$

where $0 \leq R < 1$ is the memory coefficient. Notice that EDFC transforms to DFC for $R = 0$. Periodic orbits with large period and high degree of instability may not be accessible by the original DFC. However, they can be stabilized through EDFC for suitable values of the parameter R. A more convenient form of EDFC can be obtained by introducing $\mathbf{z}(t) \equiv \sum_{m=1}^{\infty} R^m \mathbf{x}(t - mT)$ as follows

$$\dot{\mathbf{x}} = \mathbf{f}(t, \mathbf{x}) + \mathbf{K}_D\Big((1 - R)\mathbf{z}(t - T) - \mathbf{x}(t)\Big) \tag{2.13}$$

where, $\mathbf{z}(t) = \mathbf{x}(t) + R\mathbf{z}(t - T)$. Obviously, the presentation of EDFC according to Eq.(2.13) is more suitable for numerical simulations, as well as experimental

implementations. Adaptive versions of DFC with automatic adjustment of the delay time and the control gain have also been proposed [42], which significantly simplifies implementation of DFC specially to autonomous systems.

From a practical point of view, the experimental implementation of DFC is very convenient. This method of control provides a simple, robust, and efficient approach to stabilize unstable periodic orbits of chaotic systems. The controlled system can be treated as a black box, since DFC does not require any analytical knowledge about the target orbit beyond its period T. It is a reference-free method of controlling chaos that can be realized experimentally trough analogue hardware, even if only a single output of the system is available [43]. Therefore, it is appealing to experimentalist. Despite the great success of DFC in practical situations, evaluating the control performance and the stability properties of the target orbit is complicated. In fact, the dynamics of the systems controlled by DFC takes place in an infinite dimensional function space. Therefore, conventional tools and classical theories developed to study the behavior of finite dimensional systems are not available to analyze the controlled systems. Consequently, numerical and analytical investigation of the stabilizing properties of DFC requires special efforts and simplifications [44].

Odd Number Limitation

In spite of the fact that analytical treatment of the control performance of DFC is difficult, some valuable analytical results have been found in the last few decades. One of the most important founding concerns the stabilizing torsion free

periodic orbits of dynamical systems. *Torsion free orbits*, which are also known as *directly unstable orbits*, belong to a class of periodic orbits whose number of real Floquet multipliers greater that unity is odd. Stabilizing this class of periodic orbits using DFC was first addressed in [8, 9]. It was claimed that torsion free orbits of dynamical systems are never stabilized by DFC for any choice of control parameters. This limitation was then extended to a wider class of delayed feedback schemes including EDFC [45]. Since then, several extensions and modifications have been proposed to overcome this limitation. To obviate this drawback, the idea of half-period delayed feedback control has been proposed [46]. However, the implementation of this approach is limited to a class of dynamical systems with certain types of symmetry. Another practical approach is to incorporate an additional unstable degree of freedom into the feedback loop to artificially enlarge the set of real Floquet multipliers greater than unity to an even number [47]. However, the orbit controlled using this approach has a complex and sometimes small basin of attraction. Consequently, the linear stability analysis of the target orbit does not always guarantee a successful performance. To obviate this drawback, some ideas such as two-step algorithm needs to be adapted for a successful implementation [48]. The limitation was refuted later, for autonomous systems based on a counterexample of a torsion free orbit emanating from the normal form of the subcritical Hopf bifurcation [49]. The correct version of the theory explaining the analytical limitation of the time delayed feedback control was then published [50]. Base on the revised version, a systematic approach of designing the control gain to stabilize torsion free orbits of autonomous systems was proposed [51]. However, the limitation is still valid for nonautonomous systems.

2.6.5 NFFC Method

A notch filter is a linear device that filters out a particular frequency from an input signal. If the input to the notch filter is denoted by u_{in}, and the output by u_{out}, then the transfer function of a typical notch filter can described by

$$g_N(s) = \frac{u_{out}(s)}{u_{in}(s)} = K_N \frac{s^2 + {\omega_T}^2}{s^2 + 2\xi\omega_T s + {\omega_T}^2} \tag{2.14}$$

where ω_T is the notch or resonance frequency, ξ is the notch filter damping, K_N is the notch filter gain, and s is the Laplace variable. As the name suggests, a single dominant notch is observed in the plot of $|\frac{g_N(i\omega)}{K_N}|$, where $i = \sqrt[2]{-1}$, at the notch frequency $\omega = \omega_T$. As a result, away from the notch frequency, a signal passing through the filter remains essentially unaltered [52].

The concept of notch filter was first used by Ahlborn and Parlitz to suppress chaos in dynamical systems [10]. They suggests a notch filter that operates based in the Wien-bridge oscillator [53; pp. 853-862]. In their approach, the intensity of the control perturbations is proportional to the deviation of the output from the input of the filter. Equation (2.15) describes a dynamical system controlled by NFFC.

$$\dot{\mathbf{x}} = \mathbf{f}(t, \mathbf{x}) + K_N\Big(u_{in}(t) - u_{out}(t)\Big) \tag{2.15}$$

In this approach, the resonance frequency is set to be equal to the fundamental frequency of the target orbit in order to filter out this frequency from the power spectrum of the chaotic signal. It is worth mention that the transfer function of DFC given by $g_D(s) = K_D\Big(e^{(-2i\pi Ts)} - 1\Big)$ has notches all coincident with the spectral lines (harmonics) of the target orbit [10]. Therefore, the target orbit is

not affected by the feedback, while the chaotic dynamics is damped out due to the feedback. NFFC filters out only a particular frequency. Consequently, it is an invasive control method, even though the controlled orbit is close to the UPO embedded in the chaotic attractor. In spite of the fact that NFFC changes the shape and the location of the target orbit in the state space, it is particularly appealing from the experimental point of view. This control algorithm can be realized through a simple electrical circuit, and therefore, it is suitable to suppress chaos in fast dynamical systems.

2.7 Synchronizing Dynamical Systems

Synchronization in its most general interpretation means correlated or corresponding in-time behavior of two or more processes [54]. This phenomenon can be defined as the mutual time conformity that is characterized by the appearance of certain relations between some functionals of the processes. Based on the type of interactions between the systems components, three types of synchronization can be identified [54]:

1. Natural synchronization that refers to a synchronous behavior in disconnected systems, e.g. all precise clocks that are synchronized in the frequency domain.

2. Self-synchronization that refers to a synchronous motion in properly interconnected systems without interference of any artificially introduced external forces. A classic example of the self-synchronization is the synchronous motion between a pair of pendulum clocks hanging from a light beam. This

phenomenon was perhaps first reported by Huygens in 1673. He observed that both pendulums oscillates with the same frequency.

3. Controlled-synchronization refers to a synchronous motion when there exist external forces, or artificial interconnections. This kind of synchronization occurs in the most applications of the synchronization theory such as synchronization of robotic systems [55] and synchronized oscillators in communication systems [56].

This thesis deals with the controlled-synchronization mainly, and proposes an effective chaos control algorithm that operates based on the principles of this type of synchronization. Depending on the formulation of the controlled synchronization two different classes of synchronization can be distinguished [55; pp. 7]: (*i*) internal synchronization that corresponds to a synchronous motion resulting from mutual interactions between all processes in a multi-composed system, and (*ii*) external synchronization in which a process in a multi-composed system is considered independent from the dynamics of other processes. Therefore, the synchronous motion is mainly determined by the dynamics of the independent process. In this thesis both classes of controlled synchronization are addressed. The concept of internal synchronization is incorporated into an innovative control algorithm to stabilize unstable periodic orbits embedded in the attractor of chaotic systems, and concept of external synchronization is adapted to develop an effective method to extract unstable periodic motion from chaotic time series.

2.7.1 Chaotic Synchronization

Synchronization of chaos refers to a process wherein two (or many) chaotic systems, either identical, or different, adjust a given property of their motion through a proper coupling [57]. Identifying a synchronized state between chaotic systems is not a trivial process. At the first glance, it seems that chaotic systems defy synchronization. Even two identical chaotic systems, started from slightly different initial conditions, evolve in time in an unsynchronized manner, due to the sensitivity of the systems' response to initial conditions. However, this perception was refuted by Pecora, and Carroll more that three decades ago [58]. They identified a synchronous motion as the equality of the state variables in unidirectionally coupled identical chaotic systems. The concept of synchronization in the context of chaotic systems is not restricted to the equality of the systems' states that occurs in identical systems. In fact, many different types of synchronization namely complete or identical synchronization [58], phase synchronization [59], lag synchronization [60], and generalized synchronization [61] have been studied in the past.

Complete synchronization is the simplest form of synchronization. It normally takes place in properly coupled identical chaotic systems that leads to a perfect correlation of the chaotic trajectories. This means that the trajectories of coupled systems remain in step with each other in the course of time. Generalized synchronization extends the concept of complete synchronization to nonidentical coupled chaotic systems. This type of synchronization relates the state of one system to a given function of the state of the other systems. It transforms to complete

synchronization when the given function is defined by the equality of the systems' state at all time. Nonidentical systems may experience phase synchronization before reaching to the generalized synchronization. This stage is characterized by an intermediate regime in which the phase lock is achieved, while the amplitude remain almost uncorrelated. The lag synchronization is a stage between the phase synchronization and the generalized synchronization. It corresponds to the locking of the both phases and the amplitudes of the coupled systems, however with the presence of time lag. Imperfect phase [62], and intermittent lag synchronization [63] have also been observed in coupled chaotic systems. These types of synchronization refer to a synchronous motion interrupted by occasional bursts when the system's trajectory passes through certain regions in the attractor.

From a different perspective, all types of chaotic synchronization can be classified as controlled synchronization. The external synchronization is achieved when a unidirectional coupling exists between two subsystems. In this situation, one subsystem evolves freely, but drives the evolution of the other subsystem. In other words, one subsystem (response system) follows a proper function of the dynamics of the other subsystem (drive system). This configuration is also known as the master-slave configuration. A totally different configuration is achieved when a bidirectional coupling exists between the subsystems. This situation produces an internal synchronization that adjusts the rhythm of the both subsystems to a common synchronized behaviour.

This thesis investigates the synchronization of a chaotic system with a nonchaotic system defined by a system of harmonic oscillators. Both internal and

external synchronization is addressed in the context of the generalized synchronization.

2.8 Summary

Chapter 2 introduced deterministic time-continuous dissipative dynamical systems as the focus of this thesis. It provided background knowledge required to identify chaos and inherent properties of it in dissipative systems. The concept of controlling chaos was then introduced as an effective way to prevent chaos from deteriorating dynamical behavior of the system. In addition, a review on major contributions in the area of controlling chaos was provided, which allows identifying a set of desirable properties of an effective control technique. Finally, the concept of synchronization in chaotic systems was addressed, which serves as a basis to develop an innovative method of controlling chaos in the next chapter.

Chapter 3

Proposed Methodology

3.1 Introduction

This chapter introduces HO synchronization as a synchronization between a system of harmonic oscillators and a given dynamical system, and investigates its applications in the area of controlling chaos. Section 3.2 provides a mathematical description of HO synchronization, and investigates its performance in the context of periodic evolutions. Section 3.3 reveals that a bidirectionally coupled version of HO synchronization leads to an innovative method of controlling chaos, called HO feedback control. This section addresses the theoretical aspects of the proposed control method, and investigates its stabilizing properties using Floquet theory. Section 3.4 utilizes the same concept of synchronization in order to develop a novel method of detecting unstable periodic orbits from chaotic time series, called HO time series analysis. It reveals that the information obtained from the detected orbit significantly simplifies control parameter design of HO

feedback control. Section 3.5 addresses a different, but related application of HO synchronization. It develops a systematic transformation of a time delay system to a well-organized system of ordinary differential equations, called HO transformation. This section investigates the applications of the proposed transformation in evaluating the stability properties of equilibrium solutions and periodic orbits of time delay systems. HO transformation is then used to study the relation between EDFC and HO feedback control. Finally, stabilizing torsion free orbits using HO feedback control is discussed. Section 3.6 reveals that a truncated version of HO feedback control does not suffer from the so-called odd number limitation.

3.2 HO synchronization

HO synchronization is defined as a synchronization in a coupled system described by

$$\dot{\mathbf{x}} = \mathbf{f}(t, \mathbf{x}) \tag{3.1}$$

$$\dot{\mathbf{A}}_n = in\omega\mathbf{A}_n + \mathbf{K}_n\Big(\mathbf{x} - \sum_{m\in\mathbb{U}} \mathbf{A}_m\Big), \qquad n \in \mathbb{U} \tag{3.2}$$

where $i = \sqrt{-1}$ is the imaginary unit, ω is the frequency constant, $\mathbb{U} \subset \mathbb{Z}$ such that, if $n \in \mathbb{U}$, then $-n \in \mathbb{U}$, and $\mathbf{K}_n$ is a $D \times D$ coupling matrix such that $\mathbf{K}_n$ is the complex conjugate of $\mathbf{K}_{-n}$. Equations (3.1) and (3.2) define an external synchronization problem, in which the nonlinear system $\dot{\mathbf{x}} = \mathbf{f}(t, \mathbf{x})$ drives a system of harmonic oscillators $\dot{\mathbf{A}}_n = in\omega\mathbf{A}_n$ through the coupling $\mathbf{K}_n\Big(\mathbf{x} - \sum_{m\in\mathbb{U}} \mathbf{A}_m\Big)$. It is called HO synchronization, due to the central role of harmonic oscillators in its structure. This section investigates the evolution of the coupled system, when $\mathbf{x}$ is a periodic solution.

3.2.1 HO Manifold

This section derives an explicit expression defining the evolution of the coupled system on a synchronization manifold, when the drive system has a periodic solution. Suppose that $\mathbf{x}_T$ denotes a periodic solution of $\dot{\mathbf{x}} = \mathbf{f}(t, \mathbf{x})$, whose Fourier expansion can be described by

$$\mathbf{x}_T = \sum_{m=-\infty}^{\infty} \mathbf{x}_m e^{im\omega_T t} \tag{3.3}$$

where $\mathbf{x}_m$ is the complex Fourier coefficient, and $\omega_T = \frac{2\pi}{T}$ is the fundamental frequency of the periodic evolution. Equation (3.2) suggests that $\mathbf{A}_n$ may exhibit a periodic evolution with the same frequency, which can be described by

$$\mathbf{A}_{n\,T} = \sum_{m=-\infty}^{\infty} \mathbf{a}_{mn} e^{im\omega_T t} \tag{3.4}$$

Substituting Eqs. (3.3) and (3.4) into Eq. (3.2) and equating the coefficient of each harmonic on the both sides yields

$$\big(in\omega - im\omega_T\big)\mathbf{a}_{nm} + \mathbf{K}_n\Big(\mathbf{x}_m - \sum_{l\in\mathbb{U}} \mathbf{a}_{lm}\Big) = 0, \qquad n \in \mathbb{U}, m \in \mathbb{Z} \tag{3.5}$$

Equation (3.5) represents a linear system of algebraic equations leading to a unique solution for $\mathbf{a}_{nm}$, provided that

$$\det\left(\mathbf{I} + \sum_{n\in\mathbb{U}} \frac{\mathbf{K}_n}{im\omega_T - in\omega}\right) \neq 0, \qquad m \in \mathbb{V}^c \tag{3.6}$$

where $\mathbf{I}$ is the $D \times D$ identity matrix, $\mathbb{V} \subset \mathbb{Z}$ such that $\mathbb{V} = \{m \mid m\omega_T - n\omega = 0, n \in \mathbb{U}\}$, and $\mathbb{V}^c$ is the complement of $\mathbb{V}$ with respect to $\mathbb{Z}$. Solving Eq. (3.5) for $\mathbf{a}_{nm}$ yields an explicit expression for $\mathbf{A}_{n\,T}$ as follows:

$$\mathbf{A}_{n\,T} = \begin{cases} \mathbf{c}_n e^{in\omega_T t} + \displaystyle\sum_{m\in\mathbb{V}^c} \frac{\mathbf{K}_n}{im\omega_T - in\omega}\mathbf{c}_m e^{im\omega_T t}, & n = \frac{\omega_T}{\omega} m \,\forall\, m \in \mathbb{V} \\ \displaystyle\sum_{m\in\mathbb{V}^c} \frac{\mathbf{K}_n}{im\omega_T - in\omega}\mathbf{c}_m e^{im\omega_T t}, & n \neq \frac{\omega_T}{\omega} m \,\forall\, m \in \mathbb{V} \end{cases} \tag{3.7}$$

where the constants $\mathbf{c}_m$ are defined by the coordinates of the periodic solution $\mathbf{x}_T$, whose Fourier expansion is described by

$$\mathbf{x}_T = \sum_{m\in\mathbb{V}} \mathbf{c}_m e^{im\omega_T t} + \sum_{m\in\mathbb{V}^c} \Big(\mathbf{I} + \sum_{n\in\mathbb{U}} \frac{\mathbf{K}_n}{im\omega_T - in\omega}\Big)\mathbf{c}_m e^{im\omega_T t} \tag{3.8}$$

Equation (3.6) guarantees a unique correspondence between $\mathbf{c}_m$ and $\mathbf{x}_m$. Eliminating the constants $\mathbf{c}_m$ from Eqs. (3.7) and (3.8) yields an explicit expression of a synchronization manifold defined by $\mathcal{H}_\omega\big(\mathbf{x}, \mathbf{A}_n\big) = 0$, where

$$\mathcal{H}_\omega\big(\mathbf{x}, \mathbf{A}_n\big) = \sum_{n\in\mathbb{U}} \mathbf{A}_n - \mathbf{x} + \frac{1}{T}\sum_{m\in\mathbb{V}^c} \left(\mathbf{I} + \sum_{n\in\mathbb{U}} \frac{\mathbf{K}_n}{im\omega_T - in\omega}\right)^{-1} \int_0^T \mathbf{x}(t-z)e^{im\omega_T z}\,\mathrm{d}z \tag{3.9}$$

$\mathcal{M}_\mathcal{H} = \{(\mathbf{x}, \mathbf{A}_n) \mid \mathcal{H}_\omega\big(\mathbf{x}, \mathbf{A}_n\big) = 0\}$ is called HO manifold representing periodic evolutions of the coupled system. It is invariant under the flow of the coupled system, provided that the drive system has a periodic solution. Notice that similar to the lag synchronization, there is a delay coordinate in the manifold equation. In addition to the existence and the from of the HO manifold, its stability is an important property, which is addressed in section 3.3, where Eq. (3.9) is used to develop an effective method of controlling chaos called HO feedback control.

3.2.2 Truncated HO synchronization

The idea of truncated HO synchronization is based on selecting a suitable set $\mathbb{U}$ and a frequency constant ω in order to simplify the structure of HO manifold. To do so, $\mathbb{U}$ and ω are assigned such that the term

$$\mathcal{H}_0 = \frac{1}{T}\sum_{m\in\mathbb{V}^c} \left(\mathbf{I} + \sum_{n\in\mathbb{U}} \frac{\mathbf{K}_n}{im\omega_T - in\omega}\right)^{-1} \int_0^T \mathbf{x}(t-z)e^{im\omega_T z}\,\mathrm{d}z \tag{3.10}$$

has a negligible contribution on the configuration of the HO manifold. Substituting Eq. (3.3) into Eq. (3.10) reveals the building blocks of $\mathcal{H}_0$ as follows:

$$\mathcal{H}_0 = \sum_{m \in \mathbb{V}^c} \left(\mathbf{I} + \sum_{n \in \mathbb{U}} \frac{\mathbf{K}_n}{im\omega_{_T} - in\omega} \right)^{-1} \mathbf{x}_m e^{im\omega_{_T} t} \tag{3.11}$$

where $\mathbf{x}_m$ is the m^{th} term in the Fourier expansion of $\mathbf{x}_T$. Equation (3.11) is well defined through the condition of Eq. (3.6). The fact that $\mathbf{x}_m$ vanishes exponentially fast with respect to m [64], where $\mathbf{x}_T$ is a continuously differentiable function, suggests that the magnitude of $\mathcal{H}_0$ is controlled by the smallest positive integer in the set $\mathbb{V}^c$ denoted by k. This motivates the idea of selecting a suitable frequency constant ω and a number set $\mathbb{U}$ leading to a sufficinetly large k. It can be verified that $\mathbb{V} = \mathbb{U}$ when $\omega = \omega_{_T}$. In this situation, the contribution of $\mathcal{H}_0$ on the configuration of HO manifold is arbitrarily small, if the smallest positive integer missing from the set $\mathbb{U}$ is sufficiently large. Elimination $\mathcal{H}_0$ from the definition of HO manifold leads a simplified version Eq. (3.9) called truncated HO manifold defined by $\mathcal{H}^k_{\omega_{_T}}(\mathbf{x}, \mathbf{A}_n) = 0$, where

$$\mathcal{H}^k_{\omega_{_T}}(\mathbf{x}, \mathbf{A}_n) = \sum_{m \in \mathbb{U}} \mathbf{A}_m - \mathbf{x} \tag{3.12}$$

Here, k is the smallest positive integer missing from the set $\mathbb{U}$. The deviation of the truncated manifold from the original manifold vanishes, when $k \to \infty$. This thesis deals with truncated HO synchronization mainly, due to its simplicity in theoretical investigations and practical applications. The full version of HO synchronization is addressed to study the relation between EDFC and HO feedback control in section 3.5.2, and also to investigate stabilizing torsion free orbits of nonautonomous systems in section 3.6.

3.3 HO Feedback Control

This section investigates the performance of HO synchronization, when the drive system is chaotic. In this situation, $\mathcal{H}_\omega(\mathbf{x}, \mathbf{A}_n) = 0$ represents an unstable invariant manifold, as the drive system has infinitely many unstable periodic solutions. In fact, evolutions described by the unstable orbits of the chaotic system correspond to the evolution of the coupled system on the HO manifold. This section utilizes this fact to develop an innovative method of controlling chaos, called HO feedback control. The proposed method aims to control chaos by stabilizing HO manifold of the coupled system. To do so, a bidirectionally coupled version of HO synchronization, as described by Eqs. (3.13) and (3.14), is considered.

$$\dot{\mathbf{x}} = \mathbf{f}(t, \mathbf{x}) + \mathbf{K}_H \mathcal{H}_\omega(\mathbf{x}, \mathbf{A}_n) \tag{3.13}$$

$$\dot{\mathbf{A}}_n = in\omega \mathbf{A}_n + \mathbf{K}_n \Big(\mathbf{x} - \sum_{m \in \mathbb{U}} \mathbf{A}_m \Big) \tag{3.14}$$

where $\mathbf{K}_H$ is a $D \times D$ control gain matrix. The underlying idea of HO feedback control is based on the fact that $\mathcal{H}(\mathbf{x}, \mathbf{A}_n) = 0$ is still an invariant under the flow of the controlled system. Therefore, a successful performance of HO feedback control does not change the dynamics of the system, but stabilizes its periodic behaviour through the feedback $\mathbf{K}_H \mathcal{H}_\omega(\mathbf{x}, \mathbf{A}_n)$.

Notice that the contribution of the delay coordinate $\mathbf{x}(t-z)$ in the definition of HO manifold complicates the analysis of the controlled system. This section investigates the performance of a truncated version of HO feedback control that utilizes the concept of the truncated HO synchronization to simplify the structure of the controlled system.

3.3.1 Truncated HO Feedback Control

The system controlled by the truncated HO feedback control is described by

$$\dot{\mathbf{x}} = \mathbf{f}(t, \mathbf{x}) + \mathbf{K}_H \mathcal{H}^k_{\omega_T}(\mathbf{x}, \mathbf{A}_n) \tag{3.15}$$

$$\dot{\mathbf{A}}_n = in\omega_T \mathbf{A}_n + \mathbf{K}_n \Big(\mathbf{x} - \sum_{m \in \mathbb{U}} \mathbf{A}_m \Big) \tag{3.16}$$

where $\mathcal{H}^k_{\omega_T}(\mathbf{x}, \mathbf{A}_n)$ represents truncated HO manifold. Taking Eq. (3.8) into account reveals that the orbit of the controlled system and the orbit of the free system have identical k^{th} order Fourier expansion. This implies that the intensity of the control perturbations stays vanishingly small for sufficiently large k.

Boundedness of the Controlled System

An important property of the system (3.16) is the boundedness of its response, when x represents a periodic evolution. Casting Eq. (3.16) in the vector form of

$$\dot{\mathbf{A}} = \Psi \mathbf{A} + \mathbf{K}\mathbf{x} \tag{3.17}$$

where $\mathbf{A} = [\ldots, \mathbf{A}^\top_{-m}, \ldots, \mathbf{A}^\top_m, \ldots]^\top$ is the vector of harmonic oscillators, $\mathbf{K} = [\ldots, \mathbf{K}^\top_{-m}, \ldots, \mathbf{K}^\top_m, \ldots]^\top$ is the generalized coupling matrix, Ψ is the coefficient matrix of $\mathbf{A}$, and the superscript $\top$ denotes the transpose of a matrix, reveals that $\mathbf{A}$ represents abounded response for a periodic x, provided that Ψ is a stable matrix. The characteristic equation defining the eigenvalues of the the coefficient matrix Ψ can be described by

$$\det \Big(\mathbf{I} + \sum_{n \in \mathbb{U}} \frac{\mathbf{K}_n}{\lambda_\Psi - in\omega_T} \Big) = 0 \tag{3.18}$$

where λ_Ψ is the eigenvalue of Ψ. The coupling matrix $\mathbf{K}_n$ needs to be assigned such that $\mathrm{Re}(\lambda_\Psi) < 0$. This criterion guarantees not only a bounded response, but also the existence of HO manifold as described by Eq. (3.6). It is worth noting than in many practical applications, only a single state of the system is available. In these situations, $\mathbf{K}_n$ consists of a single nonzero diagonal element denoted by κ_n corresponding to the available state. If κ_n is chosen to be a real number, $\mathrm{Re}(\lambda_\Psi) < 0$ is satisfied, if $\kappa_0 > 0$, and the rest of the coupling strengths are of the same sign satisfying $\sum_{n\in\mathbb{U}} \kappa_n > 0$. This condition defines admissible values of the coupling strength independently from any aspect of the controlled system. It is important in practical applications, where no analytical knowledge about the dynamical system is available. Any set of coupling strength κ_n satisfying this condition guarantees a bounded response, while the stability of the target orbit can be achieved by adjusting the control gain K_H, experimentally. The details are provided in Appendix A.

Stability of the Controlled Orbit

The performance of the truncated HO feedback control can be investigated through the linear stability analysis of the controlled orbit. The linearized equations around the controlled orbit reads

$$\delta\dot{\mathbf{x}} = \mathbf{J}(t)\,\delta\mathbf{x} + \mathbf{K}_H\Big(\sum_{m\in\mathbb{U}} \delta\mathbf{A}_n - \delta\mathbf{x}\Big) \tag{3.19}$$

$$\delta\dot{\mathbf{A}}_n = in\omega\delta\mathbf{A}_n + \mathbf{K}_n\Big(\delta\mathbf{x} - \sum_{m\in\mathbb{U}} \delta\mathbf{A}_n\Big) \tag{3.20}$$

where $\mathbf{J}(t) = \mathbf{J}(t+T)$ is the Jacobian of the free system evaluated on the controlled orbit. Equations (3.19) and (3.20) represent a homogeneous system of linear equa-

tions with periodic coefficients, whose stability can be analyzed in the the context of Floquet theory. The fundamental matrix solution of the linearized system Φ can be defined by the well-organized matrix equation

$$\dot{\Phi}(t) = \begin{bmatrix} \mathbf{J}(t) - \mathbf{K}_H & \cdots & \mathbf{K}_H & \cdots & \mathbf{K}_H & \cdots \\ \vdots & \ddots & \vdots & & \vdots & \\ \mathbf{K}_{-m} & \cdots & -im\omega_T I - \mathbf{K}_{-m} & \cdots & -\mathbf{K}_{-m} & \cdots \\ \vdots & & \vdots & \ddots & \vdots & \\ \mathbf{K}_m & \cdots & -\mathbf{K}_m & \cdots & im\omega_T I - \mathbf{K}_m & \cdots \\ \vdots & & \vdots & & \vdots & \ddots \end{bmatrix} \Phi(t) \quad (3.21)$$

where $m \in \mathbb{U}$. The characteristic equation defining the stability properties of the controlled orbit is defined by

$$\det\left(\Phi(T) - e^{\lambda T} I'\right) = 0 \quad (3.22)$$

provided that $\Phi(t_0) = \mathbf{I}'$, where $\mathbf{I}'$ is the identity matrix of appropriate order defined by the cardinality of the set $\mathbb{U}$. Apparently, λ is a function of coupling matrices $\mathbf{K}_n$ and control gain $\mathbf{K}_H$. In order to achieve stability, the real part of the leading Floquet exponent has to change its sign from positive to negative for some values of the control parameters. The implementation of truncated HO feedback control is addressed in chapter 4 through numerical simulations and experimental realizations.

3.4 HO Time Series Analysis

Unstable periodic orbits embedded in chaotic attractors play fundamentally important role in understanding chaotic dynamics. Presence of such orbits

is not only an evidence of determinism, but also an important concept based on which several properties of chaotic attractors such Lyapunove exponents, fractal dimension and topological entropy can be defined [65]. Identifying unstable periodic orbits within chaotic attractors is important not only from a theoretical point of view, but also it is an essential step in many practical situations. A particularly important application is found in controlling chaotic systems, where *a priori* knowledge of the shape and the location of the periodic orbit is often required to establish the control [5]. As suggested by Eq. (3.11), knowing the frequency content of the target orbit significantly simplifies control parameter design of truncated HO feedback control by identifying the oscillators whose absence from the feedback loop has negligible effect on the configuration of HO manifold. Therefore, developing a simple and efficient method to identify unstable periodic motions embedded in a chaotic signal is important from both theoretical and practical points of view.

Detecting unstable orbits from experimental data has been addressed in several publications, and various methods have been proposed. Classical methods of extracting periodic orbits utilize the recurrence properties of a chaotic attractor in the full state space [66], or on a Poincaré section of the system [67, 68]. They follow the evolution of the trajectory in the state space, and record the moment when the trajectory returns to a small neighborhood of some recurrent point. The statistical analysis is then conducted to determine whether the recurrent point belongs to an unstable orbit, or improve the initial estimation of it. More recent publications propose a different approach. They suggests utilizing advanced techniques such as neural network [69], directed weighted complex network [70],

or Kalman filters [71] to estimate the vector field of the underlying dynamics, through which the periodic orbit can be detected. An important building block of the previously proposed method is reconstruction of the chaotic attractor from a time history of the system using state space embedding methods such as method of delays [34]. It is important to note that reconstructing the system's attractor in a pseudo state space is not a trivial task. Extracting the embedding parameters such as the embedding dimension and the value of the delay can be challenging, specially from noisy time series. Moreover, identifying a Poincaré section, or estimating the vector field of the underlying system can be complicated by the fact that no analytical knowledge of the system is available in many practical situations.

This section proposes a novel algorithm of detecting unstable periodic motions in experimental chaotic data, called HO time series analysis. In contrast to previously proposed methods that require state space reconstruction, or an estimation of the vector filed of the underlying dynamics, the proposed method does not require any information about the system beyond a recorded time history. HO time series analysis utilizes the fact that any chaotic trajectory visits arbitrary small neighborhood of unstable periodic orbits during its temporal evolution in the chaotic attractor. It employs the concept of HO synchronization considering a periodic orbit embedded in the chaotic attractor corresponds to the evolution of the coupled system on HO manifold. This implies that the magnitude of $\mathcal{H}_\omega(\mathbf{x}, \mathbf{A}_n)$ indicates the divination of the system from a periodic orbit. The target unstable orbit can be detected when $\mathcal{H}_\omega(\mathbf{x}, \mathbf{A}_n)$ is within a small threshold.

3.4.1 Implementation of HO Time Series Analysis

To implement the idea of HO time series analysis, the concept of truncated HO synchronization is utilized. The fact that higher frequency components of the unstable orbit have negligible contributions on the configuration of HO manifold suggests an accurate approximation to the synchronization manifold defined by $\mathcal{H}^k_{\omega_T}(A_n, y) = 0$ for sufficiently large k, where

$$\mathcal{H}^k_{\omega_T}(\mathbf{A}_n, y) = \sum_{m=-k}^{k} \mathbf{A}_m - y \tag{3.23}$$

$$\dot{\mathbf{A}}_n = in\omega\mathbf{A}_n + \kappa_n\Big(y - \sum_{m=-k}^{k} \mathbf{A}_m\Big) \tag{3.24}$$

Here, $y = y(t)$ is a recorded time history of the chaotic system, and κ_n is the coupling strength. To implement the idea of HO time series analysis the first step is to solve Eq. (3.24) for $\mathbf{A}_n$. To do so, the following vector form of Eq. (3.24) is addressed.

$$\dot{\mathbf{A}} = \Psi\mathbf{A} + \mathbf{K}y \tag{3.25}$$

Assuming a sufficiently small sampling period Δt, the Euler exponential integrator can be used to approximate A_n at each consecutive sampling time as follows:

$$\mathbf{A}(t_{m+1}) = e^{\Psi\Delta t}\mathbf{A}(t_m) + \Psi^{-1}\Big(e^{\Psi\Delta t} - I'\Big)\kappa y(t_m), \qquad m = 1, 2, \ldots, L \tag{3.26}$$

where L is the length of the recorded time history of the system. For a fixed sampling period, the constant quantities $e^{\Psi\Delta t}$ and $\Psi^{-1}(e^{\Psi\Delta t} - I')\kappa$ are evaluated once for the whole integration process. The next step is to detect unstable orbits by evaluating the deviation of the system from HO manifold. HO time series analysis suggests monitoring the root mean square value (RMS) of the quantity

$\mathcal{H}^k_{\omega_T}(y, A_n)$ over one period of the orbit as follows

$$R_{\omega_T}(t_m) = \sqrt{\frac{\sum_{i=0}^{N-1} \left(\mathcal{H}^k_{\omega_T}(A_n(t_m + i\Delta t), y(t_m + i\Delta t))\right)^2}{N}}, \quad m = 1, \ldots, L - N, \tag{3.27}$$

where N denotes the number of samples per period. The system starts evolving in a small neighborhood of an unstable orbit, whose size is controlled by a prescribed threshold ε, when $R_{\omega_T}(t_m) < \varepsilon$.

The proposed algorithm can be extended to cover the situations, in which the period of unstable orbits is not explicitly known. Suppose that identifying periodic orbits in the frequency range of $[\omega_{min}, \omega_{max}]$ is desirable. The prescribed range of frequency can be discretized according to

$$\omega_j = \omega_{min} + j\,\frac{\omega_{max} - \omega_{min}}{N_\omega}, \qquad j = 0, 1, \ldots, N_\omega \tag{3.28}$$

where N_ω is the resolution of the discretization. HO time series analysis suggests monitoring a weighted time average of the quantity $R_{\omega_j}(t_m)$ over the prescribed rage of frequency as described by

$$\bar{R}(\omega_j) = \frac{\sum_{l=1}^{L-N} w_l R_{\omega_j}(t_l)}{\sum_{l=1}^{L-N} w_l}, \qquad j = 0, 1, \ldots, N_\omega \tag{3.29}$$

where the weights w_l are assigned based on the fact that the values of $R_{\omega_j}(t_l)$ around a local minimum are significantly more important that the values of $R_{\omega_j}(t_l)$ in other regions, when it comes to detecting unstable orbits. This section suggests $w_l = \frac{1}{R_{\omega_j}(t_l)^\alpha}$, where $\alpha \geq 1$. To identify the period of an unstable orbit, HO time series analysis utilizes the fact that the values of $\bar{R}(\omega_j)$ decreases when ω_j approaches the fundamental frequency of the unstable orbit. Therefore, the fundamental

frequency of unstable orbits can be detected when the plot of $\bar{R}(\omega_j)$ with respect to ω_j exhibits local minima.

It is worth noting that the period of the target orbits is a critically important piece of information in many chaos control techniques such as EDFC, NFFC, OGY and HO feedback control. This section offers a straightforward algorithm to extract the period of unstable orbit through set of simple calculations. The effectiveness of the proposed approach is demonstrated in chapter 4 using time series obtained from numerical simulations as well as experiments.

It is worth mentioning that $\mathbf{A}_n = \mathbf{a}_n e^{in\omega t}$ is the predicted solution to Eq. (3.24), if the system evolves sufficiently close to HO manifold for one period of an unstable orbit. However, the actual value of $\mathbf{A}_n$ may differ slightly from the predicted value by the fact that the periodic orbits are unstable. Assuming N samples per period of the unstable orbit, an improved estimation of the Fourier coefficient $\mathbf{a}_n$ can be obtained by applying the root mean square regression as follows

$$\mathbf{a}_n = \frac{1}{N}\sum_{m=0}^{N-1} \mathbf{A}_n(t_m) e^{-in\omega t_m}. \tag{3.30}$$

This regression not only improves the accuracy of the result especially for noisy time series, but also allows extracting an explicit expression for the detected orbit in the form of Fourier expansion, which can be used to control chaos thorough PFC control algorithm.

3.5 HO Transformation

Stability analysis of time delay systems is complicated by the fact that the evolution of such systems takes place in an infinite dimensional function space. Consequently, the classical theories and the conventional tools developed to analyze finite dimensional systems are not available for time delay systems. To obviate this drawback, various methods of representing time delay systems with a finite dimensional approximation have been proposed. In semi-discretization method [72], the time is divided into smaller intervals over which the delayed term is considered as a constant value of the history function at the beginning of the interval, or as a linear combination of the history function at the beginning and end of the interval. This approach leads to a system of ODEs, whose solution can be calculated for each time interval. The solution of the ODEs then can be used to construct the state transition matrix whose eigenvalues decide the stability. In time finite element approach [73], the solution is assumed through a set of basis functions defined only over the designated finite element. Substituting the assumed solution in to the time delay system yields a map that relates the solution of the system in past to the current time. The stability of time delay system then can be evaluated using the stability of the associated map. In the finite difference method [74], a grid is generated spanning the current time and the maximum delay. The time derivatives at the grid points are approximated using the forward or central difference formulas leading to a large finite dimensional approximation to the original time delay system. In different approach, time delay systems are reformulated in the from of PDEs in which the time delay is treated

as a spatial coordinate. Discretization methods such as Galerkin method then can be used to approximate the PDEs through certain spatial integration by a system of ODEs [75]. This section proposes a novel transformation that replaces the delay coordinate through a well-organized system of couped harmonic oscillators called HO transformation. In contrast to the previously proposed method, HO transformation does not require interval discretization, or numerical integration. It is a general transformation in the sense that it is defined independently from the underlying dynamics of the delay system.

The idea of HO transformation is based on the fact that any function $\mathbf{x}(z)$ defined in the interval $z \in [t-\tau, t]$ can be presented through Fourier analysis in terms of infinite series of the form

$$x = \sum_{m=-\infty}^{\infty} \mathbf{A}_m e^{im\omega(z-t)}, \tag{3.31}$$

where $\mathbf{A}_m$ is defined by

$$\mathbf{A}_m = \frac{1}{\tau}\int_0^{\tau} \mathbf{x}(t-z)e^{im\omega_\tau z}\mathrm{d}z, \qquad \omega_\tau = \frac{2\pi}{\tau}. \tag{3.32}$$

It is worth noting that the infinite series described by Eq. (3.31) presents the periodic extension of $\mathbf{x}(z)$ for $z \notin [t-\tau, t]$. This periodic extension possibly has jump discontinuities at $z = t + m\tau$, where $m \in \mathbb{Z}$. It is important to note that Fourier expansion (3.31) converges to the average of two one-sided limits of the periodic extension of $\mathbf{x}(z)$ at such points. Therefore, evaluating this expansion at $z = t - \tau$ yields

$$\sum_{m=-\infty}^{\infty} \mathbf{A}_m = \frac{1}{2}\big(\mathbf{x}(t) + \mathbf{x}(t-\tau)\big). \tag{3.33}$$

Taking Eq. (3.33) into account, and noting that $\frac{\partial \mathbf{x}(t-z)}{\partial t} = -\frac{\partial \mathbf{x}(t-z)}{\partial z}$, differentiating

Eq. (3.32) with respect to t yields

$$\dot{\mathbf{A}}_n = in\omega_\tau \mathbf{A}_n + \frac{2}{\tau}\Big(\mathbf{x}(t) - \sum_{m=-\infty}^{\infty} \mathbf{A}_m\Big). \tag{3.34}$$

$$\mathbf{x}(t-\tau) = 2\sum_{m=-\infty}^{\infty} \mathbf{A}_m - \mathbf{x}(t). \tag{3.35}$$

HO transformation can be described through Eqs. (3.34) and (3.35). It offers a systematic replacement of delayed coordinate $\mathbf{x}(t-\tau)$ in time delay system through a well-organized system of coupled harmonic oscillators. One of the key features of this transformation is its generality in the sense that it is defined independent from the vector filed describing the dynamics of the system, which facilitates its application in a wide range of practical situations.

It is worth noting that the replacement of delayed coordinate through Eqs. (3.34) and (3.35) leads to a special case of HO synchronization, in which $\omega = \omega_\tau$, $\mathbb{U} = \mathbb{Z}$, and $\mathbf{K}_n = \frac{2}{\tau}\mathbf{I}$. This implies that HO synchronization describes a general synchronization scheme a subclass of which can be presented by time delay systems. However, in practice, only a truncated version of HO transformation with a finite number of coupled harmonic oscillators can be used. Therefore, the convergence rate of the solutions obtained by the truncated HO transformation to the solution of the original time delay system is an important issue to address.

3.5.1 Truncated HO Transformation

The truncated HO transformation replaces the delayed coordinate through the truncated version of Eqs. (3.34) and (3.35) according to

$$\dot{\mathbf{A}}_n = in\omega_\tau \mathbf{A}_n + \frac{2}{\tau}\Big(\mathbf{x}(t) - \sum_{m=-k}^{k} \mathbf{A}_m\Big), \tag{3.36}$$

$$\mathbf{x}(t-\tau) = 2\sum_{m=-k}^{k} \mathbf{A}_m - \mathbf{x}(t), \tag{3.37}$$

where k is the truncation limit. The truncated HO transformation is practically important, as it allows investigating the behavior of time delay system through the classical theories and conventional tools developed for finite dimensional system. Through the large area of analysis, which can be covered by the truncated HO transformation, this section investigates the success of evaluating the configuration of periodic orbits of time delay systems and their stability using truncated HO transformation.

Equations (3.36) and (3.37) suggest that the convergence rate of the truncated HO transformation is mainly determined by the from of the solution rather that the vector filed describing the time delay system. This section addresses the case, for which $\mathbf{x}(t)$ can be presented by

$$\mathbf{x}(t) = \mathbf{u}_{\mathbf{x}}(t)e^{\lambda t}. \tag{3.38}$$

where $\mathbf{u}_{\mathbf{x}}(t) = \mathbf{u}_{\mathbf{x}}(t+T)$ is a periodic function, and the exponent λ is a constant. It is worth noting that $\mathbf{x}(t)$ represents periodic evolutions of period T for $\lambda = 0$, and for $\lambda \neq 0$, represents the Floquet form solution to the variational equation defining the stability properties of the periodic solutions. Floquet theory suggests that $\mathbf{A}_n = \mathbf{u}_n(t)e^{\lambda t}$, where $\mathbf{u}_n(t) = \mathbf{u}_n(t+T)$ is also a periodic function of time. Expanding $\mathbf{u}_{\mathbf{x}}(t)$ and $\mathbf{u}_n(t)$ in the from of Fourier series, and replacing the results into the truncated HO transformation leads to explicit expressions for $\mathbf{x}$, and $\mathbf{A}_n$ as follows

$$\mathbf{x} = \sum_{m\in\mathbb{V}_\lambda} \mathbf{c}_m e^{(\lambda+im\omega_T)t} + \sum_{m\in\mathbb{V}_\lambda{}^c} \Big(1 + \sum_{n=-k}^{k} \frac{\frac{2}{\tau}}{(\lambda+im\omega_T) - in\omega_\tau}\Big)\mathbf{c}_m e^{(\lambda+im\omega_T)t}. \tag{3.39}$$

$$\mathbf{A}_n = \begin{cases} \mathbf{c}_n e^{(\lambda+im\omega_{_T})t} + \sum\limits_{m\in\mathbb{V}_\lambda{}^c} \dfrac{\frac{2}{\tau}}{(\lambda+im\omega_{_T})-in\omega_\tau}\mathbf{c}_m e^{(\lambda+im\omega_{_T})t}, & n=\frac{\omega_{_T}}{\omega}m,\ m\in\mathbb{V}_\lambda \\ \sum\limits_{m\in\mathbb{V}_\lambda{}^c} \dfrac{\frac{2}{\tau}}{(\lambda+im\omega_{_T})-in\omega_\tau}\mathbf{c}_m e^{(\lambda+im\omega_{_T})t}, & n\neq\frac{\omega_{_T}}{\omega}m,\ m\in\mathbb{V}_\lambda \end{cases}, \tag{3.40}$$

where, $\mathbb{V}_\lambda \subset \mathbb{Z}$ such that $\mathbb{V}_\lambda = \emptyset$ for $\lambda \neq 0$, and for $\lambda = 0$, $\mathbb{V}_\lambda = \{m \mid m\omega_{_T} + n\omega_\tau = 0, n \in \mathbb{Z}, -k \leq n \leq k\}$, and $\mathbf{c}_m$ are non-vanishing constants defined by the coordinates of the periodic eigenfunction $\mathbf{u}_\mathbf{x}(t)$. Incorporating Eqs. (3.39) and (3.40) into the transformation equation yields

$$\Big(e^{-2\mu_m} - 1\Big)\mathbf{c}_m = 0, \qquad m \in \mathbb{V}_\lambda, \tag{3.41}$$

$$\left(\Big(e^{-2\mu_m}+1\Big) + \Big(e^{-2\mu_m}-1\Big)\left(1+\sum_{n=-k}^{k}\frac{1}{\mu_m - in\pi}\right)\right)\mathbf{c}_m = 0, \qquad m \notin \mathbb{V}_\lambda, \tag{3.42}$$

where $\mu_m = \frac{\tau}{2}(\lambda + im\omega_{_T})$. The convergence rate of truncated HO transformation can be investigated by examining how fast the coefficient of $\mathbf{c}_m$ vanishes with respect to the truncation limit k. It is worth noting that Eq. (3.41) is automatically satisfied for $m \in \mathbb{V}_\lambda$. The vanishing rate of the coefficient of $\mathbf{c}_m$ in Eq. (3.42) is equivalent to convergence rate of the following approximation with respect to k:

$$\coth(\mu_m) \approx \sum_{n=-k}^{k}\frac{1}{\mu_m - in\pi}, \qquad m \notin \mathbb{V}_m. \tag{3.43}$$

Expression (3.43) turns to be a mathematical identity for $k \to \infty$ [76; pp. 74]. The convergence rate of the truncated approximation with respect to k can be investigated in the context of Padé approximation [77]. This approximation belongs to a class of rational approximation, that approximates a given function thorough the ratio of two power series. Under this technique, the approximant's Maclaurin expansion agrees to the Maclaurin expansion of the function it is approximating as far as possible. It is worth noting that the Padé approximation often gives

better approximation of the function than the truncated Maclaurin series. More importantly, it may still converge to the function in regions where the Maclaurin series does not converge [78; pp. 1-15]. It is worth noting that the right-hand side of Eq. (3.43) serves as a rational approximation to the function on the left-hand side. Expanding the both sides in the power series yields

$$-2\sum_{q=1}^{\infty}(-1)^q\ \frac{\zeta(2q)}{\pi^{2q}}\ \mu_m^{2q-1} \approx -2\sum_{q=1}^{\infty}(-1)^q\ \frac{\sum_{n=1}^{k}\frac{1}{n^{2q}}}{\pi^{2q}}\ \mu_m^{2q-1}, \tag{3.44}$$

where ζ is the Riemann zeta function. Comparing the both sides of Eq. (3.44) reveals that the vanishing rate of the truncation error is determined by the convergence rate of the following approximation:

$$\zeta(2q) \approx \sum_{n=1}^{k}\frac{1}{n^{2q}}. \tag{3.45}$$

Equation(3.45) is a mathematical identity defining the Riemann zeta function for $k \to \infty$. However, for finite values of k, the truncation error $E_k(q) = \zeta(2q) - \sum_{n=1}^{k}\frac{1}{n^{2q}}$ exhibits a logarithmic rate of decay. This is verified by the fact that

$$\lim_{k\to\infty}\frac{E_{k+1}(q)}{E_k(q)} = \lim_{k\to\infty}\left(1 - \frac{1}{\sum_{n=1}^{\infty}\left(\frac{k+1}{k+n}\right)^{2q}}\right) = 1, \tag{3.46}$$

$$\lim_{k\to\infty}\frac{E_{k+1}(q) - E_k(q)}{E_k(q) - E_{k-1}(q)} = \lim_{k\to\infty}\frac{k}{k+1} = 1, \tag{3.47}$$

which describes a logarithmic rate of convergence. It is important to distinguish between the problem of constructing the Padé approximation and the problem of convergence of the Padé approximation. Every power series of complex variable $\mathfrak{s}$ has a circle of convergence defined by $|\mathfrak{s}| = r_c$. If $|\mathfrak{s}| < r_c$, the series converges, and if $|\mathfrak{s}| > r_c$, it does not. If a given power series converges to a function for $|\mathfrak{s}| < r_c$, then the sequence of Padé approximants may converge for $\mathfrak{s} \in \mathbb{D}$ where

$\mathbb{D}$ is a domain larger that $|\mathfrak{s}| < r_c$ [78; pp. 3]. Note that the power series on the right side of Eq. (3.44) converge only for $|\mu_m| < \pi$. However, it still can be used to construct the Padé approximation that converges all over the complex plane except at discrete points corresponding to integer values on the imaginary axis [76; pp. 74].

To summarize, the periodic solutions of the transformed system and their stability converge logarithmically to those of the original time delay system. An improved convergence rate is found when $\tau = T$, for which the periodic solution of the transformed system exhibits an exponential rate of convergence to the periodic solutions of the original time delay system, as Eq. (3.41) is automatically satisfied for $\mathbb{V}_\lambda = \{m \mid m \in \mathbb{Z}, -k \leq m \leq k\}$.

3.5.2 Relation Between EDFC and HO Feedback Control

The relation between EDFC and a truncated version of HO feedback control has been addressed in single-output single-input systems using the transfer functions of the controllers [79] . This section utilizes HO transformation to investigates this relation in the context of HO synchronization. Consider a dynamical system controlled by EDFC, which can be described by [41]

$$\dot{\mathbf{x}} = \mathbf{f}(t, \mathbf{x}) + \mathbf{K}_D\Big((\mathbf{I} - \mathbf{R})\mathbf{z}(t - T) - \mathbf{x}(t)\Big), \tag{3.48}$$

$$\mathbf{z}(t) - \mathbf{x}(t) - \mathbf{R}\mathbf{z}(t - T) = 0. \tag{3.49}$$

where $\mathbf{R}$ is the memory coefficient, and $\mathbf{K}_D$ is the control gain. Applying HO transformation to Eqs. (3.48) and (3.49) yields

$$\dot{\mathbf{x}} = \mathbf{f}(t, \mathbf{x}) + 2(\mathbf{I} + \mathbf{R})^{-1}\mathbf{K}_D\Big(\sum_{m=-\infty}^{\infty} \mathbf{A}_m - \mathbf{x}\Big), \tag{3.50}$$

$$\dot{\mathbf{A}}_n = in\omega\mathbf{A}_n + \frac{2}{T}(\mathbf{I}-\mathbf{R})(\mathbf{I}+\mathbf{R})^{-1}\Big(\mathbf{x} - \sum_{m=-\infty}^{\infty}\mathbf{A}_m\Big), \tag{3.51}$$

where $\mathbf{A}_n$ is scaled by the factor $(\mathbf{I}-\mathbf{R})$. Analyzing Eqs. (3.50) and (3.51) in the context of HO synchronization reveals that EDFC is a special case of HO feedback control for which

$$\mathbb{U} = \mathbb{Z}, \quad \omega = \omega_{_T}, \quad \mathbf{K}_{_H} = 2(\mathbf{I}+\mathbf{R})^{-1}\mathbf{K}_{_D}, \quad \mathbf{K}_n = \frac{2}{T}(\mathbf{I}-\mathbf{R})(\mathbf{I}+\mathbf{R})^{-1}. \tag{3.52}$$

The convergence properties of HO transformation allows investigating the performance of EDFC using the truncated transformation. The fact that EDFC controlled systems belong to a class of time delay systems in which $\tau = T$ reveals that periodic solutions of the transformed system and their stability properties exhibit exponential and logarithmic rate of convergence to those of the original time delay system, respectively. This suggests that periodic orbits of EDFC controlled system and their stability can effectively be evaluated thorough the truncated HO feedback control defined by parameters

$$\mathbb{U} = \{m \mid m \in \mathbb{Z}, -k \le m \le k\}, \quad \mathbf{K}_{_H} = 2(\mathbf{I}+\mathbf{R})^{-1}\mathbf{K}_{_D}, \quad \mathbf{K}_n = \frac{2}{T}(\mathbf{I}-\mathbf{R})(\mathbf{I}+\mathbf{R})^{-1}, \tag{3.53}$$

Equation (3.53) also extends the admissible value of the memory coefficient $\mathbf{R}$, which was originally defined to be a scalar whose absolute value is less that unity, to a matrix whose eigenvalues lie inside a unit circle centered at the origin of the complex plane. This comes from the fact that HO control requires $\mathbf{K}_n = \frac{2}{T}(\mathbf{I}-\mathbf{R})(\mathbf{I}+\mathbf{R})^{-1}$ to be a stable matrix. Spectral decomposition of $\mathbf{R}$ allows defining the eigenvalues of $\mathbf{K}_n$ as follows:

$$\lambda_{\mathbf{K}} = \frac{2}{T}\frac{1-\lambda_{\mathbf{R}}}{1+\lambda_{\mathbf{R}}}, \tag{3.54}$$

where $\lambda_{\mathbf{R}}$ is the eigenvalue of $\mathbf{R}$. According to Eq. (3.54), $Re(\lambda_{\mathbf{K}}) < 0$, if and only if $\mid \lambda_{\mathbf{R}} \mid < 1$, which defines the region inside the unit circle centered at the origin of the complex plane.

Filtering Properties of EDFC, NFFC, and HO Feedback Control

The filtering properties of truncated HO feedback control, EDFC, and NFFC are addressed in this section using the transfer functions of the controllers. For a single-input single-output systems, the transfer functions of truncated HO feedback control, EDFC, and NFFC can be defined by Eqs. (3.55), (3.56), and (3.57), respectively.

$$G_H(s) = -K_H\Big(1 + \sum_{m\in\mathbb{U}} \frac{\kappa_m}{s - im\omega_{_T}}\Big)^{-1}, \tag{3.55}$$

$$G_D(s) = -K_D \frac{1 - e^{-sT}}{1 - Re^{-sT}}, \tag{3.56}$$

$$G_N(s) = K_N \frac{s^2 + \omega_{_T}{}^2}{s^2 + \frac{\omega_T}{Q}s + \omega_{_T}{}^2}. \tag{3.57}$$

Figure 3.1 plots $|\frac{G_N(i\frac{\Omega}{\omega_T})}{K_N}|$, $|\frac{G_H(i\frac{\Omega}{\omega_T})}{K_H}|$, and $|\frac{G_E(i\frac{\Omega}{\omega_T})}{K_D}|$, with respect to the dimensionless frequency $\frac{\Omega}{\omega_T}$. As illustrated in the Fig. 3.1(a), the plot of $|\frac{G_N(i\frac{\Omega}{\omega_T})}{K_N}|$ has only one notch that drops to zero at the $\Omega = \omega_{_T}$. This implies that NFFC is only able to filter out the fundamental frequency of the target orbit from the signal. Figure 3.1(b) plots $|\frac{G_H(i\frac{\Omega}{\omega_T})}{K_H}|$ that corresponds to truncated HO feedback control. It illustrates a number of notches equal to the truncation limit $k = 20$ that drop to zero at integer multiples of the fundamental frequency of the target orbit, while higher harmonics are corrupted in the feedback loop. Figure 3.2(c) plots $|\frac{G_H(i\frac{\Omega}{\omega_T})}{K_H}|$ for the same parameters, but updated $\mathbb{U} = \{m \mid m \in \mathbb{Z}, -20 \leq m \leq 20, m \neq$

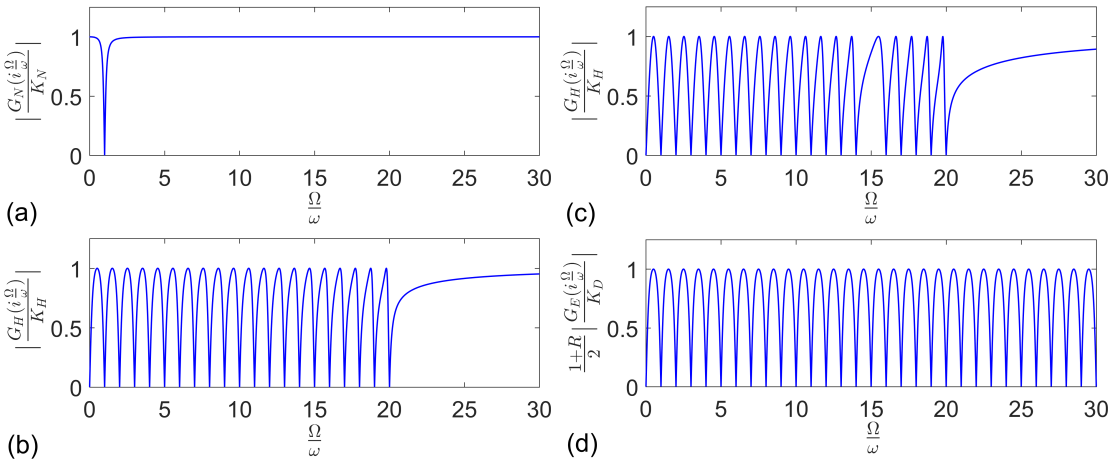

Figure 3.1: Magnitude of the transfer functions: (a) NFFC for $Q = 4$. (b) Truncated HO feedback control for $\kappa_n = 0.2$ and $\mathbb{U} = \{m \mid m \in \mathbb{Z}, -20 \leq m \leq 20, \}$. (c) Truncated HO feedback control for $\kappa_n = 0.2$ and $\mathbb{U} = \{m \mid m \in \mathbb{Z}, -20 \leq m \leq 20, m \neq 15, m \neq -15\}$. (d) EDFC for $R = 0.25$.

$15, m \neq -15\}$. It illustrate the flexibility of truncated HO feedback control in selective elimination of a frequency from the feedback loop without affecting its filtering properties at other frequencies. In contrasts to truncated HO control that only filters out a finite number of frequencies defined by the set $\mathbb{U}$, the plot of $|\frac{G_E(i\frac{\Omega}{\omega_T})}{K_D}|$ suggests that EDFC is capable of filtering out all the multiple integers of the fundamental frequency from the signal, as it corresponds to $\mathbb{U} = \mathbb{Z}$.

Figure 3.1 suggests that all three types of controller can be classified as filters, but with different filtering properties. EDEC filters out an infinite number of harmonics, and therefore, has the best filtering properties. It seems that the superior filtering property of EDFC is a relative merit of this version over the truncated versions of HO feedback control. However, section 3.6 reveal that the frequency content of the feedback loop of EDFC is the main reason why this control technique suffers from the so-called odd number limitation, when dealing with torsion free orbits of nonautonomous systems. On the other hand, the absence

of high frequency oscillators from the feedback loop of truncated HO feedback control does not affect the coordinates of the periodic orbit in the state space, but enables stabilizing torsion free orbits of nonautonomous systems.

3.6 Stabilizing Torsion Free Orbits

This section investigates the performance of HO feedback control in stabilizing torsion free orbits using linear stability analysis of the controlled system. Consider the variational equation defining the deviation of the controlled system from the target period orbit, which can be described by

$$\delta\dot{\mathbf{x}} = \mathbf{J}(t)\delta\mathbf{x} + K_H\mathcal{H}_\omega(\delta\mathbf{x}, \delta\mathbf{A}_n) \tag{3.58}$$

$$\delta\dot{\mathbf{A}}_n = in\omega\delta\mathbf{A}_n + K_n\Big(\delta\mathbf{x} - \sum_{m\in\mathbb{U}}\delta\mathbf{A}_m\Big) \tag{3.59}$$

The Floquet form solution of the variational equation can be described by $\delta\mathbf{x} = \mathbf{u}_\mathbf{x}(t)e^{\lambda t}$, and $\delta\mathbf{A}_n = \mathbf{u}_n(t)e^{\lambda t}$. This section investigates the condition under which $\lambda = 0$ is an eigenvalue of the coupled system. To reveal the significance of analyzing this case, consider a unidirectional coupling between the dynamical system and the system of harmonic oscillators in which $\mathbf{K}_H = 0$. In this situation, two separate sets of Floquet exponents can be distinguished. The first set of exponents is associated with the periodic orbit of the free system λ_0, and the second set of exponents is defined by $\lambda = \lambda_\Psi$, where λ_Ψ is the eigenvalue of the coefficient matrix Ψ. A successful control requires $Re(\lambda_\Psi) < 0$. This implies that the stability of orbits with odd number of positive exponents in λ_0 requires at least one exponent changes the sign of its real part from positive to negative along the real axis as $\mathbf{K}_H$ increases, since the complex eigenvalues appear in conjugate pairs. Therefore,

analyzing Eq. (3.58) and (3.59) for $\lambda = 0$ is critically important as it describes the stability requirement of torsion free periodic orbits.

For $\lambda = 0$, the variational equation can be written as

$$\dot{\mathbf{u}}_{\mathbf{x}} = \mathbf{J}(t)\mathbf{u}_{\mathbf{x}} + K_H \mathcal{H}_\omega(\mathbf{u}_{\mathbf{x}}, \mathbf{u}_n) \tag{3.60}$$

$$\dot{\mathbf{u}}_n = in\omega\mathbf{u}_n + K_n\Big(\mathbf{u}_x - \sum_{m\in\mathbb{U}} \delta\mathbf{u}_m\Big) \tag{3.61}$$

The fact that $\mathbf{u}_{\mathbf{x}}(t)$ and $\mathbf{u}_n(t)$ are periodic function with period T implies that their evolution always take place on the manifold defined by $\mathcal{H}_\omega(\mathbf{u}_{\mathbf{x}}, \mathbf{u}_n) = 0$. This cancels out the feedback term form Eq. (3.60), and leaves

$$\dot{\mathbf{u}}_{\mathbf{x}} = \mathbf{J}(t)\mathbf{u}_{\mathbf{x}} \tag{3.62}$$

For autonomous systems, there always exists an exponent $\lambda = 0$ corresponding to an eigenfunction satisfying Eq. (3.62). This implies that $\lambda = 0$ can be a solution to the eigenvalue problem with algebraic multiplicity two. This is the situation based on which the odd number limitation was refuted for autonomous systems [50]. In contrast to autonomous systems for which one Floquet exponent always exists at the origin of the complex plane, for nonautonomous systems such a condition is not satisfied. Consequently, $\lambda = 0$ leads to the trivial solution $\mathbf{u}_{\mathbf{x}} = 0$ of the eigenvalue problem. In other words, torsion free orbits of nonautonomous systems cannot be stabilized by the full version of HO feedback control for any choice of control gains. This extends the so-called odd number limitation of the time delayed feedback scheme when dealing with nonautonomous systems to HO feedback control.

A similar analysis reveals that truncated HO feedback control does not suffer from this limitation. This control method incorporates a simplified version

of HO manifold as described by Eq. (3.12) into the feedback loop leading to a non-vanishing control perturbations $\mathbf{K}_H\big(\mathcal{H}^k_{\omega_T} - \mathcal{H}_\omega\big)$ for $\lambda = 0$. In this situation, the variational system can be be described by the following single equation

$$\dot{\mathbf{u}}_\mathbf{x} = \mathbf{J}(t)\mathbf{u}_\mathbf{x} + \frac{\mathbf{K}_H}{T}\sum_{m\in\mathbb{U}^c}\left(\mathbf{I} + \frac{1}{i\omega_T}\sum_{n\in\mathbb{U}}\frac{\mathbf{K}_n}{m-n}\right)^{-1}\int_0^T \mathbf{u}_\mathbf{x}(t-z)e^{im\omega_T z}\,\mathrm{d}z \qquad (3.63)$$

The second term on the right-hand side of Eq. (3.63) represents the effect the truncated term $\mathcal{H}_0$ on the control perturbations. Although $\mathcal{H}_0$ has a negligible contribution to the configuration of the periodic orbit, it can have a significant effect on its stability properties. $\lambda = 0$ is a solution to the eigenvalue problem, if there exist $\mathbf{K}_H$ and $\mathbf{K}_n$ leading to a non-trivial solution $\mathbf{u}_\mathbf{x}(t)$ satisfying Eq. (3.63). Further analytical treatment of this equation can be complicated due to the existence of the delay coordinate. An alternative approach is to find $\mathbf{K}_H$ and $\mathbf{K}_n$ directly from monodromy matrix associated with the matrix equations (3.21). In this approach, $\mathbf{K}_H$ and $\mathbf{K}_n$ need to be determined such that

$$\det\Big(\Phi(\mathbf{K}_H, \mathbf{K}_n, T)\Big) = 0, \qquad (3.64)$$

Equation (3.64) can be treated numerically to find a suitable set of control parameters. A successful implementation of this approach is provided in chapter 4, where torsion free orbits of a chaotic Duffing oscillators are stabilized using truncated HO feedback control.

3.7 Summary

This chapter introduced the concept of HO synchronization, and addressed its applications in the area of controlling chaos. It proposed a reference-free method of controlling chaos through the bidirectionally coupled version of HO

synchronization. The proposed method is called HO feedback control, which requires only the period of the target orbit to establish the control. The main draw back associated with HO feedback control is its complex structure, which complicates its theoretical investigations and practical implantations. To overcome this limitation, the truncated version of HO feedback control was introduced. This modification of HO feedback control benefits from the fact that high frequency oscillators have negligible contributions to the control signal. It simplifies the structure of the controlled system, and facilitates its application in practical situations.

HO time series analysis was introduced next, which can serve as a complement to HO feedback control. It provides a systematically straightforward approach of detecting unstable periodic orbits in chaotic time series that does not require any information about the underlying dynamics beyond a recorded time history of the system. The information obtained from the detected orbit significantly simplifies control parameter design of HO feedback control, or can be used to control chaos, directly, through PFC method.

HO transformation was introduced, next. This transformation simplifies analysis of time delay systems by replacing the delay coordinate with a system of couped harmonic oscillator. The applications of HO transformation in evaluating periodic solutions of time delay system and their stability properties through the truncated version of the transformation was addressed. This transformation allowed investigating the relation between EDFC and HO feedback control in the context of HO synchronization.

Finally, Stabilizing torsion free orbits using HO feedback control was discussed. The linear stability analysis of the target orbits reveals the limitation of the full version of HO feedback control in stabilizing torsion free orbits of nonautonomous system. On the other hand, truncated HO feedback control overcomes this limitation by excluding high frequency oscillator from the feedback loop. Although, high frequency oscillators have negligible contributions on the configuration of the target orbit, they have significant effects in their stability properties. It is important to note that eliminating a frequency from the feedback loop is not restricted to high frequency oscillators. In situations where the frequency content of the unstable orbit is available, excluding lower frequency oscillations with negligible or vanishing amplitudes not only simplifies designing the control parameters, but also improves the performance of the controller. This is where HO time series analysis can be utilized to simplifies the control parameter design of HO feedback control.

Chapter 4

Results and Discussions

4.1 Introduction

This chapter demonstrates the success of the proposed methods of Chapter 3 in controlling chaotic systems through numerical simulations and experimental implementations. Section 4.2 addresses experimental realization of HO feedback control. It presents a successful implementation of the proposed method by controlling chaotic behavior of a transistor-based electrical circuit. Section 4.3 demonstrates the capabilities of HO time series analysis in extracting periodic motions from chaotic time series of autonomous and nonautonomous systems. It investigates the effect of noise on the quality of the detected motion, and discusses its application in controlling chaos through a simple proportional feedback controller. Section 4.4 investigates stabilizing torsion free orbits of nonautonomous systems using truncated HO feedback control. It demonstrates that the information obtained from HO time series analysis can significantly simplify control parameter

design of HO feedback control when dealing with torsion free orbits. Section 4.5 addresses the success of HO transformation in evaluating stability properties of equilibrium solutions and periodic orbits of time delay systems. It also discusses the relation between EDFC and HO feedback control in the context of HO transformation by comparing the configuration and the stability properties of orbits controlled by EDFC with those of orbits controlled by HO feedback control.

4.2 HO Feedback Control

This section addresses the implementation of HO feedback control in experimental situations. The truncated version of this controller can easily be applied to real word physical systems based on simple calculations on digital computers. Consider the control system, which can be described by Eqs. (3.15) and (3.16). Suppose that a single output of the system $y(t)$ is available for measurement and external adjustment. For sufficiently small sampling period Δt, Eq. (3.26) allows approximating the vector of harmonic oscillators $\mathbf{A}$ at each consecutive sampling time as follows:

$$\mathbf{A}(t_{m+1}) = e^{\Psi \Delta t}\mathbf{A}(t_m) + \Psi^{-1}\left(e^{\Psi \Delta t} - \mathbf{I}\right)\kappa_n y(t_m), \tag{4.1}$$

where $m = 0\,, 1\,, 2\,, \ldots$. It is worth noting that $\mathbf{Q_A} = e^{\Psi \Delta t}$ and $\mathbf{Q}_y = \Psi^{-1}(e^{\Psi \Delta t} - \mathbf{I})\kappa_n$ are constant matrices for a fixed sampling frequency, and are evaluated once for the whole control process. Therefore, the control signal can be generated at each sampling time based on simple matrix multiplications as described by the block diagram shown in Fig. 4.1.

To demonstrates the efficiency of the proposed algorithm in practical sit-

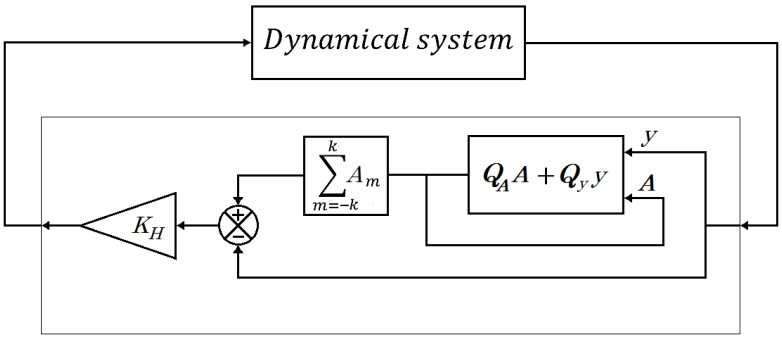

Figure 4.1: Block diagram of truncated HO feedback control

uation, this section presents a successful implementation of HO feedback control by controlling chaotic behavior of an electrical circuit through the block diagram of Fig. 4.1.

4.2.1 Controlling Chaos in an Electrical Circuit

This section addresses experimental implementation of HO feedback control through the block diagram of Fig. 4.1 to a chaotic electrical circuit illustrated in Fig. 4.2. This circuit is known as the smallest transistor-based nonautonomous chaotic circuit [12]. It shares the same structure with the original circuit presented in [12], but it has different values of the electrical components.

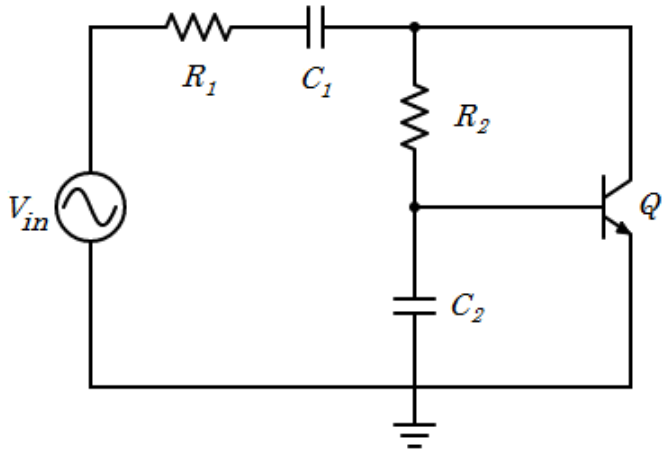

Figure 4.2: The smallest transistor-based chaotic circuit. $V_{in} = 4.5\,V/60Hz$, $R_1 = 100\Omega$, $C_1 = 136nF$, $R_2 = 820k\Omega$, $C_2 = 136nF$, and $Q = 2N2222A$.

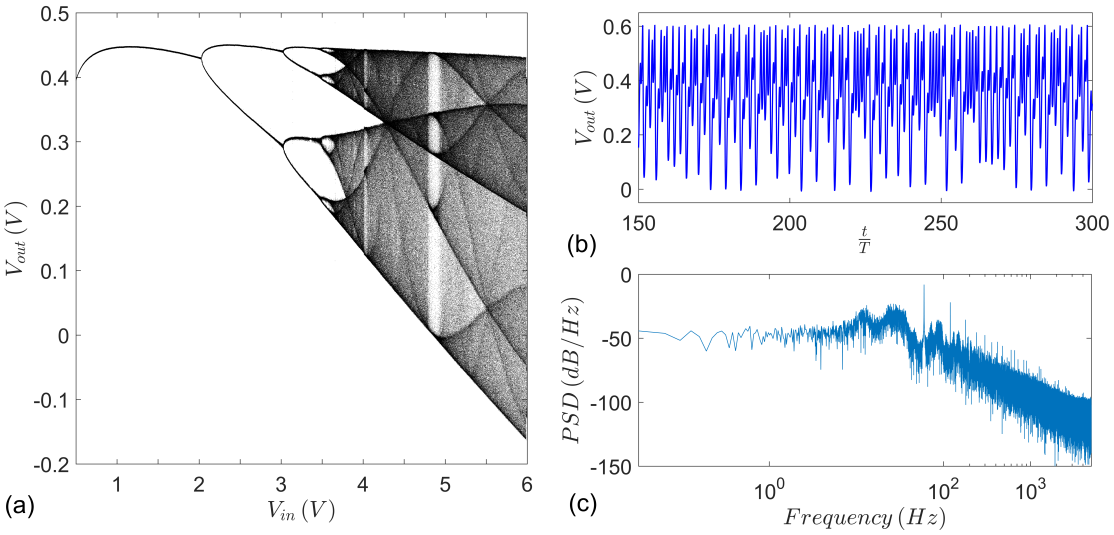

Figure 4.3: Response of the electrical circuit: (a) Bifurcation diagram. (b) Dynamics of the transistor's base voltage for $V_{in} = 4.5V$. (c). Power spectral density for $V_{in} = 4.5V$.

The bifurcation diagram of this circuit is plotted in Fig. 4.3(a), which describes the transition of a regular periodic behavior to an unpredictable chaotic response. To plot this diagram, the voltage at the base of the transistor is sampled per period of the sinusoidal voltage source as the amplitude gradually increases from $0.5V$ to $6V$. Data acquisition is conducted through *Quanser QPID* with sampling rate of $10kSps$, and processed by *Matlab* 2014a software. For any incremental increase of the amplitude, the first 50 samples are rejected to ensure that the steady state is reached, and the next 1000 samples are plotted. In other words, a component of the steady state solution on the Poincaré section is plotted as a function of amplitude of the voltage source. This diagram shows the circuit follows a sequence of period doubling bifurcations until chaos appears. Theoretically, this transition requires an infinite number of bifurcations, however, due to the inevitable noise in the experiment, some of the higher period doubling bifurcations are suppressed. Referring to Fig. 4.3(a), chaos appears at $V_{in} \approx 3.7V$,

which is accompanied by an irregular, unpredictable response. However, period-6 and period-5 windows can be distinguished in some intervals. Figure 4.3(b) plots the time history of the systems response for $V_{in} = 4.5V$ in the interval between 150 to 300 periods of the voltage source, which illustrates the chaotic behavior of the system. The power spectral density (PSD) of the measured voltage is plotted in Fig. 4.4(c). It reveals that the measured signal has a continuous broad band character, which is a sign of chaotic behaviour of the circuit. In addition to the broad band character, the spectrum consists of spikes that indicates the predominant frequency components at the harmonics of the frequency of the voltage source. These frequencies correspond to the fundamental frequency of the unstable orbits embedded in the chaotic attractors. Furthermore, Fig. 4.3(c) implies that the sampling rate of $10kSps$ is well above the limit required to an accurate reconstruction of the signal as the component correspond to the Nyquist frequency $f_N = 5kHz$ has considerably small contribution to the power of the signal. The main reason of selecting such a high sampling rate is the requirement imposed by the accuracy of the numerical integration algorithm as described by Eq. (4.1). In general, Eq. (4.1) yields a better approximation for smaller sampling period Δt.

In the implementation of HO feedback control, it is assumed that the voltage at the base of the transistor is available for measurement. In order to generate the control signal based on the measured voltage, four parameters $\mathbf{K}_n$, $\mathbf{K}_H$, ω_T and the set $\mathbb{U}$ need to be determined. In this experiment, a single output of the system is used to establish the control. Therefore, $\mathbf{K}_n$ can be thought of as a positive scalar κ_n, as it satisfies the condition $Re(\lambda_\Psi) < 0$. ω_T is determined based on the period of the unstable orbit. In non-autonomous systems, as in the present

case, the period of the unstable orbit is an integer multiple of the period of the external input. The set $\mathbb{U}$ is defined by $\mathbb{U} = \{m \mid m \in \mathbb{Z}, -k \leq m \leq k\}$, where k is the truncation limit. Finally, $\mathbf{K}_H$ is tuned experimentally to observe the desired stable periodic motion. The control signal, then, is superposed on the output of the voltage source, and feeds the circuit.

Figure 4.4 shows the results of applying HO feedback control to the chaotic circuit in order to stabilize a period-one orbit of the system. As illustrated in Figs. 4.4(a) and 4.4(b), the chaotic response of the system turns to a period-one motion once the control is switched on. The intensity of control perturbations practically vanishes, when the system exhibits a periodic evolution. Figure 4.4(c) shows the stabilized period-one response for the duration of two periods of the stabilized motion, and the error signal $E = y - \sum_{m=-k}^{k} A_m$ is depicted in Fig. 4.4(d). It is worth noting that the error signal remains considerably small, even when the measured signal experiences sharp, unsmooth changes. This implies that the stabilized motion is a solution of the same system whose free response is chaotic.

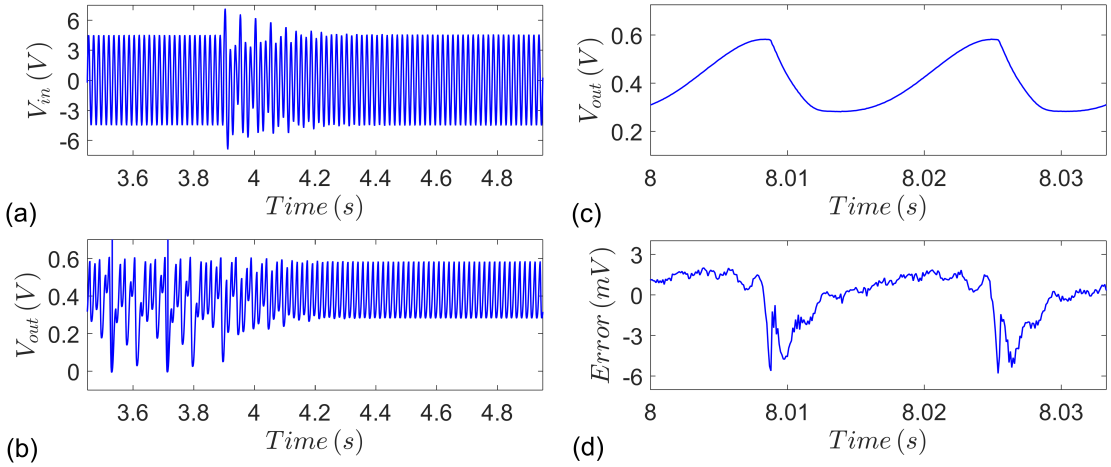

Figure 4.4: Control performance for $\kappa_n = 0.01$, $\mathbf{K}_H = 20$, $\Delta t = 0.0001\ s$, and truncation limit $k = 8$: (a) Input voltage. (b) Transistor's base voltage. (c) Stabilized period-one response. (d) Error signal with the root-mean-square value of 1.83 mV.

It is worth noting that HO feedback control is capable of stabilizing higher periodic orbits. To demonstrate this feature of HO feedback control, a period-2 orbit of the circuit is also stabilized. Figure 4.5 shows the the control performance along with the stabilized period-two motion and the associated error signal.

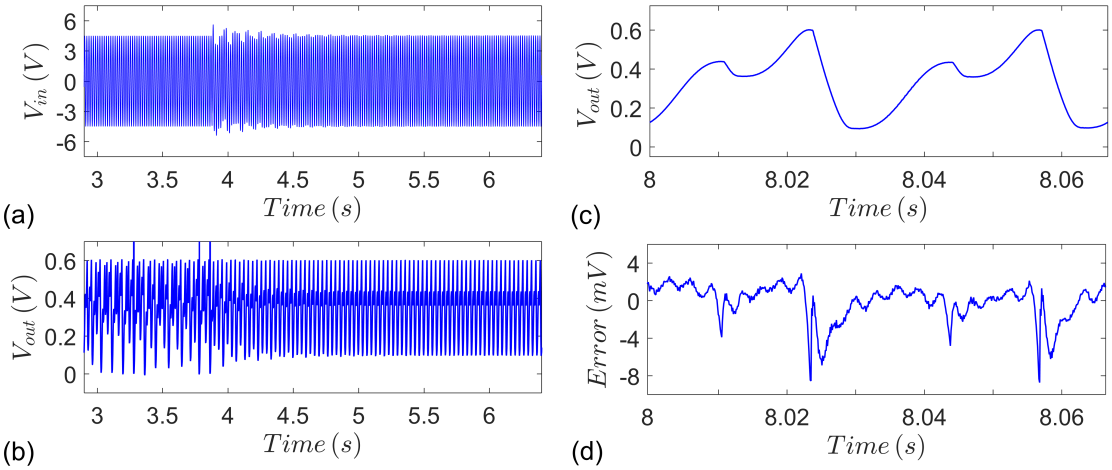

Figure 4.5: Control performance for $\kappa_n = 0.005$, $\mathbf{K}_H = 20$, $\Delta t = 0.0001\ s$, and truncation limit $k = 10$: (a) Input voltage. (b) Transistor's base voltage. (c) Stabilized period-two response. (d) Error signal with the root-mean-square error of 2.14 mV.

4.3 HO Time Series Analysis

This section demonstrates the success of HO time series analysis in extracting periodic orbits from time series obtained from numerical simulations and experiments. Extracting unstable periodic motions embedded in the chaotic time series of autonomous and nonautonomous systems is discussed. It addresses the effect of noise on the quality of the detected motion, and investigates controlling chaos using the detected unstable motion through the proportional feedback controller.

4.3.1 Detecting UPOs of Nonautonomous Systems

To exact unstable periodic motions from chaotic time series, the first step is to evaluate the vector of harmonic oscillators $\mathbf{A}$ at each consecutive sampling time according to Eq. (4.1). To do so, the coefficient matrix Ψ needs to be identified first, through the period of the orbit T and the coupling strengths κ_n. The period associated with unstable orbits of nonautonomous systems is usually explicitly known as integer multiples of the period of the external input. To guarantee a bounded solution for $\mathbf{A}$, the coupling strengths κ_n need to be assigned such that Ψ is a positive matrix. This section addressed the case in which κ_n is a positive constant, which automatically satisfies the condition $Re(\lambda_\Psi) < 0$. Once the vector of harmonic oscillators is evaluated, the root mean square value of $\mathcal{H}^k_{\omega_T}$ over one period of the target orbit can be used to detect unstable periodic motions. This quantity is denoted by $R_{\omega_T}(t)$, and is defined through Eq. (3.27). The magnitude $R_{\omega_T}(t)$ reflects the deviation of the system from the unstable orbit, and can be used to identify the moment at which the system starts evolving close to the unstable orbit.

The electrical circuit shown in Fig. 4.2 is an example of nonautonomous chaotic systems. The periods associated with unstable orbits embedded in its chaotic attractor can be identified as integer multiples of the period of the voltage source. Figure 4.3(b) plots the voltage at the base of the transistor in the interval between 150 to 300 periods of the voltage source. As illustrated, the response has a chaotic, irregular evolution while embedding a set of unstable periodic motions. The unstable periodic motions can be identified through the local minima of $R_{\omega_T}(t)$

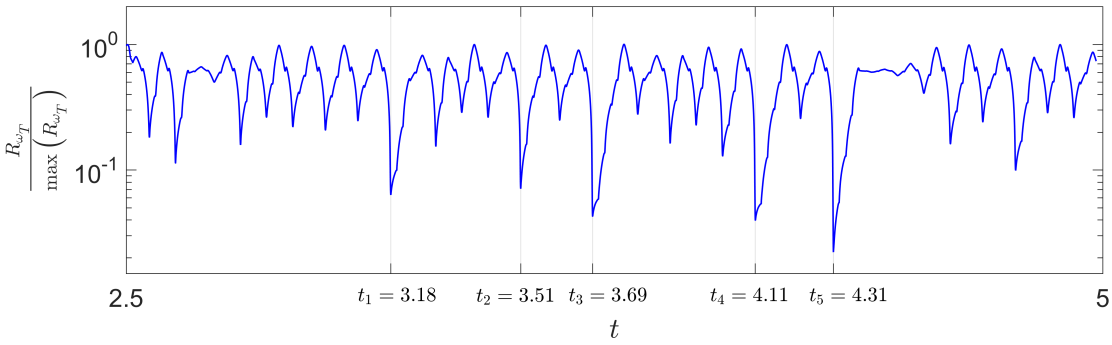

Figure 4.6: Normalized $R_{\omega_T}(t)$ for $T = \frac{1}{60}\,s$, $\kappa_n = \frac{2}{T}$, and $k = 30$.

as plotted in Fig. 4.6. Period-1 unstable orbits can be detected at $t_1 = 3.18s$, $t_2 = 3.51s$, $t_3 = 3.69s$, $t_4 = 4.11s$, and $t_5 = 4.31s$. The lower the minimum, the closer the system is to an unstable orbit. Therefore, a period-1 orbit is identified best at $t = 4.31s$, as it corresponds to a lower minimum. Figure 4.7(a) plots a period-1 unstable orbit detected at $t = 4.31s$. The detected orbit can be processed through Eq. (3.30), which does not only improve the quality of the results, but also allows developing an accurate analytical expression for the detected motion in the form of Fourier series. Figure 4.7(b) plots the Fourier series of the detected motion for duration of two periods of the orbit. It reveals that the detected motion belongs to the same system, whose stabilized response is plotted in Fig. 4.7(c).

The proposed method is also capable of extracting higher periodic orbits form chaotic time series. It is important to note that the frequency of unstable orbits of nonautonomous systems are subharmonics of the frequency of the external input. This implies that the minima of $R_{\omega_T}(t)$ may belong to an orbit whose frequency is a harmonic of the fundamental frequency of the desired orbit. Comparing the plot of $R_{\omega_T}(t)$ associated with the target frequency with those associated with its harmonics allows identifying the true moment at which the system starts evolving close to the target orbit. Figure 4.8 plots $R_{\omega_T}(t)$ for period-2

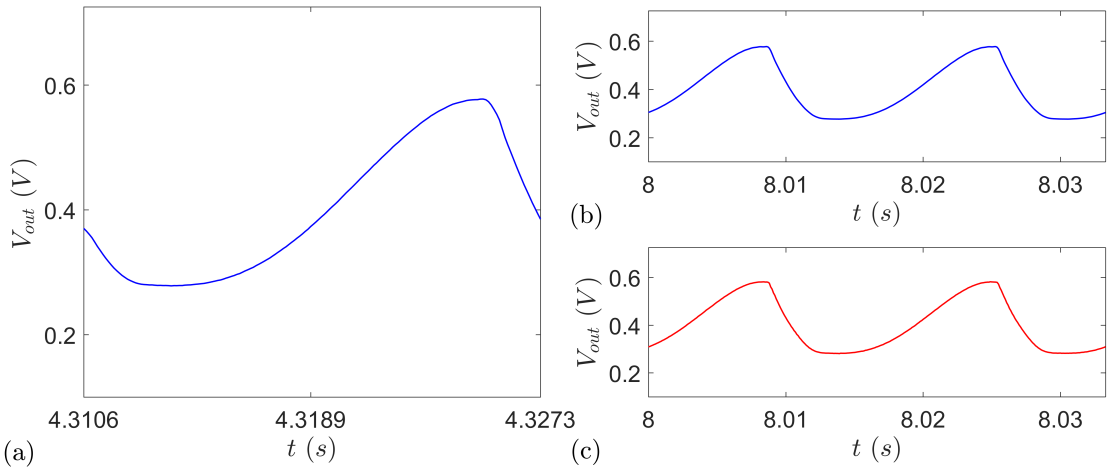

Figure 4.7: (a) Detected period-1 unstable motion. (b) Truncated Fourier series of the detected motion for $k = 30$. (c) Experimentally stabilized period-1 response.

orbits. Comparing this figure with Fig. 4.6 indicates that the system evolves close to period-1 orbits at $t_2 = 3.19s$, $t_3 = 3.71s$, $t_4 = 4.13s$, and $t_5 = 4.33s$ at least for twice the periods of the orbit. It also indicates that there is no period-1 orbit close to the system's trajectory at $t_1 = 2.68s$, and $t_6 = 4.41s$. In other words, $t_1 = 2.68s$ and $t_6 = 4.41s$ identify the true moments at which the system starts evolving close to period-2 orbits.

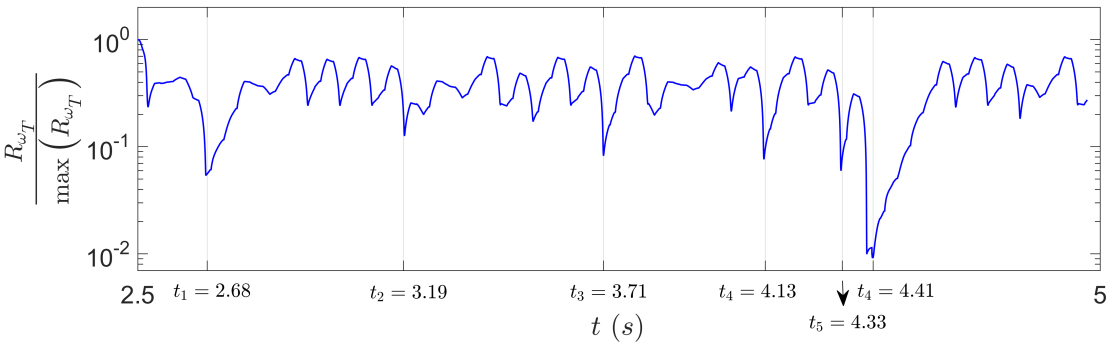

Figure 4.8: Normalized $R_{\omega_T}(t)$ for $T = \frac{1}{30}$, $\kappa_n = \frac{2}{T}$, and $k = 40$.

Figure 4.9(a) plots a period-2 unstable orbit detected in the at $t = 4.41s$. Comparing Fig. 4.9(b) with Fig. 4.9(c) reveals that the detected and the controlled orbit belong to the same system sharing the same configuration in the state space.

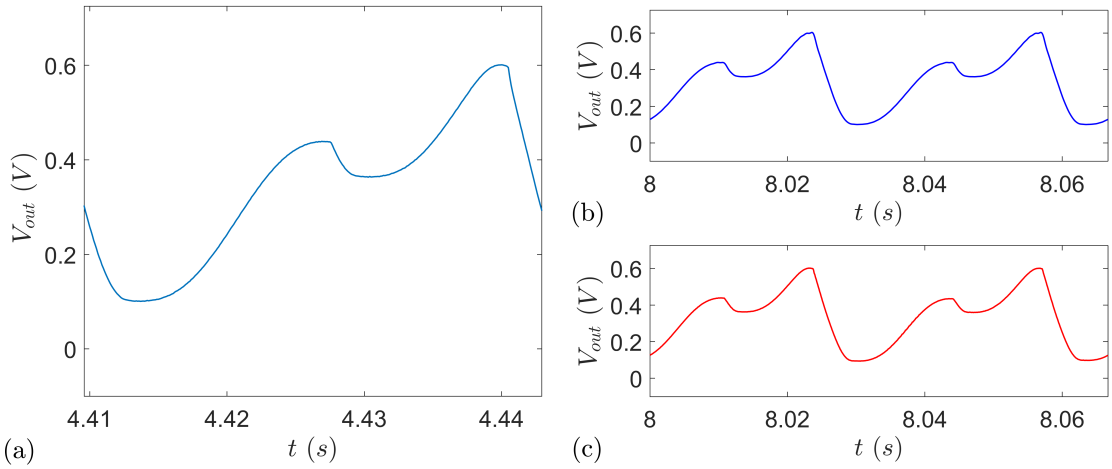

Figure 4.9: (a) Detected period-2 unstable motion. (b) Truncated Fourier series of the detected motion for $k = 40$. (c) Stabilized period-2 response.

4.3.2 Detecting UPOs of Autonomous Systems

The steps of detecting unstable periodic orbits of autonomous systems are essentially the same as nonautonomous systems. However, in contrast to nonautonomous systems, the period associated with periodic orbits of autonomous systems is not *a priori* known. To deal with this situation, section 3.4 suggests monitoring a weighted time average of $R_{\omega_T}(t)$ denoted by $\bar{R}(\omega)$ over a prescribed rage of frequency. The frequency of unstable orbits can be identified at the local minima of $\bar{R}(\omega)$. This section investigates the successes of this approach by extracting unstable periodic motions embedded in a chaotic time series of the well-known Rosselor's system, which can be described by

$$\begin{bmatrix} \dot{x}_1 \\ \dot{x}_2 \\ \dot{x}_3 \end{bmatrix} = \begin{bmatrix} -x_2 - x_3 \\ x_1 + 0.2x_2 \\ 0.2 + x_3(x_1 - 5.7) \end{bmatrix} \tag{4.2}$$

Figure 4.10 plots the normalized value of $\bar{R}(\omega)$ obtained from x_1 component of the solution in the period range from $T = 3.5$ to $T = 14$, where $T = \frac{2\pi}{\omega}$. The

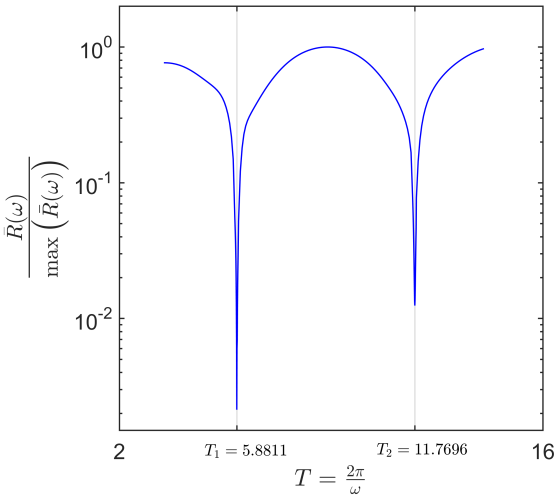

Figure 4.10: Normalized $\bar{R}(\omega)$ obtained from x_1 component of the solution for $\alpha = 2$, $\kappa = \frac{2}{T}$, and $k = 15$.

periods associated with period-1 and period-2 orbits can be distinguished through the notches at $T = 5.8811$ and $T = 11.7695$, respectively.

Figure 4.11 plots $R_{\omega_T}(t)$ for $T = 5.8811$. The moments at which the system starts evolving close to a periodic orbit can be best identified at $t_1 = 384.21$ and $t_2 = 823.73$.

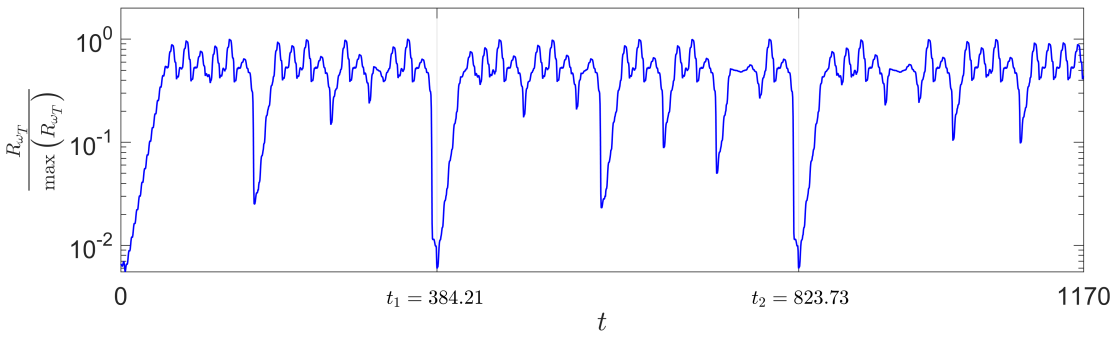

Figure 4.11: Normalized $R_{\omega_T}(t)$ for $T = 5.8811$, $\kappa_n = \frac{2}{T}$, and $k = 20$.

Figure 4.12 plots a period-1 unstable orbit detected at $t = 823.73$. To verify the accuracy of the result, the detected orbit can be used to control the chaotic behavior of system (4.2) through the proportional feedback controller [7]. To do

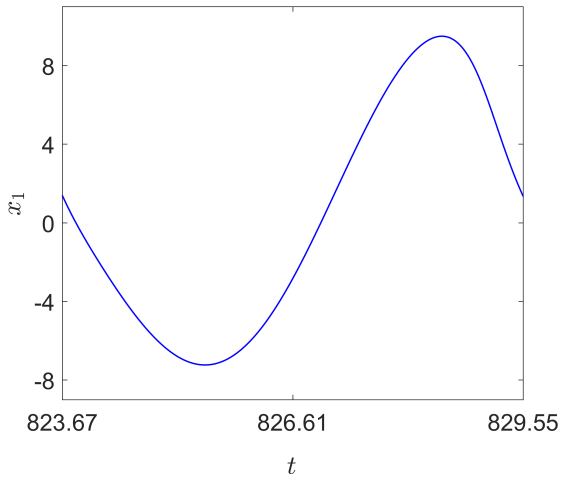

Figure 4.12: Detected period-1 unstable motion from x_{1_T} component of the solution for $T = 5.8811$, $\kappa = \frac{2}{T}$, and $k = 20$.

so, the control perturbations are applied to the first component of the vector field according to Eq. (4.3).

$$f_c = K_P\big(x_{1_T} - x_1\big) \tag{4.3}$$

where K_P is the control gain, and x_{1_T} represents the Fourier series of the detected orbit obtained through Eq. (3.30). Once the control is switched on, the magnitude of the error $E = x_{1_T} - x$ indicates whether the detected orbit belongs to the chaotic attractor of the system. The results of stabilizing period-1 orbit using the proportional feedback controller are presented in Fig. 4.13, where the dynamics of the error signal along with the detected and stabilized period-1 orbit are plotted. Once the control is switched on at $t = 294$, the magnitude of the error approaches zero and stays null, which implies that the detected orbit belongs to the same system whose free response is chaotic. This can also be verified by realizing the agreement between the detected and stabilized orbit as plotted in Fig. 4.13(b) and Fig. 4.13(c), respectively.

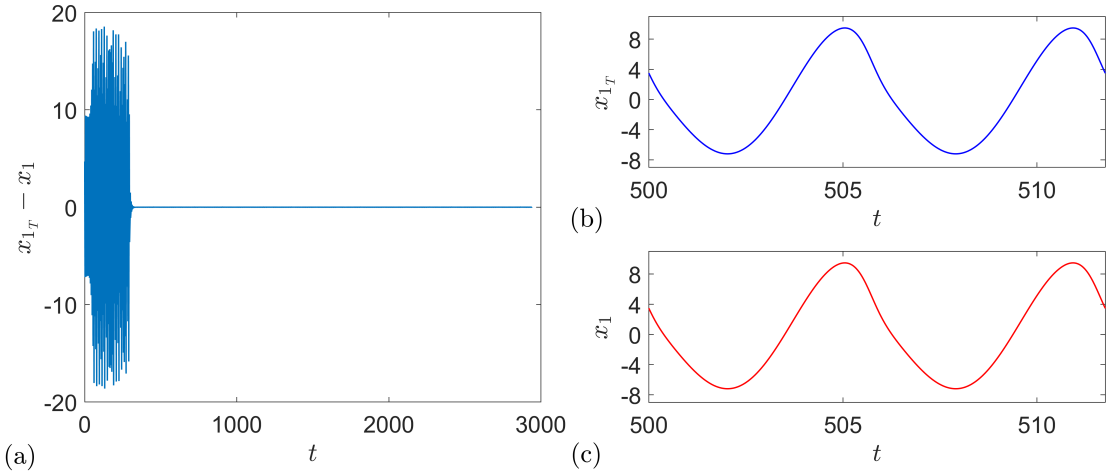

Figure 4.13: (a) Dynamics of the error signal $x_{1_T} - x$. (b) Detected period-1 orbit. (c) Stabilized period-1 orbit for $K_P = 2$.

The same approach can be applied to detect period-2 orbits of the Rosselor's system. Referring to Fig. 4.10, the period associated with a period-2 orbit can be identified at $T = 11.7695$. It is worth noting that this period is almost twice the period of the period-1 orbit implying that the minima of the error signal may correspond to a trajectory evolving twice around the period-1 orbit. Comparing the plot of $R_{\omega_T}(t)$ associated with period-1 and period-2 orbits identifies the true moments during which the system's trajectory evolves around a period-2 orbit. Figure 4.14 plots the root mean square value of the error signal for $T = 11.7695$. Comparing Figs. 4.14 and 4.11 reveals that the system evolves close to the period-1 orbits at $t_1 = 385.08$, and $t_3 = 824.61$ at least for twice the period of the orbit. The moments at which the system starts evolving around a period-2 orbit can be identified at $t_2 = 748.32$ and $t_4 = 941.63$.

Figure 4.15 plots a period-2 unstable orbit detected at $t_4 = 941.63$. The accuracy of this result can be verified by stabilizing the period-2 orbit through the

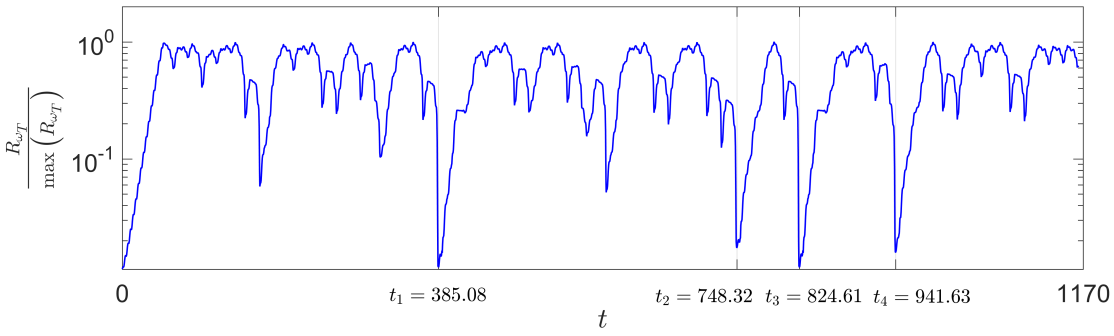

Figure 4.14: Normalized $R_{\omega_T}(t)$ for $T = 11.7696$, $\kappa = \frac{2}{T}$, and $k = 30$.

proportional controller as defined by Eq. (4.3).

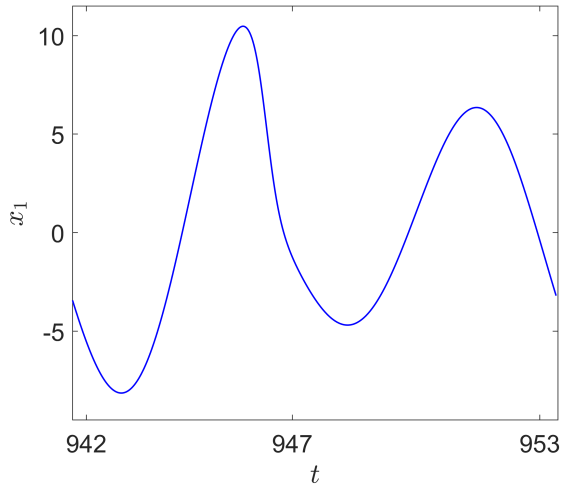

Figure 4.15: Detected period-2 unstable motion from x component of the solution for $T = 11.7696$, $\kappa = \frac{2}{T}$, and $k = 30$.

The results of stabilizing period-2 orbit using the proportional feedback controller are presented in Fig. (4.16), where the dynamics of the error signal along with the detected and stabilized period-2 orbit are plotted. The control is switched on at $t = 588$. Once the transitions die out, the magnitude of the error practically vanishes implying that the detected orbit is an unstable solution of the chaotic system. The agreement between Fig. 4.16(b) and Fig. 4.16(c) indicates that the system follows identical evolutions on both detected and stabilized orbit.

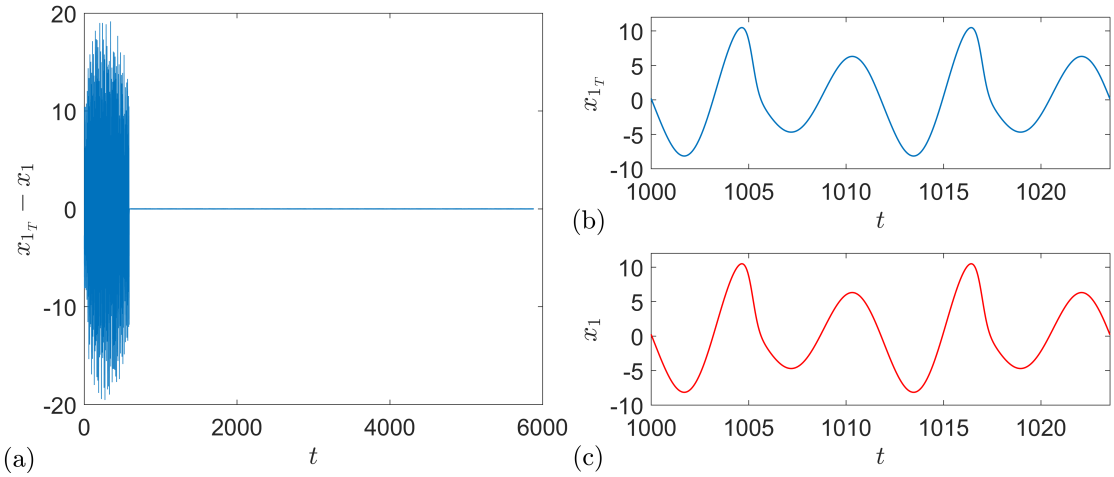

Figure 4.16: (a) Dynamics of the error signal $x_{1_T} - x$. (b) Detected period-2 orbit. (c) Stabilized period-2 orbit for $K_P = 2$.

4.3.3 Effect of Noise

The last two sections demonstrate that HO time series analysis accurately detects unstable periodic motions embedded in chaotic time series, when noise free data is available. However, noise always exists in experiments deteriorating the quality of the measurements, and eliminating valuable information from the signal. This section investigates the effect of noise on the performance of HO time series analysis. To do so, extracting periodic motions from a noisy time series of chaotic Duffing oscillator described by Eq. (4.4) is addressed.

$$\begin{bmatrix} \dot{x}_1 \\ \dot{x}_2 \end{bmatrix} = \begin{bmatrix} x_2 \\ -0.02\, x_2 - x_1 + {x_1}^3 + \cos t \end{bmatrix} \tag{4.4}$$

It is assumed that x_1 component of the solution is a measurable output of the system. The effect of noise is modeled by superimposing a random signal in the from of white noise on the output of the system. Figure 4.17 plots the dynamics of $R_{\omega_T}(t)$ along with the detected unstable motion from x_1 component of the solution for a noise free time series, and time series contaminated by a white noise

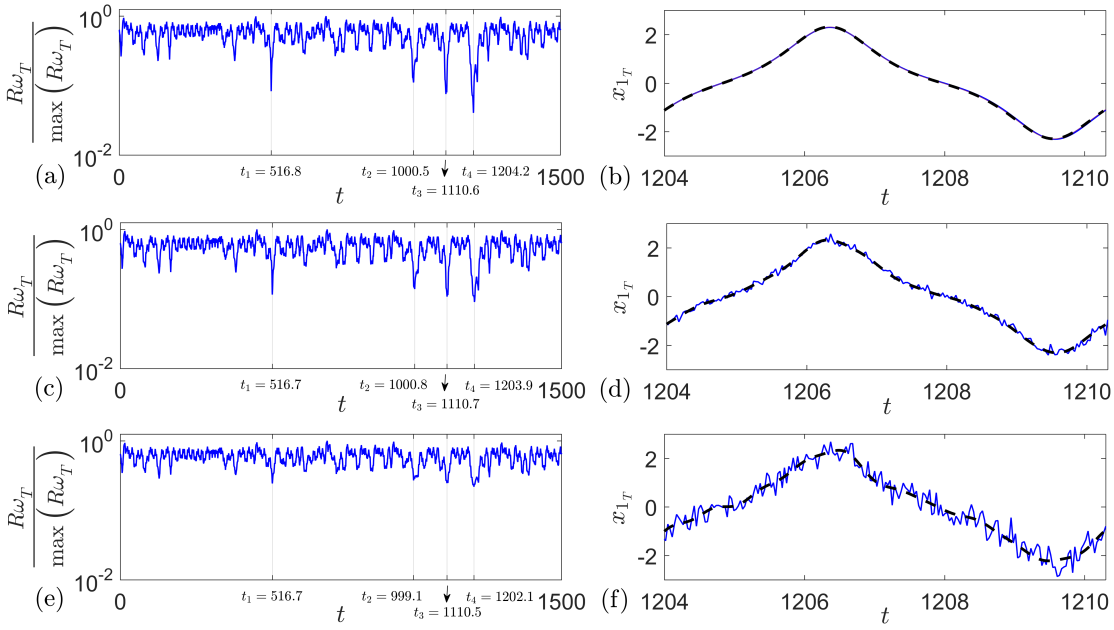

Figure 4.17: Normalized $R_{\omega_T}(t)$ along with the detected period-1 orbit (solid line), and the root mean square regression of the detected orbit (dashed line) obtained from x component of Duffing oscillator for $T = 2\pi$, $\kappa_n = \frac{2}{T}$, and $k = 10$: (a) and (b) Noise free time series. (c) and (d) Noisy time series with the signal-to-noise ratio per sample of $20dB$. (e) and (f) Noisy time series with the signal-to-noise ratio per sample of $10dB$.

source with the signal-to-noise ratio per sample of $20dB$ and $10dB$. Comparing Figs. 4.17(a), 4.17(c) and 4.17(e) reveals that HO time series analysis identifies the unstable orbits accurately even in the presence of noise as the minima of the root mean square value of the error signal for all three cases are coincident with each other. Figs. 4.17(b), 4.17(d) and 4.17(f) reveal that the noise adversely affects the quality of the detected orbit, however, the root mean square regression as described by Eq. (3.30) still provides reasonably accurate results.

To quantify the accuracy of the results in each case, the detected orbit can be used to control chaotic behavior of the Duffing oscillator through the proportional feedback controller. Figure 4.18 plots the time history of the error signal $E = x_{1_T} - x$ along with the stabilized period-1 motion. The control perturbations

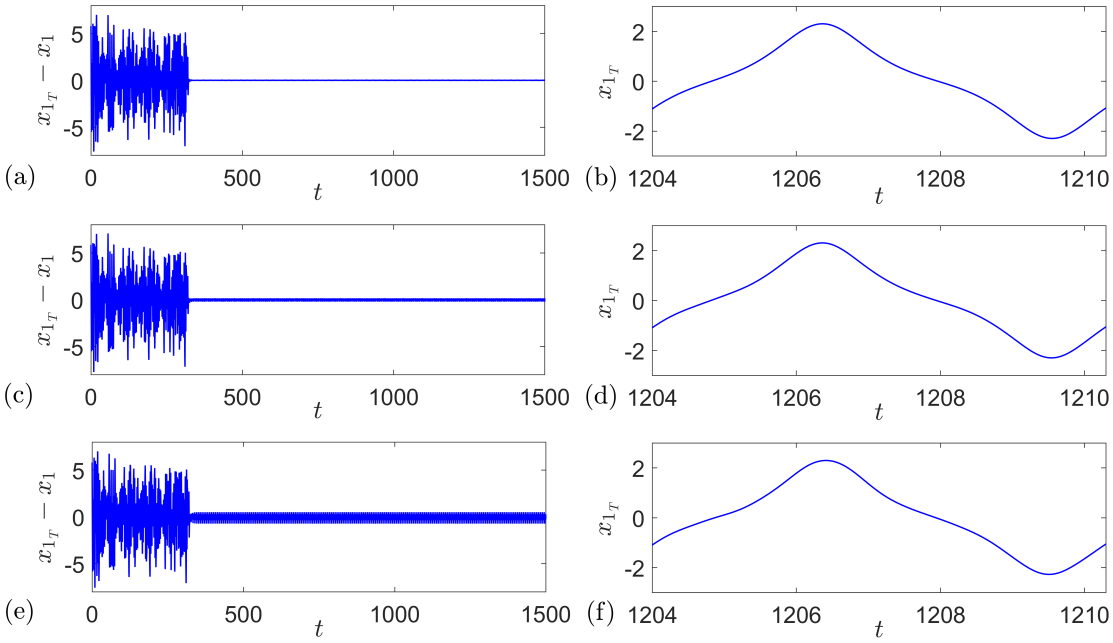

Figure 4.18: Dynamics of the error signal, and the stabilized period-1 orbit obtained from x component of Duffing oscillator for $T = 2\pi$, $\mathbf{K}_P = 0.8$, and $k = 10$: (a) and (b) Noise free time series. (c) and (d) Noisy time series with the signal-to-noise ratio per sample of $20dB$. (e) and (f) Noisy time series with the signal-to-noise ratio per sample of $10dB$.

are applied to the first component of the vector field. For the noise free data, the magnitude of the error approaches zero once the orbit attains it stability implying that the detected unstable orbit belongs to the chaotic attractor of the system. However, for noisy time series, the controller slightly changes the configuration of the orbit in the state space as magnitude of the error signal approaches a finite value, but remains reasonably small with respect to the magnitude of the stabilized orbit. This implies that HO time series analysis can effectively detect unstable periodic obits even in noisy time series.

Figure 4.19 plots the stabilized periodic orbit in the state space. For noisy time series, the stabilized orbits stay close to the orbit of the free system. This indicates that the detected orbits using HO time series analysis can effectively be

used to control chaos in practical situations and noisy environments, and serve as an alternative approach for HO feedback control. It is worth noting that the orbit depicted in Fig. 4.19 is a torsion free orbit of the free system whose Floquet exponents $\lambda_1 = 0.237$ and $\lambda_2 = -0.257$. Stabilizing this orbit using truncated HO feedback control is addressed in the next section.

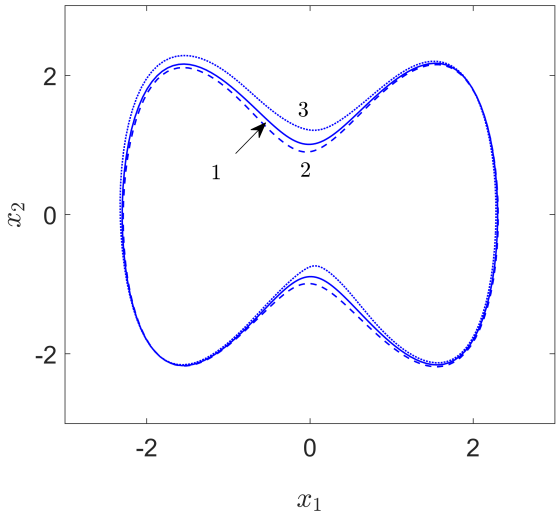

Figure 4.19: Controlled period-1 orbit using (1) noise free time series, (2) noisy time series with the signal-to-noise ratio per sample of $20dB$, and (3)noisy time series with the signal-to-noise ratio per sample of $10dB$ for $T = 2\pi$, $K_P = 0.8$, and $k = 10$.

4.4 Stabilizing Torsion Free Orbits

A major distinction between a truncated version of HO feedback control and EDFC appears when stabilizing torsion fee orbits of nonautonomous systems is concerned. The fact that EDFC inevitably involves all harmonics of the fundamental frequency in its feedback loop renders stabilizing torsion free orbits of nonautonomous systems impossible. In contrast to EDFC, truncated HO feedback control can selectively excludes higher frequency oscillator with negligible amplitudes from the feedback loop, while preserving the configuration of the tar-

get orbit in the state space. As discussed in section 3.6, this property of truncated HO feedback control enables stabilizing torsion free orbits of dynamical system. This section refutes odd number limitation in truncated HO feedback control by stabilizing torsion free orbits of Duffing oscillator (4.4).

The stability of torsion free orbits requires $\lambda = 0$ to be a solution of Eq. (4.5) for some values of the control gain $\mathbf{K}_H$ and the coupling matrices $\mathbf{K}_n$.

$$\det\Big(\Phi(\mathbf{K}_H, \mathbf{K}_n, T) - e^{\lambda T}\mathbf{I}\Big) = 0 \tag{4.5}$$

where $\Phi(\mathbf{K}_H, \mathbf{K}_n, t)$ is the fundamental matrix solution associated with the controlled orbit defined by Eqs. (3.21). Eq. (4.5) represents a multi-variable equation, which can lead to a large number of solutions for the set $\mathbb{U}$, the control gain $\mathbf{K}_H$, and the coupling matrices $\mathbf{K}_n$. This section does not intend to investigate the behavior of this equation with respect to the control parameters, analytically, but to present an algorithm to design the control parameters that leads to a stable torsion free orbit. This algorithm is explained for a single-input single-output system with real coupling strength, which can easily be extended to multiple-input multiple-out put systems with a more general coupling condition. Instead of tackling the problem directly, this section suggests a minimization algorithm that aims to minimize the real part of the leading exponent of the control orbit. Suppose that the minimization changes the sign of the real part of the leading exponent from positive to negative. For a torsion free orbit, the sign change takes place along the real axis that requires a special treatment. Two scenarios need to be addressed, separately: (i) $\kappa_m \neq 0$ at $\lambda = 0$ for all $m \in \mathbb{U}$, and (ii) there exists $m \in \mathbb{U}$ such that $\kappa_m = 0$ at $\lambda = 0$. In the first scenario, the minimization continues

until λ passes the origin from the right to the left. However, the second scenario requires further consideration. In fact the condition $\kappa_m = 0$ uncouples the m^{th} oscillator from the control system, and leaves

$$\dot{\mathbf{A}}_m = im\omega_T \mathbf{A}_m \tag{4.6}$$

Equation (4.6) has a single exponent defined by $\lambda = 0$ that appears in the minimization process. Excluding this oscillator from the system suggests that the leading exponent of the new system has a negative real part. A critical factor that decides weather this oscillator can be excluded from the feedback loop is the size of the number m. If m is sufficiently large, the oscillator can be excluded from the feedback loop without changing the coordinates of the target orbit, otherwise, the algorithm needs to be resumed with a new initial condition until this condition is fulfilled. This section addresses the case in which $\mathbb{U}$ is initially defined by $\mathbb{U} = \{m \mid m \in Z, -k \leq m \leq k\}$. The Nelder-Mead simplex algorithm [80] is used in the minimization process. This algorithm is a popular direct search method for multidimensional unconstrained minimization that attempts to minimize a scalar nonlinear function of several real variables using only the function values, without any derivative information. Thus it is suitable for this application as the information about the derivative of the objective function comes with high computational costs. This section employs a *Matlab* function *fminsearch* that formulates the Nelder-Mead simplex algorithm, which turns to be a fast and accurate algorithm of designing HO feedback control parameters. More details are provided in Appendix B.

Table 4.2 lists the control parameters leading to a vanishing solution of the

Table 4.1: The list of control parameters leading to $\lambda = 0$ for the torsion free orbits of Duffing oscillator depicted in Fig. 4.20.

Period	Coupling strength					Control gain
$T = 2\pi$	$\kappa_0 = 0.702$	$\kappa_1 = 0.298$	$\kappa_2 = 0.298$	$\kappa_3 = 0.298$	$\kappa_4 = 0.298$	$K_M = 0.300$
	$\kappa_5 = 0.297$	$\kappa_6 = 0.296$	$\kappa_7 = 0.295$	$\kappa_8 = 0.293$	$\kappa_9 = 0.286$	
	$\kappa_{10} = 0.284$	$\kappa_{11} = 0.284$	$\kappa_{12} = 0.233$	$\kappa_{13} = 0.264$	$\kappa_{15} = 0.368$	

characteristic equation for $k = 15$ and the torsion free orbit depicted in Fig. 4.20. The oscillators associated with $m = 14$ and $m = -14$ are excluded from the feedback loop through the minimization process. Note that only the coupling strength for positive values of m are presented as $\kappa_m = \kappa_{-m}$.

Figure (4.20) illustrates the results of stabilizing torsion free period-1 orbit of Duffing oscillator (4.4) using truncated HO feedback control. Figure 4.20(a) plots the stabilized torsion free period-1orbit along with the dependence of the real part of the leading exponent to the control gain $\mathbf{K}_H$. For suitably chosen coupling strength κ_n, the target orbit gains its stability when the leading exponent changes its sign from positive to negative. It remains stable until the leading exponent becomes positive again. Figure 4.20(b) plots the dynamics of the control force. It shows that the control force practically vanishes once the target orbit attains its stability. It remains null while the control is switched on. In spite of the fact that higher frequency oscillators are excluded from the feedback loop, this figure implies that proposed approach preserves the shape and the location of the target orbit in the state space.

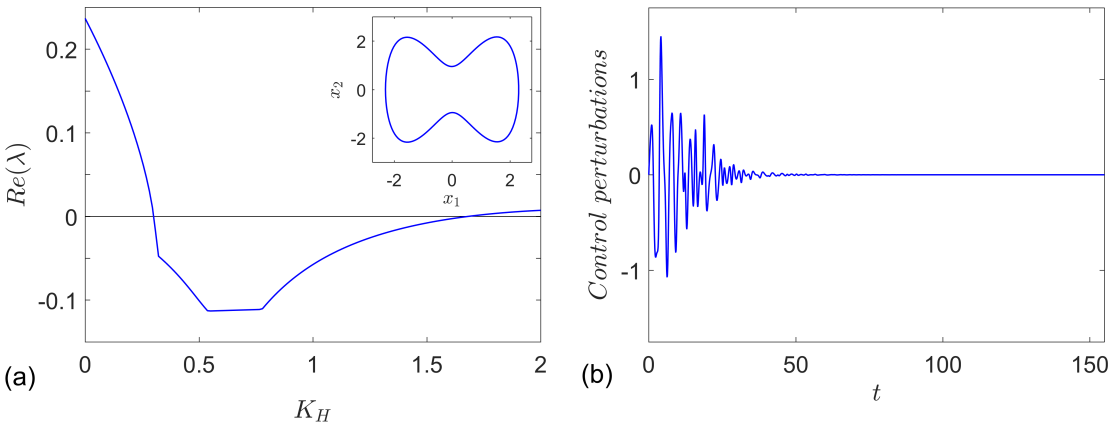

Figure 4.20: (a) The real part of the leading exponent of period-1 orbit with free exponents $\lambda_1 = 0.237$ and $\lambda_2 = -0.257$ versus $\mathbf{K}_H$ for the coupling strengths listed in Tab. 4.1. (b) Time history of the control force for $\mathbf{K}_H = 0.53$.

Figure 4.21 plots the dominant Floquet branch that governs the main stability properties of torsion free period-1 orbit. This figure illustrates the mechanism through which the target orbit gains its stability. The dominant branch enters the unit circle at the point that corresponds to $\lambda = 0$. The orbit remains stable for some interval of $\mathbf{K}_H$, until two complex conjugate branches leave the unit circle, where the orbit loose its stability again.

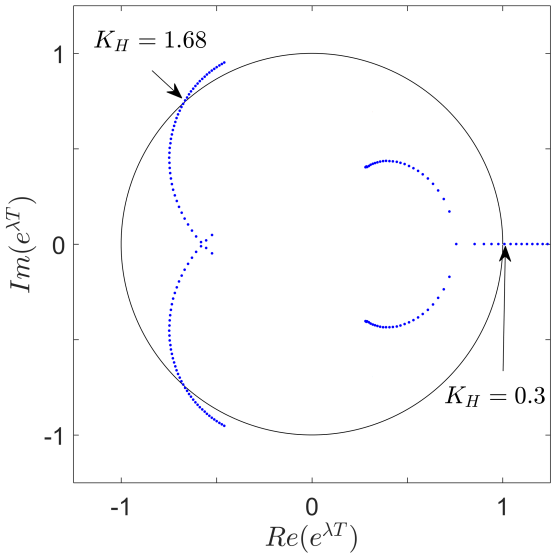

Figure 4.21: The most important Floquet branch that governs the stability properties of torsion free period-1 orbit of Duffing oscillator for the coupling strength listed in Tab. 4.1.

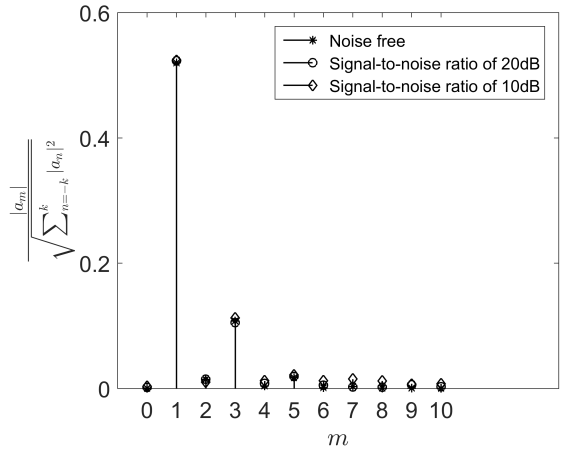

Figure 4.22: Normalized magnitude of the Fourier coefficients of the torsion free orbit depicted in Fig. 4.19 for three different levels of noise obtained from HO time series analysis. Due to the symmetry, the negative values of m are not shown.

This approach suffers from the fact that it requires explicit information about the target orbit and an accurate mathematical model of the system. To overcome this limitation in experimental situations, HO time series analysis can be used to simplify the control parameter design of HO feedback control. As illustrated in Fig. 4.22, HO time series analysis provides valuable information about the frequency content of the target orbit, even in the case of noise-contaminated data. It does not only identify the period of the target orbit, but also the oscillators with negligible amplitudes in the loop of HO feedback control. Figure 4.22 plots the normalized magnitude of the Fourier coefficients of the period-1 orbit depicted in Fig. 4.19 for three different levels of noise. This figure shows that even low frequency oscillators associated with $m = 0, 2, 4$ have small contributions on the control perturbations. It suggests that excluding any of these oscillators from the loop of HO feedback control does not practically change the coordinate of the target orbit in the state space. Figure 4.23 presents the results of stabilizing torsion free period-1 orbit of Duffing oscillator using truncated HO feedback

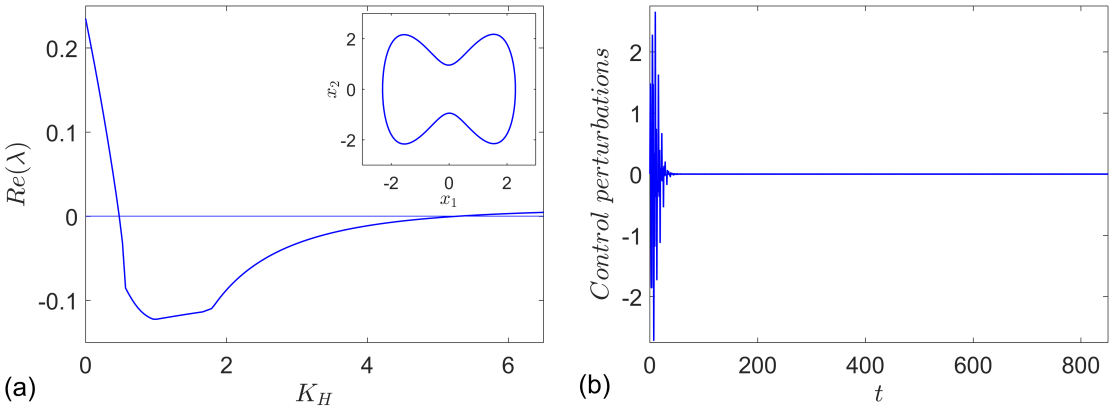

Figure 4.23: Stabilizing torsion free orbit of Duffing oscillator for $\mathbb{U}\{m \mid m \in \mathbb{Z}, -15 \leq m \leq 15, m \neq 2, m \neq -2\}$, and $\kappa_n = \frac{4}{3T}$: (a) Real part of the stabilized period-1 orbit of Duffing oscillators. (b) Dynamics of the control perturbations.

control, for $\mathbb{U}\{m \mid m \in \mathbb{Z}, -15 \leq m \leq 15, m \neq 2, m \neq 2\}$, and the simple coupling condition $\mathbf{K}_n = \frac{4}{3T}$. Figure 4.23($a$) plots the stabilized period-1 orbit of Duffing oscillator along with the dependence of the real part of the leading Floquet exponent on the control gain $\mathbf{K}_H$. Figure 4.23(b) plots the dynamics of the control perturbations. It demonstrates the stabilized orbit belongs to the chaotic attractor of the Duffing oscillator, as the magnitude of the perturbation practically vanishes once the orbit is stabilized. This figure reveals that torsion free periodic orbit of nonautonomous systems can be stabilized by truncated HO feedback control under simple condition using the information obtained from HO time series analysis.

4.5 HO Transformation

HO transformation as an effective transformation of time delay systems to ordinary differential equations is addressed in section 3.5. The present section investigates the success of this transformation in evaluating stability properties of equilibrium and periodic solutions of time delay systems through numerical

demonstrations.

4.5.1 Stability of Equilibrium Solutions

The performance of HO transformation is addressed by evaluating the stability properties of an equilibrium solution of the following system:

$$\ddot{\phi} + 2\mu\dot{\phi} + \frac{\cos(\phi)}{1+\rho\sin^2(\phi)}\Big(\tan(\phi) + \rho\dot{\phi}^2\sin(\phi) + \kappa_\phi\big(\phi(t-\tau)-\phi\big)\Big) = 0, \quad (4.7)$$

Equation (4.6) represents the oscillations of a container crane controlled by DFC. The control aims to minimize the undesirable payload pundulations ϕ around the equilibrium position $\phi = 0$ [81]. In this equation, μ is the damping coefficient, ρ is the mass ratio of the payload to the crane. The stability analysis of equilibrium state of the controlled system is complicated by the existence of the delay term in the mathematical description. This section reveals that HO transformation not only simplifies the stability analysis, but also leads to accurate and reliable results. The varitional equation describing the deviation of the system from $\phi = 0$ reads

$$\delta\ddot{\phi} + 2\mu\delta\dot{\phi} + \phi + \kappa_\phi\big(\delta\phi(t-\tau) - \delta\phi\big) = 0, \quad (4.8)$$

where $\delta\phi$ denotes the small deviation of the system from the equilibrium state. The characteristic equation defining the stability of the equilibrium state of Eq. (4.8) can be described by

$$\lambda^2 + 2\mu\lambda + \kappa_\phi\Big(e^{-\lambda\tau} - 1\Big) + 1 = 0, \quad (4.9)$$

where λ is a complex number whose real part determines the stability. Analyzing this equation is complicated due to the appearance of the exponential term. In fact, this equation leads to an infinite number of solutions for λ reflecting the

infinite dimensional state space of the system. HO transformation offers a systematically simple and efficient approach to evaluate the stability properties of the equilibrium state through an accurate finite dimensional approximation to the variational equation. Introducing $x = \delta\phi$ and $y = \delta\dot{\phi}$, and applying HO transformation to the variational equation (4.8) leads to the following state space representation of the variational equation:

$$\dot{x} = y, \tag{4.10}$$

$$\dot{y} = -2\mu y - x - 2\kappa_\phi\Big(\sum_{m=-k}^{k} \mathbf{A}_m - x\Big), \tag{4.11}$$

$$\dot{\mathbf{A}}_n = in\omega\mathbf{A}_n + \frac{2}{\tau}\Big(x - \sum_{m=-k}^{k} \mathbf{A}_m\Big). \tag{4.12}$$

Equations (4.10), (4.11) and (4.12) describe a linear system with constant coefficients whose stability is determined by the eigenvalues of the well-organized coefficient matrix as defined by

$$\psi = \begin{bmatrix} 0 & 1 & 0 & \cdots & 0 & \cdots & 0 \\ -1+2\kappa_\phi & -2\mu & -2\kappa_\phi & \cdots & -2\kappa_\phi & \cdots & -2\kappa_\phi \\ \frac{1}{\tau} & 0 & -ik\omega - \frac{1}{\tau} & \cdots & -\frac{1}{\tau} & \cdots & -\frac{1}{\tau} \\ \vdots & \vdots & \vdots & \ddots & \vdots & & \vdots \\ \frac{1}{\tau} & 0 & -\frac{1}{\tau} & \cdots & -\frac{1}{\tau} & \cdots & -\frac{1}{\tau} \\ \vdots & \vdots & \vdots & & \vdots & \ddots & \vdots \\ \frac{1}{\tau} & 0 & -\frac{1}{\tau} & \cdots & -\frac{1}{\tau} & \cdots & ik\omega - \frac{1}{\tau} \end{bmatrix}. \tag{4.13}$$

It is worth noting that HO transformation replaces the analysis of transcendental equation (4.9) with the classical eigenvalue evaluation of a constant matrix.

Figure 4.24 illustrates the stability region of the equilibrium state of the payload in $\kappa_\phi - \tau$ parameter space obtained from the truncates HO transformation.

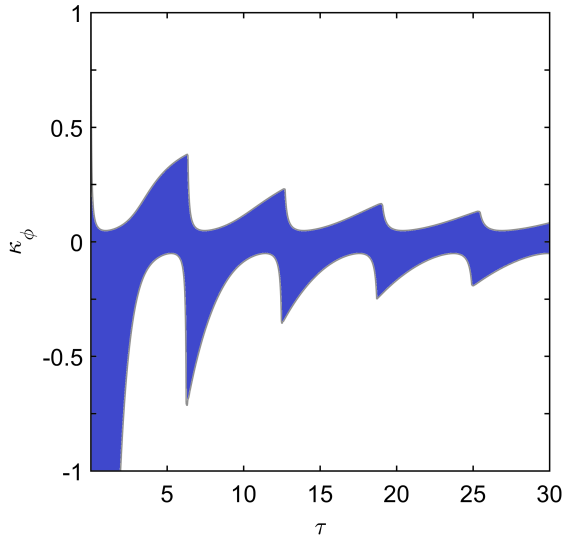

Figure 4.24: Stability region of the equilibrium state of the payload for $\mu = 0.025$ obtained from the truncated HO transformation for $k = 10$.

The shaded area corresponds to a stable equilibrium state, which matches with the results published in [81].

Figure (4.25) plots the real part of the leading exponent with respect to control gain κ_ϕ for various value of delay time τ demonstrating the significant effect of the delay time on the stability properties of the equilibrium state of the payload.

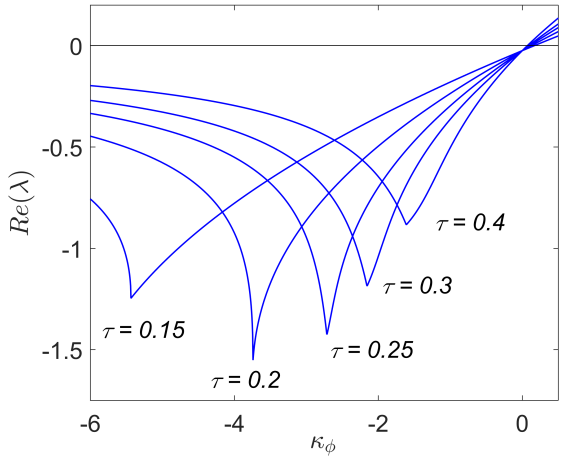

Figure 4.25: Real part of the leading exponent with respect to control gain κ_ϕ for various value of delay time τ obtained from the truncated HO transformation for $k = 10$.

4.5.2 Stability of Periodic Solutions of DDEs

Section 3.5 revealed that truncated HO transformation of EDFC controlled system leads to a system of ODEs describing the same dynamical system controlled by truncated HO feedback control for the parameters $K_H = \frac{1+R}{2}K_D$ and $K_n = \frac{2}{T}\frac{1-R}{1+R}$. This section utilizes this theoretical finding to demonstrating the success of HO transformation in evaluating stability properties of periodic orbits of time delay systems by comparing the stability properties of EDCF and HO feedback controlled orbits of Duffing oscillator (4.4).

Figure 4.26 shows the dependence of the real part of the leading Floquet exponent versus $K_D = \frac{1+R}{2}K_H$ for period-1 and period-3 orbits of Duffing oscillator controlled by truncated HO feedback control in which $\kappa_n = \frac{2}{T}\frac{1-R}{1+R}$. The results are in an excellent agreement with those obtained for the same orbits controlled by EDFC as published in [82]. These results not only demonstrate the success of HO transformation in evaluating the Floquet exponents of periodic orbits of time delay systems, but also validates the theoretical findings of section 3.5 describing the relation between EDFC and HO feedback control.

Comparing the equations describing EDFC and HO feedback control reveals that HO feedback control has the capability of treating each harmonic branches individually with different gains, while EDFC treat them all equally with identical gains. This implies that HO feedback control can lead a wider range of stability properties of the target orbit. This section demonstrates how assigning suitable values to coupling strength κ_n improves the performance of HO feedback control comparing to EDFC. To do so, one approach is to minimize the real part of

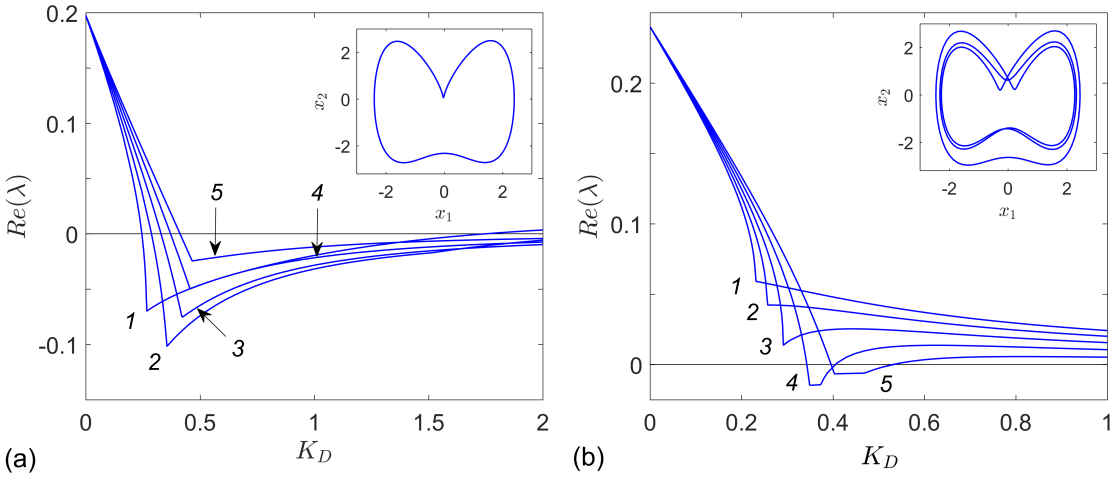

Figure 4.26: The real part of the leading Floquet exponent of periodic orbits controlled by HO feedback control versus $K_H = \frac{1+R}{2} K_D$ for the truncation limit $k = 20$ and the coupling strength $\kappa_n = \frac{2}{T}\frac{1-R}{1+R}$ at (1) $R = 0$, (2) $R = 0.2$, (3) $R = 0.4$, (4) $R = 0.6$, (5) $R = 0.8$: (a) Period-1 orbit. (b) Period-3 orbit.

the leading exponent of the target orbit with respect to the control parameters leading to a better stability properties of the controlled orbit. Obviously, the leading Folquet exponent depends on the control gain K_H, as well as the coupling strength κ_n. An optimization problem can be set up in order to minimize the real part of the leading Floquet exponent of the controlled orbit. Two cases are considered in this section: (i) $\mathbf{K}_n = \kappa$, which describes the stability of the orbit controlled by EDFC for $R = \frac{1-\frac{T}{2}\kappa}{1+\frac{T}{2}\kappa}$, and (ii) a more general condition of $\mathbf{K}_n = \kappa_n$. For the both cases, the set $\mathbb{U}$ is defined by $\mathbb{U} = m \mid m \in \mathbb{Z}, -k \leq m \leq k\}$. The same minimization algorithm of Sec. 4.4 is also used in this section. Table 4.2 lists the results of optimization problem for truncation limit $k = 19$.

Figure 4.27 plots the real part of the leading exponent of period-1 controlled orbit of Duffing oscillator (4.4) versus the control gain for the coupling strength listed in Tab. (4.2). The optimization leads to a considerably lower minimum of the

Table 4.2: Control parameters minimizing the real part of the leading Floquet exponent of the period-1 orbit of Duffing oscillator.

Control method	Control parameters				
EDFC	$R = 0.125$				$\mathbf{K}_D = 0.325$
HO	$\kappa_0 = 0.279$	$\kappa_1 = 1.327$	$\kappa_2 = 0.168$	$\kappa_3 = 0.327$	$\mathbf{K}_H = 0.457$
	$\kappa_4 = 0.300$	$\kappa_5 = 0.291$	$\kappa_6 = 0.284$	$\kappa_7 = 0.278$	
	$\kappa_8 = 0.274$	$\kappa_9 = 0.274$	$\kappa_{10} = 0.278$	$\kappa_{11} = 0.291$	
	$\kappa_{12} = 0.353$	$\kappa_{13} = 0.351$	$\kappa_{14} = 0.347$	$\kappa_{15} = 0.208$	
	$\kappa_{16} = 0.304$	$\kappa_{17} = 0.257$	$\kappa_{18} = 0.187$	$\kappa_{19} = 0.251$	

real part of the leading exponent for truncated HO feedback control comparing to EDFC, which implies a faster convergence of the nearby trajectories to the desired orbit, and provides more resistance of the stability of the response to the inevitable noise in experimental situations [82].

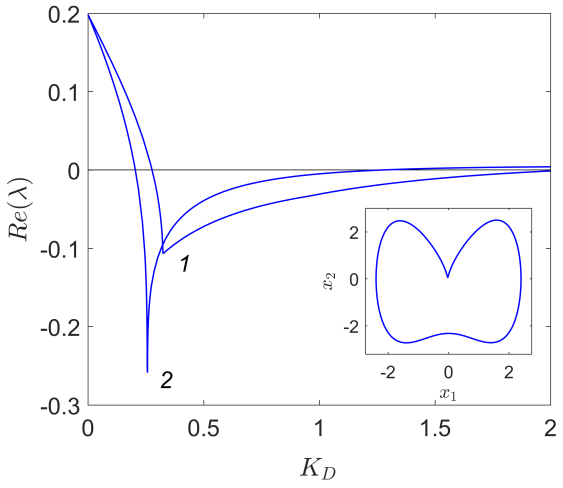

Figure 4.27: The real part of the leading exponent of a period-1 controlled orbit of Duffing oscillator versus the control gain for the coupling strength listed in Tab. (4.2) (1) EDFC (2) HO feedback control, in which $K_H = \frac{2}{1+R} K_D$ and $k = 19$.

4.5.3 Summary

This chapter addressed implementations of the proposed methods of Chapter 3 in practical situations. Section 4.1 demonstrated a successful implementation of HO feedback control in an experimental situation. It proposed an efficient realization of the control method, an demonstrated a successful implementation it by controlling chaotic behavior of an electrical circuit. Section 4.2 demonstrated the capabilities of HO time series analysis in detecting unstable periodic motion from chaotic time series. It revealed that the information obtained from HO time series analysis can be used to control chaos through proportional feedback control. This technique can be considered as a complement to HO feedback control, as it provides valuable information about the frequency content of the unstable orbit, which can be used to simplify the control parameter design of HO feedback control, especially when dealing with torsion free orbits. Section 4.3 addressed stabilizing torsion free orbits of nonautonomous system. It demonstrated that truncated HO feedback control does suffer from the odd number limitation through numerical simulation, and the information obtained from HO time series analysis. Section 4.4 discussed a different but related application of HO synchronization. It investigated the successes of HO transformation in evaluating stability properties of equilibrium and periodic solutions of time delay systems through numerical demonstrations. Finally, the relation between EDFC and HO feedback control was addressed in the context of HO transformation, which verifies the theoretical findings of Chapter 3.

Chapter 5

Contributions, Conclusions, and Future Work

5.1 Overview

This thesis introduced the concept of HO synchronization as a synchronization between a given dynamical system and a system of harmonic oscillators, and addressed its applications in the following areas:

- **Controlling chaos:** This thesis utilized the concept of HO synchronization to develop an innovative method of controlling chaos called HO feedback control. The proposed method employs an invariant manifold of the synchronized system, called HO manifold, to generate the control signal. An attractive property of the HO manifold is the fact that it is defined independently from the underlying dynamics of the chaotic system. To this end, the HO feedback control does not require any information about the dynami-

cal system beyond the period of its unstable orbits to establish the control. This thesis deals with a truncated version of HO feedback control mainly, as it features a simple structure and straightforward practical implementation. The success of the proposed method in controlling chaotic behaviour was demonstrated through numerical simulations and experimental implementations.

- **Time series analysis of chaotic system:** This thesis employed the same concept of synchronization to develop a novel method of detecting unstable periodic motions in chaotic time series. The proposed method is called HO time series analysis. It identifies unstable periodic evolutions embedded in the chaotic attractor based on the deviation of the system from the HO manifold of the synchronized system. It is superior to the previous proposed method as it does not require state space reconstruction, or any analytical knowledge about the system. It detects unstable orbits using only a recorded time history of the system. The capabilities of the HO time series analysis in extracting periodic evolutions were addressed using time series obtained from numerical simulations and experiments. It was revealed that the information obtained from HO time series analysis can be used, directly, to control chaos through PFC, and indirectly, to simplify the control parameter design of the HO feedback control.

- **Analysis of time delay systems:** This thesis proposed a novel transformation of time delay systems to a system of ordinary differential equations, called HO transformation. The proposed transformation replaces the delay coordinate by a system of coupled harmonic oscillators leading to a well-

organized finite dimensional approximation of the original time delay system. An attractive feature of the proposed transformation is its independence from the vector filed describing the system's dynamics, which simplifies its application in a wide range of practical situations. This thesis discussed an application of the HO time series analysis in evaluating stability properties of equilibrium and periodic solutions of time delay systems. The success of the HO time series analysis in linear stability analysis of time delay systems is addressed through numerical simulations and analytical investigations.

- **Relation between EDFC and HO feedback control:** This thesis utilized the HO transformation to study the relation between EDFC and HO feedback control. It revealed that, from a theoretical point of view, the HO feedback control represents a general control system, a subclass of which can be presented by EDFC. However, in practice, only truncated versions of HO control method can be used. An advantage of EDCF over truncated versions of HO feedback control is its convenience experimental realization. On the other hand, EDFC suffers from the odd number limitation, while truncated versions of HO feedback control can over come this limitation by excluding oscillators with negligible amplitudes from the feedback loop without changing the configuration of the target orbit.

5.2 List of Contributions

The main contributions of this thesis are listed as follows:

1. **HO feedback control:** This thesis proposed an innovative approach in con-

trolling chaos by synchronizing of the chaotic system with a linear system of harmonic oscillators. The proposed approach does not require any information about the chaotic system beyond the period of its unstable orbits to establish the control. It has simple structure that facilitates the theoretical investigations, as well as practical implementations.

2. **HO time series analysis:** This thesis developed a novel method of detecting unstable periodic motions in a chaotic time series using only a single time history of the system. It is a numerically efficient and practically effective method of extracting information about periodic evolutions embedded in chaotic attractors, which can be used in both theoretical investigations and practical applications.

3. **HO transformation:** This thesis proposed an effective transformation of a time delay system to a finite dimensional approximation through a well-organized system of coupled harmonic oscillators. The transformed system has a simple structure that simplifies analysis of time delay systems through the well-established methods and procedure developed for finite dimensional systems.

4. **Odd Number limitation:** This thesis addressed the odd number limitation of time delayed feedback methods using the HO transformation. It explained this limitation from a new perspective, and proposed an effective approach to overcome this limitation using the truncated HO feedback control.

5.3 Answers to the Research Questions

This section addresses the research questions outlined in section 1.2.3 through the findings and the results presented in Chapters 3 and 4, and provides insight into the potential future research.

The relation between HO feedback control and the previously proposed method, as pointed out by questions (1) and (2) is explained . The HO feedback control proposed in this thesis belongs to the continuous methods of controlling chaos, and therefore, does not suffer from the inherent limitations of discrete methods. This method is less sensitive to the level of noise as compared to OGY and OPF methods, and it benefits from the fact that the control rule is valid all over the state space. In contrast to PCF method, the HO feedback control does not require any information about the dynamical system beyond the period of its unstable orbits to establish the control, which makes it attractive for experimental implementations. Compared DFC, the HO feedback control features a simple structure, which allows straightforward theoretical investigations and numerical evaluations of the control performance. Although an effective approach of experimental realization of the HO feedback control is proposed, this method of control requires high level of computational resources, especially when dealing with fast dynamical systems with complex structures. From this perspective, DFC is superior to the truncated HO feedback control, as it features a simple experimental realization through analogue hardware. The proposed method has a desirable filtering properties that allows suppressing any desired frequency from the signal, and therefore, it is superior to NFFC that only filters out the fundamental

frequency of the target orbit.

Question (3) asks about important factors that quantify the performance of the controller. An important factor that characterizes the performance of a controller is the stability properties of the target orbit. Taking into account that the truncated HO feedback control is able to treat each harmonic oscillator individually suggests that the orbits controlled by this method feature a wider range of stability properties. In addition, the HO feedback control has the flexibility of excluding any desirable frequency from the feedback loop, which allows stabilizing torsion free orbits of nonautonomous systems by excluding high frequency oscillators from the feedback loop.

As pointed out by question (4), and effective chaos control method is a noninvasive. This property of HO feedback control is addressed through its relation with delay feedback control method. The relation between EDFC and the truncated HO feedback control was addressed in more details using HO transformation. Theoretical investigations revealed that EDFC represents a subclass of HO feedback control in which the control loop consists of infinite number of harmonics oscillators coupled through identical gains. However, in practice, only the first few frequency components determine the coordinates of the target orbit on the state space, which suggests that the truncated HO feedback control can also be classified as a noninvasive method.

Question (5) asks about the capabilities of HO feedback control in controlling real word physical systems. Section 4.2.1 revealed that the HO feedback control is an effective method of control chaos in practical situations, where the

proposed method was successfully implemented to control chaotic behavior of electrical circuit.

The limitations of HO feedback control and the proposed resolutions are the concerns of questions (6) and (7). A limitation of HO feedback control is the fact that this method requires high level of computational resources, when dealing with fast dynamical systems. To improve the performance of the proposed method, the information obtained for the HO time series analysis can be incorporated into the design process of the controller, as it provides valuable information about the frequency content of the target orbit. Another practical way of improving the control performance is to realize the proposed control method thorough analogue hardware, which makes it suitable to control fast dynamical systems.

5.4 Limitations and Proposed Resolutions

This thesis contributes to the area of control and analysis of chaotic systems, as well as develops an effective transformation that simplifies analysis of time delay systems. It addressed several theoretical and practical aspects of the proposed methods. However, some limitations still exist, and some areas require further developments, as listed as follows:

1. This thesis investigated the performance of the HO synchronization in the context of periodic evolutions. A potential extension of the present work is to investigate the application of the HO synchronization in the context of aperiodic evolutions such quasi-periodic or chaotic motions.

2. It was revealed the unstable periodic evolutions of chaotic systems can be

presented effectively through the HO manifold of the synchronized system. The HO time series analysis utilizes this fact to extract unstable periodic orbits embedded in chaotic attractors. This motivates the idea of extracting other properties of chaotic systems such as Lyaponov exponents or fractal dimensions of the chaotic attractor utilizing the same concept of synchronization, as the synchronized system represents the same set of unstable periodic orbits.

3. From a practical point of view, The Ho feedback control suffers from the fact that it requires high level of computational resources, when dealing with fast dynamical systems. An important extension of the present work includes developing an efficient computational strategy, or analogue hardware though which the HO feedback control can be implemented reliably and effectively.

4. HO transformation proposed in this thesis provides convenient tool to conduct linear stability analysis of periodic solutions of time delay systems. Investigating the application of HO transformation in evaluating nonlinear properties of the time delay systems though effective tools such as Lyapunov's direct method can be a subject of a new research project.

5. This thesis focuses mainly on truncated versions of HO feedback control, as the full version suffers from the complex structure due to the existence of delay coordinates in its structure. An interesting extension of the present work is to investigate the stabilizing properties of the full version of HO feedback control, as well as its experimental implementation by discretizing the delay coordinate through the HO transformation.

References

[1] Edward Norton Lorenz, "Deterministic nonperiodic flow," *Journal of the Atmospheric Science*, vol. 20, no. 2, pp. 130-141, March 1963.

[2] Edward Norton Lorenz, "Predictability: Does the flap of a butterfly's Wings in Brazil set off a tornado in Texas?, in "*139th meeting of the American Association for the Advancement of Science*, (Washington, D.C., December 29, 1972), 1972.

[3] Edward Norton Lorenz, The Essence of Chaos. London: UCL Press, UK, 1995, 221 pp. ISBN 1-85728-454-2.

[4] Ayub Ofulla, The Secrets of Hidden Knowledge: How Understanding Things in The Physical Realm Nurtures Life. Bloomington: Abbott Press, United States of America 2013, 546 pp. ISBN 978-1458209313.

[5] Edward Ott, Celcio Grebogi and James Alan Yorke, "Controlling chaos," *Physical Review Letters*, vol. 64, no. 11, pp. 1196-1199, March 1990.

[6] Stefano Boccaletti, Jürgen Kurths, Gennday Osipov, D. L. Valladares, and Diego Maza, "The control of chaos: theory and applications," *Physics Re-*

ports, vol. 329, no. 3, pp. 103-197, May 2000.

[7] Kestutis Pyragas, "Continuous control of chaos by self-controlling feedback," *Physics Letters A*, vol. 170, no. 6, pp. 421-428, October 1992.

[8] Wolfram Just, Thomas Bernard, Matthias Ostheimer, Ekkehard Reibold, and Hartmut Benner, "Mechanism of time-delayed feedback control," *Physical Review Letters*, vol. 78, no. 2, pp. 203-206, January 1997.

[9] Hiroyuki Nakajima, "On analytical properties of delayed feedback control of chaos," *Physics Letters A*, vol. 232, no. 3-4, pp. 207-210, July 1997.

[10] Alexander Ahlborn and Ulrich Parlitz, "Chaos control using notch filter feedback," *Physical Review Letters*, vol. 96, no. 3, pp. 034102(1-4), January 2006.

[11] Eckehard Schöll and Heinz Goerg Schuster, Hand Book of Chaos Control. Weinheim: Wiley-VCH Verlag GmbH & Co. KGaA, Germany, 2007, 849 pp. ISBN 978-3-527-40605-0.

[12] Erik Lindberg, K. Murali, and Arunas Tamasevicius, "The smallest transistor-based nonautonomous chaotic circuit", *IEEE Transactions on Circuits and Systems II: Express Briefs*, vol. 52, no. 10, pp. 661-664, October, 2005.

[13] Yuri Kuznetsov, Elements of Applied Bifurcation Theory. New York: Springer-Verlag, USA, 2004, 634 pp. ISBN 978-1-4419-1951-9.

[14] John Earman, "How determinism can fail in classical physics and how quantum physics can (sometimes) provide a cure," *Philosophy of Science*, vol. 75, no. 5, pp. 817-829, December 2008.

[15] Nicola Bellomo and Riccardo Riganti, Nonlinear Stochastic Systems in Physics and Mechanics. Singapore: World Scientific Publishing Co., Singapore, 1987, 244 pp. ISBN 9971-50-249-6.

[16] Aleksandr Mikhailovich Lyapunov, "The general problem of the stability of motion," *International Journal of Control*, vol. 55, no. 3, pp. 531-773, June 1992.

[17] Henry Poincaré, Les Méthodes Nouvelles de la Mécanique Céleste, Tome I. Gauthier-Villars et Fils, Paris, 1892.

[18] Ali Hassan Nayfeh and Balakumar Balachandran, Applied Nonlinear Dynamics, Analytical, Computational, and Experimental methods. Weinheim: Wiley-VCH Verlag GmbH & Co. KGaA, Germany, 2004, 685 pp. ISBN 0-471-59348-6.

[19] Jean-Jacques Slotine and Weiping Li, Applied Nonlinear Control. New Jersey: Printice Hall, USA, 1991, 461 pp. ISBN 0-13-040890-5.

[20] Hassan Khalil, Nonlinear Systems. New Jersey: Prentice Hall, USA, 2002, 750 pp. ISBN 0-13-067389-7.

[21] Stephen Wiggins, Introduction to Applied Nonlinear Dynamical Systems and Chaos. New York: Springer-Verlag, USA, 2003, 843 pp. ISBN 0-387-00177-8.

[22] Gaston Floquet, "Sur les équations différentielles linéaires à coefficients périodiques," *Annales de l'École Normale Supérieure*, vol. 12, pp. 47-84, 1883.

[23] , Zengqiang Chen, Yong Yang, Guoyuan Qi, and Zhuzhi Yuan "A novel hyperchaos system only with one equilibrium," *Physics Letters A*, vol. 360, no. 6, pp. 696-701, January 2007.

[24] Tamas Tel and Marton Gruiz, Chaotic Dynamics: An Introduction Based on Classical Mechanics. New York: Cambridge University Press, USA, 2006, 393 pp. ISBN 0-511-33504-0.

[25] Steven Henry Strogatz, Nonlinear Dynamics and Chaos: with Applications to Physics, Biology, Chemistry, and Engineering. New York: Perseus Books Publishing, USA, 1994, 498 pp. ISBN 0-201-54344-3.

[26] Witold Kinsner, "A unified approach to fractal dimensions," in *Proc. of the Fourth IEEE International Conference on Cognitive Informatics*, (Irvine, CA; August 8-10, 2005), pp. 58-72, 2005.

[27] David Ruelle and Floris Takens, "On the Nature of Turbulence," *Communications in Mathematical Physics*, vol. 20, no. 3, pp. 167-192, September 1971.

[28] Celso Grebigi,Edward Ott, Steven Pelikan, and James Yorke, "Strange attractors that are not chaotic," *Physica D: Nonlinear Phenomena*, vol. 13, no. 2, pp. 261-268, August 1984.

[29] Parsad Awadhesh, Negi Surendra Singh, and Ramaswamy Ramakrishna, "Strange nonchaotic attractor," *International Journal of Bifurcation & Chaos in Applied Sciences and Engineering*, vol. 11, no. 2, pp. 291-309, February 2001.

[30] Silke Steingrube, Marc Timme, Florentin Worgotter, and Poramate Manoonpong "Self-organized adaptation of a simple neural circuit enables complex robot behavior," *Nature Physics*, vol. 6, no. 3, pp. 224-230, March 2010.

[31] Ali Azimi Olyaei and Mohammad Reza Ghazavi, "Stabilizing slider-crank mechanism with clearance joints," *Mechanism and Machine Theory*, vol. 53, no. 1, pp. 17-29, February 2012.

[32] Farhad Farahanchi and Steven Shaw, "Chaotic and periodic dynamics of a slider-crank mechanism with slider clearance," *Journal of Sound and Vibration*, vol. 177, no. 3, pp. 307-324, October 1994.

[33] Y. S. Yoon, J. S. Shim, S. B. Lee, and Kenneth Willmert, "Reduction of the joint clearance effect for a planar flexible mechanism," *Journal of Mechanical Science and Technology*, vol. 9, no. 3, pp. 312-322, September 1995.

[34] Floris Takens, "Detecting strange attractor in turbulence," in [83], pp. 366-381, 1981.

[35] William Ditto, Steven Rauseo, and Mark Spano, "Experimental control of chaos," *Physical Review Letters*, vol. 65, no. 26, pp. 3211-3214, December 1990.

[36] Edward Ott and Mark Spano, "Controlling chaos," *Physics Today*, vol. 48, no. 5, pp. 34-40, May, 1995.

[37] Troy Shinbrot, Edward Ott, Celso Grebogi, and James York, "Using chaos to direct trajectories to target," *Physical Review Letters*, vol. 65, no. 26, pp. 3215-3218, December 1990.

[38] Ricardo Lima and Marco Pettini, "Suppression of chaos by resonant parametric perturbations", *Physical Review A*, vol. 41, no. 2, pp. 726-733, January 1990.

[39] Alexander Frankov, Robin Evans, and Boris Andrievsky, "Control of chaos: methods and applications in mechanics," *Philosophical Transactions of the Royal Society*, vol. 364, no. 1846, pp. 2279-2307, July 2006.

[40] E. R. Hunt, "Stabilizing high-period orbits in a chaotic system: the diode resonator," *Physical Review Letters*, vol. 67, no. 15, pp. 1953-1955, October 1991.

[41] Joshua Socolar, David Sukow, and Daniel Gauthier, "Stabilizing unstable periodic orbit in fast dynamical systems," *Physical Review E*, vol. 50, no. 4, pp. 3245-3248, October 1994.

[42] Achim Kittel, Jürgen Parisi, and Kestutis Pyragas, "Delayed feedback control of chaos by self-adapted delay time," *Physics Letters A*, vol. 198, no. 5-6, pp. 433-436, March 1995.

[43] Klaus Hohne, Hiroyuki Shirahama, Chol-Ung Choe, Hartmut Benner, Kestutis Pyragas, and Wolfram Just, "Global Properties in an experimental realization of time delayed feedback control with an unstable control loop," *Physical Review Letters*, vol. 98, no. 21, pp. 214102(1-4), May 2007.

[44] Dennis Tweten and Brian Mann, "Spectral element method and delayed feedback control of chaos," *Physical Review E*, vol. 86, no. 4, pp. 046214 (1-7), October 2012.

[45] Hiroyuki Nakajima and Yoshisuke Ueda "Limitation of generalized delayed feedback control," *Physica D*, vol. 111, no. 1-4, pp. 143-150, January 1998.

[46] Hiroyuki Nakajima and Yoshisuke Ueda "Half-period delayed feedback control for dynamical systems with symmetry," *Physical review E*, vol. 58, no. 2, pp. 1757-1763, August 1998.

[47] Kestutis Pyragas, "Control of chaos via an unstable delayed feedback controller," *Physical Review Letters*, vol. 86, no. 11, pp. 2265-2268, March 2001.

[48] Arunas Tamasevicius, Gytis Mykolaitis, Viktoras Pyragas, and Kestutis Pyragas, "Delayed feedback control of periodic orbits without torsion in nonautonomous chaotic systems: theory and experiment," *Physical Review E*, vol. 76, no. 2, pp. 026203 (1-6), August 2007.

[49] Bernold Fiedler, Valentin, Michael Georgi, Philipp Hövel, and Eckehard Schöll, "Refuting the odd-number limitation of time-delayed feedback control," *Physical Review Letters*, vol. 98, no. 11, pp. 114101 (1-4), March 2007.

[50] Edward Hooton and Andreas Amann, "Analytical limitation for time-delayed feedback control in autonomous systems," *Physical Review Letters*, vol. 109, no. 15, pp. 154101 (1-5), October 2012.

[51] Kestutis Pyragas and Viktor Novicenko "Time-delayed feedback control design beyond the odd-number limitation," *Physical Review E*, vol. 88, no. 1, pp. 012903 (1-6), July 2013.

[52] Walter Grantham and Amit Athalye, "Notch filter feedback control for k-period motion in a chaotic system," in [JMTL97], pp. 142-157, 1997.

[53] Ulrich Tietze, Christoph Schenk, and Eberhard Gamm, ELECTRIC CIRCUIT: HANDBOOK FOR DESIGN AND APPLICATION. New York: Springer-Verlag, USA, 2004, 1523 pp. ISBN 978-3-540-78655-9.

[54] Iliya Blekhman, Alexander L'vovich Fradkov, Henk Nijmeijer, and Alexander Yu Pogtomsky "On self-synchronization and controlled synchronization," *Systems & Control Letters*, vol. 31, no. 5, pp. 299-305, August 1997.

[55] Alejandro Rodriguez Angeles, SYNCHRONIZATION OF MECHANICAL SYSTEMS. Eindhoven: University Press Facilities, Netherlands, 2002, 158 pp. ISBN 90-389-2634-7.

[56] Kevin Cuomo and Alan victor Oppenheim, "Circuit implementation of synchronized chaos with application to communications," *Physical Review Letters*, vol. 71, no. 11, pp. 65-68, November 1993.

[57] Stefano Boccaletti, Celcio Grebogi, Ying-Cheng Lai, Hector Mancini, and C. S. Zhou "The synchronization of chaotic systems," *Physics Reports*, vol. 366, no. 1-2, pp. 1-102, August 2002.

[58] Louis Peccora and Thomas Carroll, "Synchronization in chaotic systems," *Physical Review Letters*, vol. 64, no. 8, pp. 821-825, February 1990.

[59] Michael Rosenblum, Arkady Pikovsky, and Jürgen Kurths "Phase synchronization of chaotic oscillators," *Physical Review Letters*, vol. 76, no. 11, pp. 1804-1807, March 1996.

[60] Michael Rosenblum, Arkady Pikovsky, and Jürgen Kurths, "From phase to lag synchronization in coupled chaotic oscillators," *Physical Review Letters*, vol. 78, no. 22, pp. 4193-4196, June 1996.

[61] Nikolai Rulkov, Mikhail Sushchik, Lev Tsimring, and Henry Abarbanel "Generalized synchronization of chaos in directionally coupled chaotic systems," *Physical Review E*, vol. 51, no. 2, pp. 980-994, February 1995.

[62] Michael Zaks, Eun-Hyoung Park, Michael Rosenblum, and Jürgen Kurths, "Alternating locking ratios in imperfect phase synchronization," *Physical Review Letters*, vol. 82, no. 21, pp. 4228-4231, May 1999.

[63] Stefano Boccaletti and D. L. Valladares, "Characterization of intermittent lag synchronization," *Physical Review E*, vol. 62, no. 5, pp. 7497-7500, November 2000.

[64] Arieh Iserles and Syvert Norsett, "From high oscillation to rapid approximation I: modified Fourier expansions," *IMA Journal of Numerical Analysis*, vol. 28, no. 4, pp. 862-887, April 2008.

[65] Ditaz Auerbach, Predrag Cvitanovic, Jean-Pierre Eckmann, Gemunu Gunaratne, and Itamar Procaccia, "Exploring chaotic motion through periodic orbits," *Physical Review Letters*, vol. 58, no. 23, pp. 2387-2389, June 1987.

[66] Daniel Lathrop and Eric Kostelich, "Characterization of an experimental strange attractor by periodic orbits," *Physical Review A*, vol. 40, no. 7, pp. 4028-4031, October 1989.

[67] Paul So, Edward Ott, Steven Schiff, Daniel, Kaplan, Tim Sauser, Celso

Grebogi, "Detecting unstable periodic orbits in chaotic experimental data," *Physical Review Letters*, vol. 76, no. 25, pp. 4705-4708, June 1996.

[68] Paul So, Edward Ott, Tim Sauser, Bruce Gluckman, Celso Grebogi, Steven Schiff "Extracting unstable periodic orbits from chaotic time series data," *Physical Review E*, vol. 55, no. 5, pp. 5398-5417, May 1997.

[69] Huanfei Ma, Wei Lin, and Ying-Cheng Lai, "Detecting unstable periodic orbits in high-dimensional chaotic systems from time series: Reconstruction meeting with adaptation," *Physics Review E*, vol. 87, no. 5, pp. 050901R(1-5), May 2013.

[70] Zhong-Ke Gao and Ning-De Jin, "A directed weighted complex network for characterizing chaotic dynamics from time series," *Nonlinear analysis: Real World Applications*, vol. 13, no. 2, pp. 947-952, April 2012.

[71] David Walker and Micheal Small, "Detecting unstable fixed points using Kalman filters with constraints," *IEEE transactions on circuits and systems I*, vol. 53, no. 12, pp. 2818-2827, December 2006.

[72] Tamas Insperger and Gabor Stepan, "Semi-discretization method for delayed systems," *International Journal for Numerical Methods in Engineering*, vol. 55, no. 5, pp. 503-518, October 2002.

[73] Nitin Garg, Brian Mann, Nam Kim, and Mohammad Kurdi, "Stability of a time-delyaed system with parametric excitation," *Journal of Dynamic Systems, Measurement, and Control*, vol. 129, no. 2, pp. 125-135, May 2006.

[74] Jian-Qiao Sun, "A method of continuous time approximation of delayed

dynamical systems," *Communications in Nonlinear Science and Numerical Simulations*, vol. 14, no. 4, pp. 998-1007, April 2009.

[75] Anwar Sadath and C. P. Vyasarayani, "Galerkin approximations for stability of delay differential equations with time periodic coefficients," *Journal of Computational and Nonlinear Dynamics*, vol. 10, no. 2, pp. 0210111(1-7), March 2015.

[76] David Bailey, Jonathan Borwein, Neil Calkin, Russell Luke, Roland Girgensohn, and Victor Moll, Experimental Mathematics in Action. Boca Raton: CRC Press, USA, 2007, 337 pp. ISBN 978-1-568-81271-7.

[77] Henri Padé, "Sur la repr´esentation approch´ee d'une fonction pour des fractions rationelles," Annales Scientifiques De l'École Normale Supérieure, vol. 9, no. 1, pp. 1-93, 1892.

[78] George Baker and Peter Graves-Morris, Padé Approximation.: New York, Cambridge University Press, USA, 1996, 746 pp. ISBN 978-0-521-45007-2.

[79] Viktoras Pyragas and Kestutis Pyragas, "Relation between the extended time-delayed feedback control algorithm and the method of harmonic oscillators" *Physical Review E*, vol. 92, no. 2, pp. 022925(1-7), August 2015.

[80] J. A. Nelder and R. Mead "A simplex method for function minimization," *The Computer Journal*, vol. 7, no. 4, pp. 308-313, April 1965.

[81] Thomas Erneux, Tamas Kalmar-Nagy, "Nonlinear stability of a delayed feedback controlled container crane," *Journal of Vibration and Control*, vol. 13, no. 5, pp. 603-616, May 2007.

[82] Kestutis Pyragas, "Controlling chaos via extended delay feedback," *Physics Letters A*, vol. 206, no. 6, pp. 323-330, October 1995.

[83] David Anthony James and Lia-Sang Young (eds.), Dynamical System and Turbulence, Warwinck 1980. New York: Springer-Verlag, USA, 1981, 390 pp. ISBN 978-3-540-11171-9.

[84] Kevin Judd, Alistair Mees , Kok Lay Teo, and Thomas Vincent (eds.), Chaos and Control. Boston: Birkhauser, USA, 1997, 333 pp. ISBN 978-1-4612-7540-4.

[85] M. Biehler, "Sur une classe d'équations algébriques dont toutes les racines sont réelles ," *Journal für die Reine und Angewandte Mathematik*, vol. 87, pp. 350-352, 1879.

[86] C. Hermite, "Sur les nombre des racines d'une équation algébrique comprise entre des limites données," *Journal für die Reine und Angewandte Mathematik*, vol. 52, pp. 39-51, 1856.

[87] Ming-Tzu Ho, Aniruddha Datta, and S. P. Bhattacharyya, "Generalization of the Hermite-Biehler theorem," *Linear Algebra and its Applications*, vol. 303, no. 12, pp. 135-153, December 1999.

[88] Jefrrey Lagarias, James Reeds, Margaret Wright, and Paul Wright, "Convergence properties of the Neldwer-Mead simplex method in low dimensions," *SIAM Journal of Optimization*, vol. 9, no. 1, pp. 112-147, January 1998.

[89] Robert Devaney, An Introduction to Chaotic Dynamical Systems. Cambridge, Massachusetts: Westview Press., USA, 2003, 335 pp. ISBN

978-0-813-34085-2.

[90] Annalisa Crannell, "The role of transitivity in Devaney's definition of chaos," *The American Mathematical Monthly*, vol. 102, no. 9, pp. 788-793, November 1995.

[91] J. Banks, J. Brooks, G. Cairns, G. Davis, and P. Stacey, "On Devaney's Definition of Chaos.," *The American Mathematical Monthly*, vol. 99, no. 4, pp. 332-334, April 1992.

Reference Span

1856-1899	1990-1994	1995-1999	2000-2004	2005-2009	2010-2016
15	14	22	13	17	10

Appendix A

Boundedness of the Response

This appendix provides the proof of the results presented in section 3.3, which includes the necessary condition imposed on the coupling matrices $\mathbf{K}_n$ to guarantee a bounded response of the controlled system. Suppose that Ψ in Eq.(3.17) is a diagonalizable matrix, which can be written as

$$\Psi = \mathbf{P}_\Psi \Lambda {\mathbf{P}_\Psi}^{-1} \tag{A.1}$$

Here, $\mathbf{P}_\Psi$ is a matrix whose columns are the right eigenvectors of Ψ, and Λ is a diagonal matrix whose the m^{th} diagonal element λ_{Ψ_m} is the eigenvalues of Ψ corresponding to the m^{th} column of $\mathbf{P}_\Psi$. Introducing a new variable $\mathbf{C} = \mathbf{P}_\Psi \mathbf{A}$ leads to the following scalar equation:

$$\dot{C}_m = \lambda_{\Psi_m} C_m + \sum_{l=1}^{D\times D_\mathbb{U}} \sum_{j=1}^{D} {\mathbf{P}_\Psi}^{-1}{}_{ml} \, \mathbf{K}_{lj} \mathbf{x}_j, \tag{A.2}$$

where C_m is the m^{th} component of the vector $\mathbf{C}$, and $D_\mathbb{U}$ is the cardinality of the set $\mathbb{U}$. The solution to Eq. (A.2) can be found as

$$C_m(t) = e^{\lambda_{\Psi_m}(t-t_0)} C_m(t_0) + \int_{t_0}^{t} e^{\lambda_{\Psi_m}(t-\tau)} \sum_{l=1}^{D\times D_\mathbb{U}} \sum_{j=1}^{D} {\mathbf{P}_\Psi}^{-1}{}_{ml} \, \mathbf{K}_{lj} \mathbf{x}_j(\tau) \, \mathrm{d}\tau. \tag{A.3}$$

For $\mathrm{Re}(\lambda_{\Psi_m}) > 0$, C_m is unbounded as $t \to \infty$. However, for $\mathrm{Re}(\lambda_{\Psi_m}) < 0$, an upper limit for C_m can be found as

$$|C_m(t)| \leq |C_m(t_0)| + \frac{1}{|\lambda_{\Psi_m}|} \sum_{j=1}^{D} \sum_{l=1}^{D \times D_{\mathbb{U}}} |{\mathbf{P}_\Psi}^{-1}{}_{ml}||\mathbf{K}_{lj}| M_j, \tag{A.4}$$

where M_j is a positive number such that $|\mathbf{x}_j| \leqslant M_j$. Additionally, for $\mathrm{Re}(\lambda_{\Psi_m}) < 0$, Eq. $(A.3)$ implies that the effect of the initial condition $C_m(t_0)$ on the steady state motion vanishes, as $t \to \infty$.

Equation $(A.5)$ defines the m^{th} eigenvector of matrix Ψ, and the corresponding eigenvalue λ_{Ψ_m} as

$$\left(im\omega - \lambda_{\Psi_m}\right) \mathbf{P}_{\Psi ml} - \mathbf{K}_m \sum_{n \in \mathbb{U}} \mathbf{P}_{\Psi nl} = 0, \qquad l = 1, \ldots, D \times D_{\mathbb{U}} \tag{A.5}$$

Assuming $\lambda_{\Psi_m} \neq im\omega$, the eigenvalue problem can be solved for $\mathbf{P}_{\Psi ml}$ as

$$\mathbf{P}_{\Psi ml} = \frac{\mathbf{K}_m}{\lambda_{\Psi_m} - im\omega} \mathbf{F}_l \tag{A.6}$$

Here, $\mathbf{F}_l$ is a constant vector. Substituting Eq. (A.6) into Eq. (A.5) yields the following homogeneous algebraic equation for vector $\mathbf{F}_l$:

$$\left(\mathbf{I} + \sum_{n \in \mathbb{U}} \frac{\mathbf{K}_n}{\lambda_{\Psi_m} - in\omega}\right) \mathbf{F}_l = 0 \tag{A.7}$$

In order to avoid the trivial solution $\mathbf{F}_l = 0$, the determent of the coefficient matrix needs to be zero.

$$\det\left(\mathbf{I} + \sum_{n \in \mathbb{U}} \frac{\mathbf{K}_n}{\lambda_{\Psi_m} - in\omega}\right) = 0 \tag{A.8}$$

Equation $(A.8)$ defines the eigenvalues of matrix Ψ. A successful synchronization requires $\mathbf{K}_n$ to be determined such that $Re(\lambda_{\Psi_m}) < 0$.

In many practical situations, only a single state of the system is available. In this situation, coupling matrix $\mathbf{K}_n$ consists of only a single diagonal element

corresponding to the valuable state, denoted by κ_n. If κ_n is chosen to be a real number, the boundedness condition leads to a simpler criteria. Here, the results are presented for $\mathbb{U} = \{m \mid m \in \mathbb{Z}, -k \leq m \leq k\}$, which can easily be extended to a more general set $\mathbb{U}$. The boundedness condition is satisfied, if and only if,

$$\begin{cases} \kappa_m \times \kappa_{m+1} > 0, & m \neq 0 \\ \kappa_0 > 0 \\ \sum_{m=-k}^{k} \kappa_m > 0 \end{cases} \tag{A.9}$$

This is a useful result specially when designing a controller in experimental situations.

The condition given by Eq. (A.9) can be proven using Hermite-Biehler theorem [85, 86]. This appendix follows the description of this theorem as presented in [87]. For scalar coupling strength κ_n, Eq. (A.8) can be written in a polynomial form with real coefficients as follows:

$$\lambda_\Psi \prod_{n=1}^{k} \left({\lambda_\Psi}^2 + n^2\omega^2 \right) + \kappa_0 \prod_{n=1}^{k} \left({\lambda_\Psi}^2 + n^2\omega^2 \right) + \sum_{n=1}^{k} 2{\lambda_\Psi}^2 \kappa_n \prod_{\substack{m=1 \\ m\neq n}}^{k} \left({\lambda_\Psi}^2 + m^2\omega^2 \right) = 0. \tag{A.10}$$

Equation (A.10) can be cast into $\lambda_\Psi \delta_o({\lambda_\Psi}^2) + \delta_e({\lambda_\Psi}^2) = 0$, where $\lambda_\Psi \delta_o({\lambda_\Psi}^2)$ and $\delta_e({\lambda_\Psi}^2)$ are made up of odd and even powers of λ_Ψ, respectively. According to Hermit-Biehler theorem, the roots of Eq. (A.10) are all located on the left side of the complex plane if and only if, (i) the roots of $\lambda_\Psi \delta_o(-{\lambda_\Psi}^2)$ and $\delta_e(-{\lambda_\Psi}^2)$ have simple real interlacing roots, and (ii) the coefficients of the characteristic equation are all of the same sign. Notice that the polynomial $\delta_o(-{\lambda_\Psi}^2)$ has exactly $2k+1$

roots described by

$$\lambda_{\Psi_{o_n}} = n\omega, \qquad n = -k, \cdots, k \tag{A.11}$$

The roots of the polynomial $\delta_e(-{\lambda_\Psi}^2)$ are located between the successive roots of $\delta_o(-{\lambda_\Psi}^2)$, if and only if $\delta_e(-{\lambda_{\Psi_{o_p}}}^2) \times \delta_e(-\lambda^2_{\Psi_{o_{p+1}}}) < 0$ where $p = -k, \cdots, k-1$.

$$\delta_e(-{\lambda_{\Psi_{o_p}}}^2) = p^2\omega^2\kappa_p \prod_{\substack{m=1 \\ m\neq p}}^{k} \left(m^2 - p^2\right)\omega^2 \tag{A.12}$$

$$\delta_e(-\lambda^2_{\Psi_{o_{p+1}}}) = (p+1)^2\omega^2\kappa_{p+1} \prod_{\substack{m=1 \\ m\neq p+1}}^{k} \left(m^2 - (p+1)^2\right)\omega^2. \tag{A.13}$$

The condition $\delta_e(-{\lambda_{\Psi_{o_p}}}^2)\times\delta_e(-\lambda^2_{\Psi_{o_{p+1}}}) < 0$ is satisfied, if and only if $\kappa_p \times \kappa_{p+1} > 0$, which is the first condition of Eq. (A.9).

Referring to Eq. (A.10), The second condition requires $\kappa_0 > 0$ since the constant term $\kappa_0 \prod_{n=1}^{k} n^2\omega^2$ needs to be positive, which is the second condition of Eq. (A.9).

To prove the third condition, Eq. (A.2) is written as

$$\left(\lambda_\Psi + \kappa_0 + 2\sum_{n=1}^{k}\kappa_n\right)\prod_{n=1}^{k}\left({\lambda_\Psi}^2 + n^2\omega^2\right) - \sum_{n=1}^{k} 2\kappa_n n^2\omega^2 \prod_{\substack{m=1 \\ m\neq n}}^{k}\left({\lambda_\Psi}^2 + m^2\omega^2\right). \tag{A.14}$$

Considering the first two conditions of Eq. (A.9), all the coefficients of Eq. (A.10) are of the same sign, if an only if $\kappa_0 + 2\sum_{n=1}^{k}\kappa_n > 0$, which is the third condition of Eq. (A.9).

Appendix B

Nelder-Mead Simplex Algorithm

Nelder-Mead simplex algorithm is an efficient direct search algorithm for unconstraint minimization of a scalar function of several real variables. It is an iterative method of minimization that starts with an initial estimate of the function minimizer and updates it through a set of simple transformation of reflection, expansion, contraction, and shrinkage at each iteration [88]. Suppose that the problem evolves a d dimensional vector of variables. The Nelder-Mead algorithm starts with a simplex in a d dimensional space, along with $d+1$ vertices, each of which is a point in the d dimensional space. The initial simplex is formed by creating d points around the initial estimate of the function minimizer along the each axis spanning the d dimensional space. At each iteration, it generates an new point trough the aforementioned transformations, and compares the function value at the new point with the function values at the vertices of the current simplex. At the end of the iteration, it generates a new simplex by replacing one of the vertices by a new point. The process is repeated until the radius of the

simplex is smaller that a prescribed threshold, or the function values are close to each other at the end of two consecutive iterations.

The Nelder-Mead simplex algorithm is a numerically efficient algorithm, as each iteration requires small number of function evaluations. Furthermore, it does not require any information about the derivative of the function in the minimization process. This algorithm is practically effective when designing the parameter of the HO feedback control through minimizing the real part of leading exponent of the controlled orbit. This problem can be formulated as the minimization of a scalar function that returns the real part of the leading exponent as a function of control parameters K_H and κ_n. The minimization process is illustrated in Fig. $B.1$. The function describing the real part of the leading exponent of the control system is identified by the dashed rectangle.

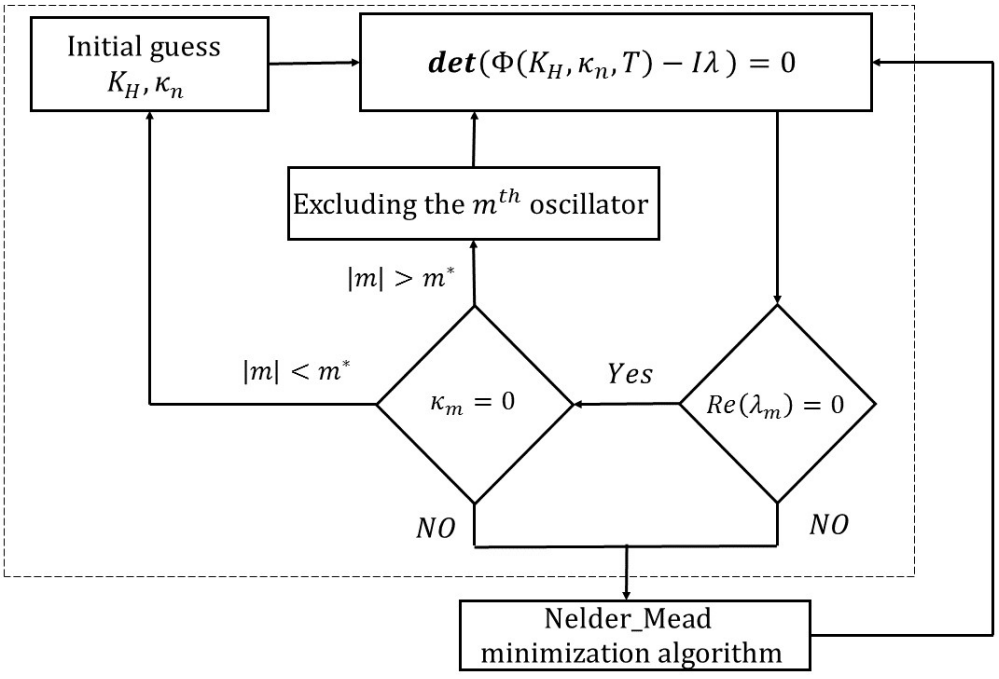

Figure B.1: Minimization algorithm of the real part of the leading exponent of controlled orbit. m^* denotes a prescribed limit of the desired frequency range.

Appendix C

Supplementary Figures

C.1 Introduction

This appendix includes supplementary figure of the experiment explained in Sec. 4.2.1, ion which, the chaotic behavior of the electrical circuit shown in Fig. C.1 is controlled. This circuit is an adaptation of the electrical chaotic circuit described in [12], whose electrical element are designed such that circuit exhibits chaotic behavior for lower frequency of the input voltage.

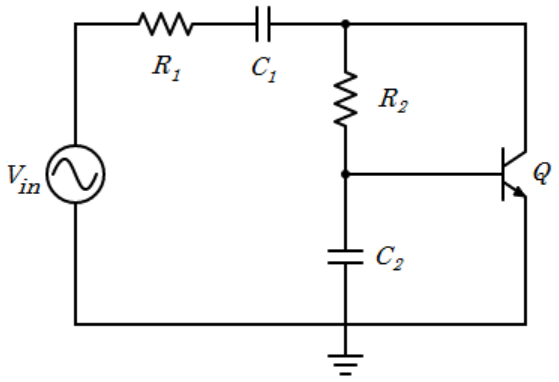

Figure C.1: The smallest transistor-based chaotic circuit. $V_{in} = 4.5V/60Hz$, $R1 = 100$, $C1 = 136nF$, $R2 = 820k$, $C2 = 136nF$, and $Q = 2N2222A$.

C.2 Implementation

The actual circuit, along with the specification of each component, is illustrated in Fig. C.2.

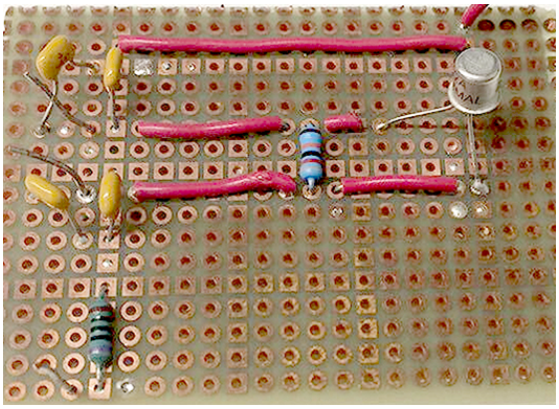

Figure C.2: The smallest transistor-based chaotic circuit. $V_{in} = 4.5V/60Hz$, $R1 = 100$, $C1 = 136nF$, $R2 = 820k$, $C2 = 136nF$, and $Q = 2N2222A$.

Figure C.2 represents an oscilloscope screenshot of a two dimensional projection of the chaotic attractor for $V_{in} = 4.5V$. Not that the dot-like shape of the figure is due to the limitation of the oscilloscope in presenting the continuous output of the circuit.

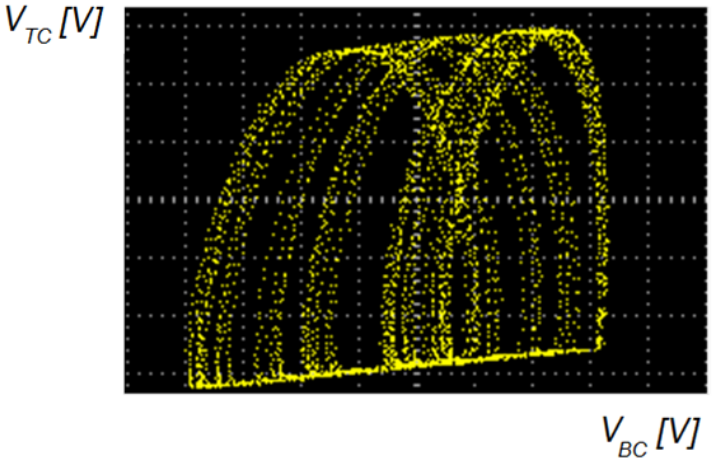

Figure C.3: The chaotic attractors of the circuit. The horizontal axes represents the transistor's base voltage V_{TB} and the vertical axes represents its collector voltage V_{TC}.

The block diagram of the HO feedback control, as well as a complete description of the implementation of this control method are explained in Sec. 4.2.1. Figure C.3 represents the result of successful implementation of HO feedback control, where the stabilized period-one orbit embedded in the chaotic attractor is illustrated. The effect of noise and environmental disturbance can be identified through the small fluctuations of the stabilized orbit.

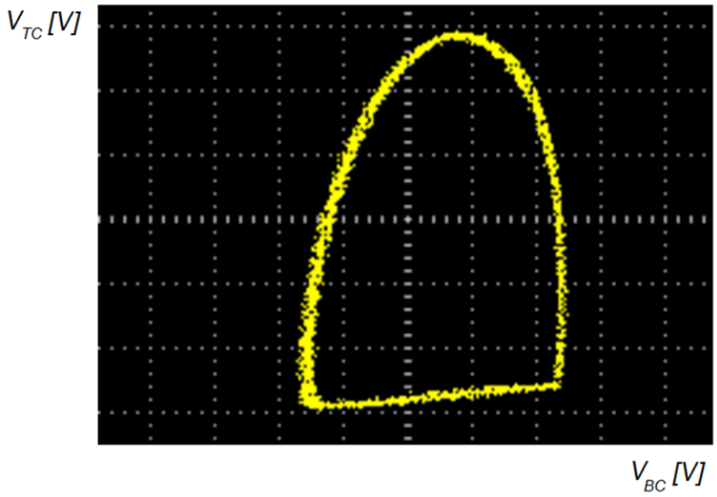

Figure C.4: The stabilized period-one orbit. The horizontal axes represents the transistor's base voltage V_{TB} and the vertical axes represents its collector voltage V_{TC} .

The dynamics of the control perturbations is plot in Fig. C4, which confirms the success of stabilization of the target orbit, as its magnitude remains small with respect to the input voltage V_{in}.

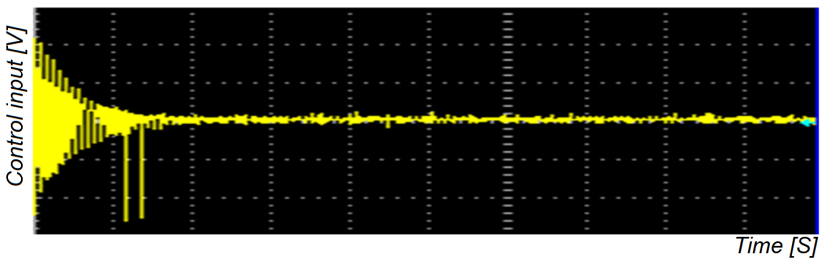

Figure C.5: The dynamics of the error signal

Appendix D

Devaney's Definition of Chaos

D.1 Introduction

Devaney's definition of chaos for discrete dynamical systems is one of the most popular and most widely known [89]. It says a function $f : \mathbb{M} \to \mathbb{M}$ is chaotic if

1. f is *topological transitive* that is, for any pair of non-empty sets $\mathbb{U}$ and $\mathbb{V}$ in $\mathbb{M}$, there is some $k > 0$ such that $f^{[k]}(\mathbb{U}) \cap \mathbb{V} \neq \emptyset$.

2. The periodic orbits of f are dense in $\mathbb{M}$; and

3. f displays the famous condition, sensitive dependence on initial conditions: there is a number $\delta > 0$ depending only on $\mathbb{M}$ and f, so that in every non-empty open subset of $\mathbb{M}$, one can find a pair of points whose eventual iterates under f are separated by a distance of at least δ [90].

Here $\mathbb{M}$ is generally a subset of $\mathbb{R}^n$, and $f^{[k]}$ means f composed with itself k times.

D.2 Discussion

Devaney's definition of chaos defines a function $f : \mathbb{M} \to \mathbb{M}$ on a metric space $\mathbb{M}$ to be chaotic if it satisfies three conditions: topological transitive, having dense set of periodic points, and sensitive dependence on initial conditions. Essentially, transitivity says that the function f draws open sets close together. Sensitivity, on the other hand, says f draws things apart. The condition that f has a dense set of periodic orbits is referred to as an *element of regularity* [89; pp. 50]. Among these three conditions, the third condition, sensitive dependence on initial conditions, is widely understood as the central idea in chaos. However, Banks et al [91] have proven that if f is continuous, then the third condition is redundant, that is the first two conditions imply the third. This fact reveals the topological, rather than metric, nature of chaos.